Structural Background of Force Generation in Myosins

PhD Thesis

by Boglárka Várkuti

Supervisor: András Málnási-Csizmadia, DSc

Associate Professor

Structural Biochemistry Doctoral Program

Doctoral School in Biology

Program Leader: Prof. Nyitray László, DSc

Head of the School: Prof. Erdei Anna, DSc

Eötvös Loránd University, Faculty of Science

Institute of Biology, Department of Biochemistry

Budapest, 2013

Content

I. Summary

P-loop NTPase activation by partner molecules is ubiquitous among various motor and signaling systems. Despite its significance in eukaryotic cell functioning, the structural mechanism of activation is still unrevealed. F-actin serves as a track for myosin's motor functions and activates its ATPase activity by several orders of magnitude, enabling actomyosin to produce effective force against load. We have described a conserved actin-binding region of myosin that we named 'activation loop', which interacts with the N-terminal segment of actin. We have demonstrated by biochemical, biophysical and *in vivo* approaches that the interaction between activation loop and actin accelerates the movement of the lever arm, stimulating myosin's ATPase activity and resulting in efficient force generation. The binding of actin to myosin's activation loop specifically increases the ratio of mechanically productive to futile myosin heads, leading to efficient muscle contraction.

The knowledge of the initial state of the powerstroke is inevitable to understand the structural rearrangements occurring upon actin activation. Therefore, we have created the structural model of the weak-binding actomyosin complex, the initial structure of powerstroke by *in silico* docking and molecular dynamics simulations. We found that actin-binding induced significant structural changes in the pre-powerstroke state of myosin. It resulted in the further up movement of the up-lever conformation and the further closure of the closed switch II loop, thereby creating an 'extra primed' state of myosin. Activation loop is specifically responsible for the formation of the extra primed state of myosin, as the elimination of the interaction between activation loop and actin N-terminal region by *in silico* mutations abolished, while the elimination of other actin-binding interactions did not revoke the extra primed state of myosin.

Capturing structurally unidentified states within the multistep process of the powerstroke of myosin would further help to reveal insights into the structural mechanism of force generation. Recently, a possible intermediate powerstroke state of myosin has been detected in the presence of ADP and blebbistatin, a myosin II specific inhibitor. The crystallization of the myosin-ADP-blebbistatin complex has been hindered due to the low affinity of blebbistatin to the myosin-ADP complex. In order to overcome this problem, we have synthesized para-azidoblebbistatin, a photoreactive derivative of blebbistatin, which can be covalently cross-linked to myosin in its different structural states. In the absence of UV irradiation, azidoblebbistatin exhibits identical inhibitory properties to those of blebbistatin. By a series of UV irradiation and application of para-azidoblebbistatin, we could covalently saturate myosin in the presence of ADP with its inhibitor. Our further aim is to crystallize the para-azidoblebbistatin-myosin-ADP complex, thereby reveal the atomic structure of a yet undetermined myosin state of the powerstroke.

II. Összefoglaló (Summary in Hungarian)

A P-hurok NTPáz család tagjainak kötőpartner molekulák általi alloszterikus aktivációja számos motor és jelátviteli rendszerben előfordul. Annak ellenére, hogy e fehérjék aktivációja az eukarióta sejt működéséhez elengedhetetlen, magának az aktivációnak a szerkezeti mechanizmusa mindmáig ismeretlen. Az F-aktin amellett, hogy sínként szolgál a miozin motorfunkciójának betöltéséhez, egyben aktiválja is annak ATPáz aktivitását, lehetővé téve ezzel a hatékony erőkifejtést. Csoportunk egy konzervált aktinkötő miozin régiót fedezett fel – melynek az aktivációs hurok nevet adta −, mely az aktin N-terminális részével létesít kapcsolatot. Biokémiai, biofizikai és *in vivo* kísérletekkel igazoltuk, hogy az aktivációs hurok és aktin közötti interakció felelős a miozin ATPáz aktivitásának aktin általi aktivációjáért, ami a hatékony erőgenerálást eredményezi. Az aktin az aktivációs hurokkal kialakuló interakción keresztül specifikusan növeli a hatékony erőkar lecsapások arányát (aktinkötött lecsapás) az úgynevezett haszontalan lecsapásokkal szemben (nem aktinkötött lecsapás), ami a hatékony erőkifejtéshez elengedhetetlen.

Mivel az erőkar lecsapás kiindulási állapotának szerkezeti ismerete elengedhetetlen az aktin aktivációkor bekövetkező szerkezeti átrendeződés megértéséhez, *in silico* dokkolással és molekuladinamikai szimulációval létrehoztuk a gyengén kötő aktomiozin komplex szerkezeti modelljét, ami az erőkar lecsapás kiindulási állapotát képviseli. Az eredményeink azt mutatják, hogy az aktin szignifikáns szerkezeti változásokat indukált a *pre-powerstroke* (aktin nélküli, felhúzott erőkarú, gyenge aktinkötő) miozin állapot szerkezetében, ahhoz történő kötésekor. A miozin felhúzott erőkara még inkább felhúzott állapotba került, illetve a zárt switch 2 tovább záródott, ezáltal létrehozva a miozin úgynevezett „extra felhúzott" állapotát. Az aktivációs hurok specifikusan felelős a miozin extra felhúzott állapotának kialakulásáért, mivel az aktivációs hurok és aktin N-terminális régió közötti interakciót megszüntető *in silico* mutációk az extra felhúzott miozin állapot megszűnését okozták, míg más aktinkötő miozin régiók nem felelősek az extra felhúzott miozin állapot kialakulásáért.

A többlépéses erőkar lecsapás mindmáig ismeretlen szerkezeti állapotainak felderítése nagymértékben elősegítené az erőgenerálás szerkezeti mechanizmusának megértését. Nemrégiben egy olyan miozin állapotot figyeltek meg ADP és blebbisztatin − egy miozin II specifikus inhibitor − jelenlétében, mely a miozin erőgenerálásának egy lehetséges átmeneti állapotát képviseli. A miozin-ADP-blebbisztatin komplex kristályosítására tett kísérletek azonban kudarcba fulladtak, a blebbisztatin miozin.ADP komplexhez való alacsony affinitása miatt. A problémát megoldandó, előállítottuk a blebbisztatin azido szubsztituált származékát, mely UV besugárzás alkalmazásával kovalensen kereszt köthető különböző állapotú

4

miozinokkal. UV fény hiányában a blebbisztatin és azidoblebbisztatin miozin inhibíciós tulajdonságai teljes mértékben megegyeznek. ADP jelenlétében a miozint para-azidoblebbisztatinnal UV indukált keresztkötési ciklusok alkalmazásával kovalensen telítettük, így lehetőség nyílt a miozin-ADP-azidoblebbistatin komplex kristályosítására. Célunk, hogy ennek az átmeneti erőgenerálási miozin állapotnak az atomi szerkezetét megismerjük.

III. Introduction

In this thesis I will present some of the milestones of the research on a motor enzyme, myosin and different aspects of its functional mechanism. Although 'myosinology' is an extensively studied field in motor enzyme research, there are still intriguing questions regarding the very basis of muscle contraction: what is the mechanism of force-generation? What structural changes are induced in myosin upon binding to actin that triggers muscle contraction? In this study, I will try to shed light on some specific moments of these very complex questions.

Molecular Motors in the Cell

Molecular motors are enzymes with the ability of converting energy into motion or mechanical power. One should note, that – unlike macroscopic motors – in the 'thermal bath' of a living cell, molecular motors are exposed to such a surrounding, where the fluctuations caused by the thermal noise cannot be neglected. Nevertheless, these nanomachines working efficiently and in concert within a cell, sustain the life of living organisms. The energy for their mechanical performance can have different origins. ATP synthases make use of proton gradients while performing rotation which motion is exploited to synthesize ATP, therefore they are also called *rotor* proteins. Additionally, in the absence of proton gradient, they hydrolyze ATP while performing work [1]. Besides the many other known proton gradient-driven motors (e.g. bacterial flagella), there are protein complexes that utilize ion gradients, such as Ca^{2+} for motion (spasmin in the protozoa Vorticella). A huge variety of other type of motor proteins evolved to make use of high-energy containing compounds. Most of these motors hydrolyze nucleoside triphosphates (NTPs, or their deoxy forms), and they are called NTPases (nucleoside triphosphatases). We can further differentiate them to GTPases (guanosine triphosphatases e.g. microtubules, dynamins) or ATPases (adenosine triphosphatases e.g. dynein, kinesin, actin, myosin or helicases), according to the type of NTP they hydrolyze. Within the cell, ATP is produced continuously from catabolic processes, creating a ~5-fold higher concentration of ATP than its hydrolysis products, ADP and Pi (phosphate). Therefore, ATP hydrolysis is accompanied by a huge negative free energy change (ATP→ADP+Pi: -30.5 kJ/mol, ATP→AMP+PPi: -45.6 kJ/mol). The hydrolysis products are also stabilized by having more resonance forms, by their ionization and their higher degree of solvation, all of which contribute to the high free energy change. Sometimes the group transfer

(Pi, PPi or AMP) from the ATP molecule to the sidechain of the enzyme, but mostly the hydrolysis of ATP itself at the binding site creates structural changes that enable the performance of mechanical work. As these motor proteins use chemical energy to create mechanical work, the process is called *chemomechanical energy transduction.*

Besides rotors, there is a huge variety of motor proteins in the cell which act linearly along a track to a specific direction. These *linear motors* can perform motion on the cytoskeleton (myosins on actin and kinesins/dyneins on microtubules), have a nucleic acid track/binding partner (helicases, polymerases), or create motion by the polymerization/depolymerization of themselves (actin, tubulin).

The Diverse Myosin Superfamily

Myosin is a superfamily consisting of more than 2000 molecular motors that are capable of hydrolyzing ATP and generating force: translocating/thethering actin filaments or translocating cargo on actin filaments. These motors are ubiquitous to eukaryotic cells, and recent philogenetic analysis groups them into 35 classes based on sequence homology of their head domains (**Figure 1**.) [2]. A member of the myosin II class was the first to be isolated from muscle fibres (which are also called conventional myosins) [3].
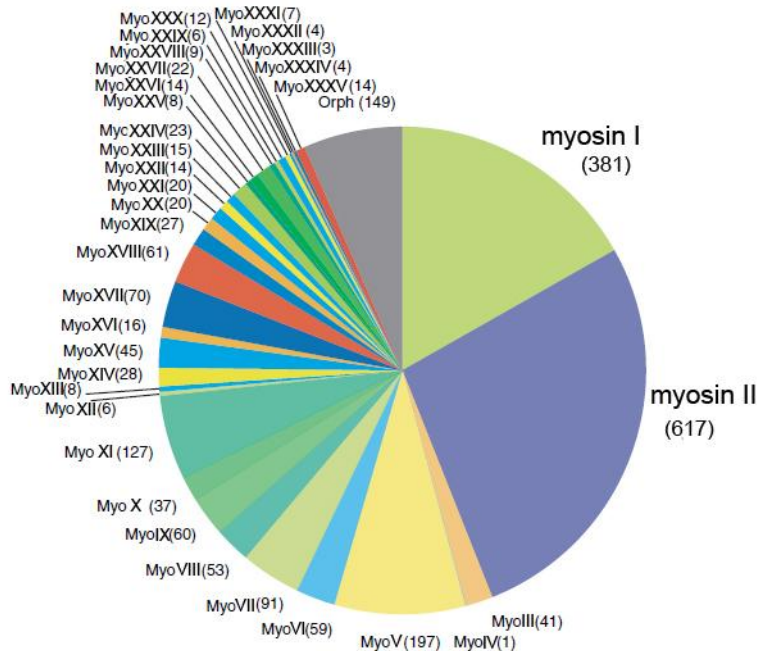
Figure 1. The pie-chart of the members of the myosin superfamiliy. The number of myosins in each class is shown (numbers in brackets). All myosins that cannot be classified yet are considered as orphan myosins (Orph). Figure is modified based on Figure 1 from [2].

As these myosins have two heads, they were given the number II. Myosin II itself is a diverse class, it integrates myosins that carry out muscle contraction, cell division, cell movement or sustain cell shape. They are usually grouped into skeletal+cardiac myosins, vertebrate smooth muscle+non-muscle myosins, *Dictyostelium*+*Acanthamoeba*-type myosins

and yeast-type myosins. Their common characteristic is to self-assemble through their tail regions and exhibit their function in a variety of filamentous structures [4]. Class I myosins were the first unconventional myosins to be identified from *Acanthamoeba*. They are not capable of dimerizing through their tail region, as they lack such coiled-coil forming sequences essential for it [5, 6]. This results in having a single head, consequently they were given the number I. Their role is in cytoskeletal reorganization and organelle translocation. All other myosins are assigned to a number referring to the order of their discovery. Another remarkable class among myosins is myosin V, which is a double-headed, high duty ratio motor, resulting in its processive feature. Processivity is the ability of a single molecule to undergo multiple interactions with actin without detaching from it, and the duty ratio is the ratio of the occupancy of the strong actin-bound states to the occupancy of all the states (bound and unbound). Processivity makes myosin V suitable for organelle/vesicle transport, membrane trafficking and polarized cell growth [7]. A unique nature of myosin VI is to travel towards the minus end of the actin filament, as all other known myosins act towards the opposite direction. This is possible with a 'reverse gear' inserted between the head and the neck of the protein [8]. Myosin VI molecules are located in the hair cells of the organ of Corti, possibly responsible for recycling and endocytosis. There are plant specific myosins taking part in cell division (myosin VIII), and many other myosins are supposed to be involved in intracellular signaling (myosin III, IX) [9]. There are myosin classes from which little is known, and some are only known as partial cDNA sequences derived by RT-PCR. With the help of PCR, many new myosins have been identified in the past decade.

Despite the large functional variety of myosins, they share a common mechanism of chemomechanical energy transduction, conducted by the conserved N-terminal head (motor domain) that all myosins possess (**Figure 2.**). Besides the motor domain, myosins have two other major functional domains that are more diverse among the myosin classes i.e. a neck and a tail.
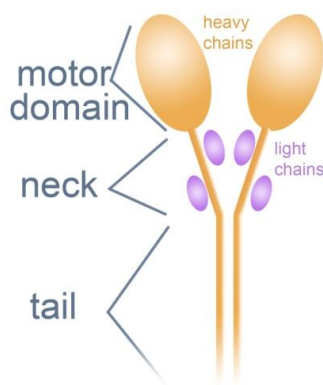
Figure 2. Schematic representation of a conventional hexamer myosin II. Myosin II consists of two heavy chains (~220 kDa each) that dimerize at their tail region, and four light chains (two essential and two regulatory, ~20 kDa each). The N-terminal regions of the heavy chains create the catalytic motor domains, which is followed by a neck region. The neck is variable in length, and contains the binding sites of the light chains. The two α-helices of the heavy chains create a coiled-coil rod, the tail region.

Motor domains are typically composed of 720-780 amino acids, and contain the nucleotide and actin-binding sites [10, 11]. Usually motor domains are located at the N-terminal part of the myosin, however some myosins (e.g. *Drosophila* non-muscle myosin II or myosin III) have large amino-terminal extensions preceding the motor domain [12, 13]. Basic structural elements of the actin- or nucleotide-binding sites are well conserved among myosins, with a few regions that correspond to the flexible linkers between conserved regions [14]. Insertion or deletion of amino acid residues comparing various isoforms can be found mainly on the surface of the molecules, the length of structures within the core of the protein is remarkably conserved [15, 16].

The following functional region of myosin is the neck region. The α-helix of the neck is stabilized by the binding of light chains. In case of myosin II, two kinds of light chains bind to each neck region, the essential and regulatory light chains. Their names originate from investigations with smooth muscle and scallop myosin, where they regulate the ATPase activity of myosin [17, 18] and muscle contraction [19]. There are consensus sequences involved in their binding, which are called 'IQ motifs' (IQXXXRGXXXR). The number of IQ motifs in the neck region vary among myosin classes. As an example, in the case of myosin V there are five of them. Also, in many classes, variable numbers of calmodulin molecules associate with the neck region, in addition to other types of light chains. Besides being the binding site of the regulatory proteins, the neck also serves as an extension of the motor domain acting as a lever throughout the force generation of myosin.

The tail region is the most diverse domain among myosins, sequentially, structurally and functionally too. It serves for anchoring myosin so it can move relative to the actin filaments. Myosin II molecules can self-assemble in low ionic strength through their tails into thick filaments, with their multiple heads being capable of translocating actin. In skeletal muscle, these thick filaments are bipolar, and they move actin from both sides towards their centre. Myosin I cannot dimerize, but it can anchor itself to membranes. Other myosins, like myosin V have cargo binding domains at the C-terminal of their tails.

Besides the three major regions, some myosins possess SH3-like or protein kinase domains preceding the motor domain. Additional domains in the tail region (such as SH2, PDZ, Ras association or ubiquitin associated domains) can also be found.

We should also mention some main forms of regulation among myosins. One of it is indirect, when myosin's ATPase activity is modulated by a steric hindrance of its binding to the actin filament. An example for this is skeletal myosin II, regulated by the troponin(C, I and T)-tropomyosin complex which sterically hinders the binding of myosin to the actin filament at low Ca^{2+} concentrations (~10^{-7} M). At high Ca^{2+} concentrations (~10^{-5} M), troponin C binds

Ca^{2+} which induces conformational changes of the troponin-tropomyosin complex resulting in the uncovering of the myosin-binding site on the actin filament [20]. Another form of regulation involves the modulation of myosin itself by the varying Ca^{2+} concentrations within the cell, either directly or indirectly. Smooth muscle and non-muscle myosin II are activated by the phosphorilation of their RLC regulated by Ca^{2+} indirectly, with the contribution of myosin light chain kinases [21, 22]. In the case of mollusk myosin II, Ca^{2+} concentration directly influences its activity by binding to their ELC [23, 24]. There are myosins that can be regulated by both RLC phosphorilation and the troponin-tropomyosin complex e.g. tarantula leg myosin [25, 26]. The ATPase activity of myosin I and VI can be modulated by the direct phosphorilation of their heavy chains i.e. of amino acids located in a surface-loop of the molecules [27, 28]. Although the ATPase activity of myosin V in the presence of actin is activated by micromolar concentrations of Ca^{2+}, Ca^{2+} also inhibits the binding of calmodulin molecules to the IQ motifs of myosin V, thereby abolishing its processivity [29, 30]. It is likely that Ca^{2+} is not the physiologically important activator of myosin V and there may be other mechanisms involved in its regulation e.g. binding of cargo to the molecule.

Early Research of Myosin

Discovery of Actin and Myosin

The name 'myosin' was given to a viscous extract from muscle fibres by Kühne [31]. As the solution from muscle had enzymatic properties, he named it myo-enzyme: myosin. Many years later, Engelhardt and Lyubimova described for the first time that myosin catalyses ATP hydrolysis to ADP and Pi, which is referred to as the myosin's ATPase activity [32]. Although many experiments have been carried out on myosin, scientists did not realize that the extract was not one protein, but a mixture of proteins, until Albert Szent-Györgyi and his colleagues working in Szeged demonstrated it. Ilona Banga and Albert Szent-Györgyi could separate the extract to a low and a high viscosity solution (named myosin A and B), and showed that ATP can decrease the viscosity of myosin B [33]. Due to the lack of communication during World War II, such effect of ATP on the viscosity of the myosin solution was also discovered independently by Needham *et al* [34] . Preparing threads from myosin B and adding boiled muscle juice to them shortened the threads, as Albert Szent-Györgyi demonstrated [35]. The active compound causing the shortening was later identified to be ATP. Soon it became clear, that myosin A was one protein, which they kept to call as myosin, and myosin B was a mixture of myosin and another protein, which they named actin.

Both proteins were isolated and characterized first by Brunó Straub and Albert Szent-Györgyi [36, 37]. Interestingly, actin is still prepared by practically the same protocol. They also showed the existence of actin in two forms: at low salt concentration the globular monomer form is present (G-actin), while increasing the salt concentration makes G-actin to polymerize into fibrous actin (F-actin) [38]. The group at Szeged also demonstrated that magnesium increased the steady-state ATPase activity of actomyosin [39], and that ATP had a duel function depending on ionic strength. At low ionic strength it caused contraction of the fibers, at high ionic strength it caused the dissociation of actin and myosin [40]. Tamás Erdős discovered that the state 'rigor mortis' was due to ATP depletion of the actomyosin muscle fibers [41]. Additionally, Endre Biró and Andrew G. Szent-Györgyi detected that steady-state ATPase of actomyosin increased during contraction [42]. Although first it was not universally accepted, soon Albert Szent-Györgyi made conclusive *in vitro* experiments to prove that the contractile event of muscles is based on ATP and the actomyosin system [43]. He demonstrated, when magnesium and ATP containing solution was added to oriented actomyosin filaments, they contracted as the original muscle tissue. Neither actin nor myosin filaments alone behaved in such a manner. With these results Albert Szent-Györgyi and his group have laid down the fundaments of myosin research and opened up a new phase of muscle biochemistry.

In order to assign the different functions (ATPase activity, actin binding, filament formation) to different regions of myosin, researchers used proteolitic fragmentation of the molecule. The approach was initiated by János Gergely [44] and Perry [45] independently. Tryptic digestion resulted in two populations of fragments when sedimenting by ultracentrifugation at high ionic strength, one of which seemed to bind to actin. The slowly sedimenting component was named light meromyosin (LMM) and the faster sedimenting component was named heavy meromyosin (HMM) (**Figure 3**.). Andrew G. Szent-Györgyi suggested another separation method, which depended on the different solubility of the fragments: HMM was soluble even at low ionic strength, whereas LMM formed paracrystals, making it easy to separate them under such conditions [46]. This finding was important in further research, as it made HMM a very useful experimental object to investigate the enzymatic properties of myosin. The LMM paracrystals showed similar periodicity in the electron microscope [47] as the obtained fundamental fiber period by X-ray analysis in the work of Huxley [48]. Further analysis of the fragments revealed, that LMM is a coiled-coil structure responsible for filament formation, and HMM retains the ATPase activity and actin binding properties of myosin. Overdigestion of HMM by trypsin results in S1 and S2 subfragments [49] (**Figure 3.**). Papain or chymotrypsin can split myosin into a rod and S1 fragments. S1 is able to bind actin and fully preserve myosin's ATPase activity [50], while S2

is a helical and flexible structure [51, 52]. S1 is not only the fully active part of myosin, but it is also a cross-bridge of the muscle fiber, acting as a minimal model for muscle [53]. It appeared that LMM together with S2 forms the rod of myosin, LMM being the core of the myosin filaments while myosin heads can reach out of the filament through the flexible S2. Electron microscopy has also revealed that myosin II has two globules (heads) at one end [54], proving that myosin II is made up of two parallel peptide chains, in contrast to previous proposals of a three-chained structure [55].
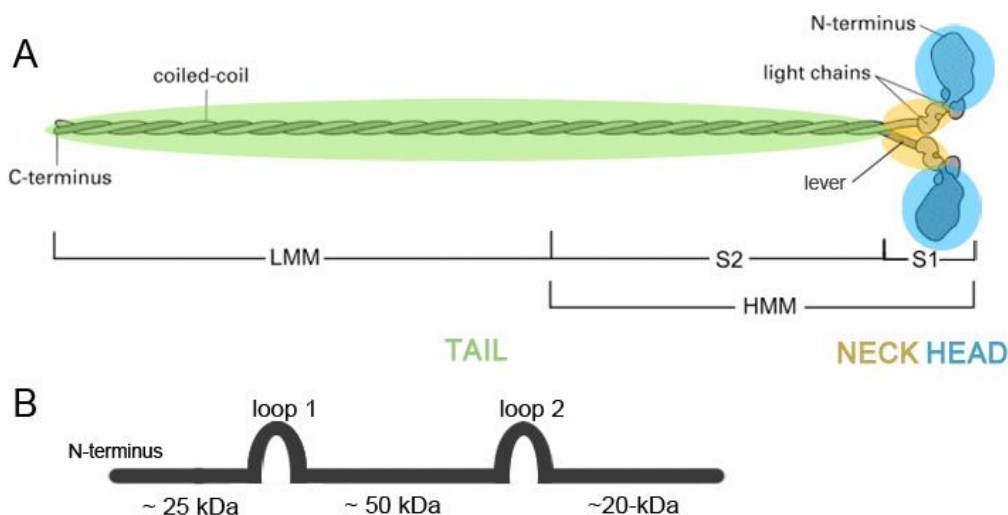
Figure 3. Proteolytic fragmentation of myosin II. (A) Various proteases cleave myosin II at the junctions LMM/HMM or S1/S2. LMM together with S2 forms the tail of myosin, which is a coiled-coil α-helix. HMM (~140 kDa) is a two-headed dimer that is interconnected through S2. S1 (~120 kDa) contains the motor domain and the lever with the light chain binding sites, forming a sole crossbridge. Therefore, HMM is made up of two crossbridges. The figure is modified based on [3]. **(B)** Loop 1 and loop 2 cleavage sites within the head result in three fragments of the head, which remain associated under native conditions.
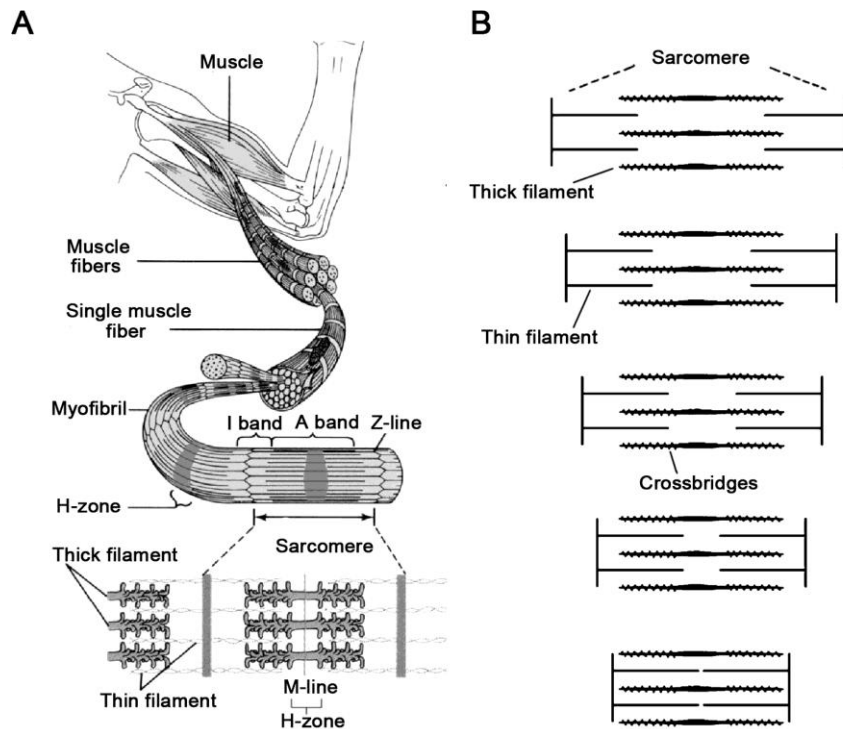
Researchers could further cleave S1, as the head contains extremely sensitive proteolytic sites, which are accesible by various proteases [56-60]. These sites are within flexible loops on the surface of the head, termed loop 1 and loop 2. One site is about 25 kDa and the other is 75 kDa from the amino terminus, resulting in three fragments of S1 after cleavage: the amino-terminal 25-kDa fragment, the central 50-kDa fragment and the carboxy-terminal 20-kDa fragment. These fragments are also named Bálint-fragments, after Miklós Bálint who discovered them [60]. Later it turned out that these fragments do not constitute independently folding domains of the head, and only dissociate under denaturating conditions. The loop 2 cleaved N-terminal fragment of S1 (25 kDa+50 kDa fragments) is still active enzimatically, though it binds actin more weakly than the intact molecule [61-63]. The remaining 20 kDa fragment associated with light chain is named the regulatory domain [64].

Myosin fragments were proved to be crucial in exploring the various functions of the molecule as well as guiding our understanding towards how muscles work. HMM and S1 are

used widely in kinetic, actin binding studies or *in vitro* motility assays, while rod and LMM are used in structural and filament assembly experiments.

The Structure of the Muscle and the Principles of Contraction

Vertebrate striated skeletal muscle consists of muscle fibers, each surrounded with a sarcolemma (**Figure 4.**). One muscle fiber is a fusion of several cells, having multiple nuclei, and containing many myofibrils. Myofibrils are made up of myofilaments. Electron microscopy revealed the existence of two kinds of myofilaments: 1.6 µm long thick filaments (located in the A-band), and 1 µm long thin filaments (anchored to the Z-line and stretching to the H-zone) [65, 66]. The thick filament was identified to be myosin, while the thin filament is actin. The intercalating thin and thick filaments between two Z-lines form the sarcomere, the contracting, functional unit of the muscle. I-bands of the striated muscle contain only thin filaments, and central Z-lines, where thin filaments anchor. A-bands of the muscle fibres contain thin and thick filaments, central H-zones with M-lines, which is a zone of myosin rods only.

The idea of the *sliding filament theory* came from the observation that under contraction, the length of the A-band is constant, while the length of the I-band shortens [67, 68]. It was discovered independently by two groups of researchers, A.F. Huxley & Niedergerke and H.

Figure 4. The structure of the muscle and the basis of contraction. (A) Ultrasctructure of the muscle. Skeletal striated muscle is made up of sarcomeres, which build up to filaments, fibrils, fibers then muscle. Striation comes from two zones with high or low refractive indexes observed by light microscopy: the anisotropic A-band and the isotropic I-band. (B) Model of the sliding filament. The sarcomere shortens as the crossbridges of thick filaments pull thin filaments towards the center of the sarcomere, without any change in the length of the myofilaments. Figure was modified based on [3].

Huxley & Hanson, publishing their results in the same issue of Nature journal. As thick filaments propel thin filaments towards the center of the sarcomere during contraction, the lengths of the filaments do not change. It explains the constancy of the A-band and the changes in the I-band and H-zone. This mechanism is possible due to the bipolar structure of the thick filaments, as myosins associate through their tail region with their heads pointing to opposite directions. These observations revolutionized muscle studies, as previous theories took it for granted, that muscle contraction was a result of the length change of long polymer-like molecules.

Soon it became clear, that the contraction of the sarcomere is driven by the crossbridges attaching to and 'pulling' on actin [66, 69]. It took a few years to discover, that the shape of the crossbridges change during the cycle, changing the angle of the head relative to the actin filament [70]. As X-ray diffraction and electron microscopy showed, the resting muscle contains heads perpendicular to the filaments (90°), while in ATP depleted muscle (rigor), myosin heads protrude from the thick filaments creating an acute angle (45°). Thus, the *swinging crossbridge theory* was created, proposing that these angle changes take place while myosin is attached to the actin filament, which leads to the shortening of the sarcomere [71]. The idea was widely accepted, though it took many years to find direct evidence for it.

**The First Chemomechanical Model of Actomyosin**

Thorough investigation of the crossbridge cycle started with S1 and HMM fragments of myosin. Transient kinetics was introduced to explore the steps of the cycle [72]. The first kinetic model of actomyosin was proposed by Lymn and Taylor, whose four step model is still valid today (**Figure 5.**) [73]. It was based on the findings, that ATP is hydrolyzed by actin-detached myosins and that a burst of ATP hydrolysis occurs − nearly stoichiometric with the myosin heads − upon ATP addition. The burst could only be detected, when the active site was not occupied, indicating that the dissociation of the products limits the rate of the actomyosin cycle.
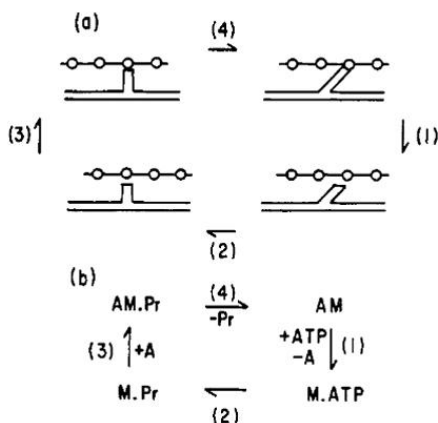
Figure 5. The chemomechanical Lymn-Taylor cycle of actomyosin ATPase. (A) The mechanical cycle of actomyosin. Actin filament is represented as globules on a string, while the crossbridge is a protrusion of the thick filament. **(B) The chemical cycle of actomyosin.** Actin is A, myosin is M and the hydrolyzed product is Pr. This figure is in its original form as it was published by Lymn and Taylor in 1971 [73].

Combining the mechanical with the chemical cycle, the chemomechanical cycle is the following: as ATP binds to rigor (strong binding) actomyosin (I), it reduces the affinity of myosin to actin, causing myosin to rapidly dissociate from the actin filament. The crossbridge then undergoes a conformational change, while ATP is hydrolyzed (2). Myosin, with the bound hydrolysis products, rebinds to actin (3). This is followed by the dissociation of the hydrolysis products and the swing of the crossbridge moving the actin filament (4). This step is called the *powerstroke*, and in this model force production is associated with the conformational change of the crossbridge and the release of the products. The release of products enables the rebinding of ATP, thus the cycle starts again. Although the Lymn-Taylor cycle says little about the intrinsic structural changes, it is still a very useful basis for more complex models, as it summarizes all the physical and chemical changes of the action of actomyosin that can be detected macroscopically. However, it turned out, that to understand the structural changes that occur during the crossbridge cycle, the determination of the structures of myosin and actin at atomic resolution was necessary. This took more than twenty years.

Throughout these years, on the basis of intense electron micrographic studies of acto-S1 complexes the swinging crossbridge model (that was used in the Lymn-Taylor cycle as well) was gradually modified into the *swinging lever-arm hypothesis* (**Figure 6.**). A model was proposed for the changes of crossbridge conformation [74], which could only be proved much later [75], after the three dimensional structure of the myosin crossbridge was revealed by X-ray diffraction experiments. The swinging lever gives explanation to why the changes in crossbridge orientation were not visible under the electron microscope: only a small fraction of the crossbridge itself (the lever) moves during the cycle. Furthermore, it has gradually become clear that only a small fraction of the total crossbridges takes part in contraction at a time, making the detection of active crossbridges difficult.
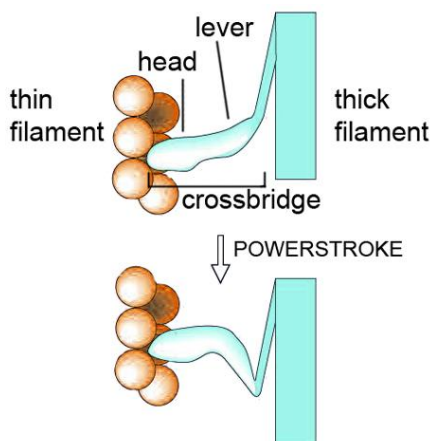
Figure 6. The swinging lever-arm. The swinging crossbridges needed revision and were replaced by swinging levers. The figure illustrates, that only the distal part of the crossbridges move during the powerstroke. The lever serves to amplify the small changes occurring in the head during actin binding, leading to powerstroke. We must note, that according to this theory, the interacting surface of actomyosin does not necessarily change during powerstroke. Figure modified based on [74].

Several new and innovative techniques had been developed to understand the enzyme mechanism of myosin at the molecular level before the first crystal structures were determined. These include the application of fluorescence energy transfer [76], single molecule measurements and optical traps [77, 78], or *in vitro* motility assays [79]. In such assays, the sliding velocity of the fluorescent actin filaments propelled forth by a myosin-coated surface could be quantified. Tension induced by single myosins acting on actin attached to a thin glass needle could be determined [77], which technique was further developed by holding the actin filament between beads in a laser trap [80]. The other great progress achieved in this era is the recombinant expression of myosin constructs. The expression of S1, motor domain and many mutant forms of myosin in *Dictyostelium* [81, 82] and the expression of myosin fragments in insect cells using baculovirus as a vector [83-85] paved the way to the determination of many three dimensional atomic structure of myosin.

Atomic Structures of Different States in the Actomyosin Enzyme Cycle

Structural Features of Actin

The atomic structure of actin from the actomyosin system was discovered first. As only the monomer G-actin can be crystallized [86-88], there are only models of the F-actin [89, 90] (**Figure 7**). G-actin is made up of two domains, a DNase-binding and a myosin binding domain. A large cleft separates the two domains, which is the binding site of ATP and Ca/Mg. Each domain can be separated to two subdomains. One creates parts of the nucleotide binding pocket, the other is involved in actin-actin interactions [86]. The ATPase activity of actin is not related to its interactions with myosin, neither to muscle contraction. It drives the continuous polymerization/depolimerization of the actin filaments. ATP-bound G-actin associate to the developing + end of the filament (barbed end). When actin hydrolyzes ATP, Pi is released and the ADP-bound actin monomer dissociates from the other, - end (pointed end) of the filament. As the filaments have polarity, myosins are also committed to one direction of the actin filament, either proceeding towards the + or the − end.

When creating F-actin models, G-actin crystals are fit into the three dimensional electron density map obtained from electron cryo-microscopy (called electron micrographic map or EM map). In the refinement, the four subdomains of the actin monomer are allowed to move as independent solid bodies. The result is a left-handed actin filament, with each monomer turning 166° from the previous one, providing the filament a double helical shape. The polymerization of the actin filament involves a relative rotation of 20^0 between the two

major domains, creating flat monomers in the filament. This flat form is needed to stabilize the F-actin [90].
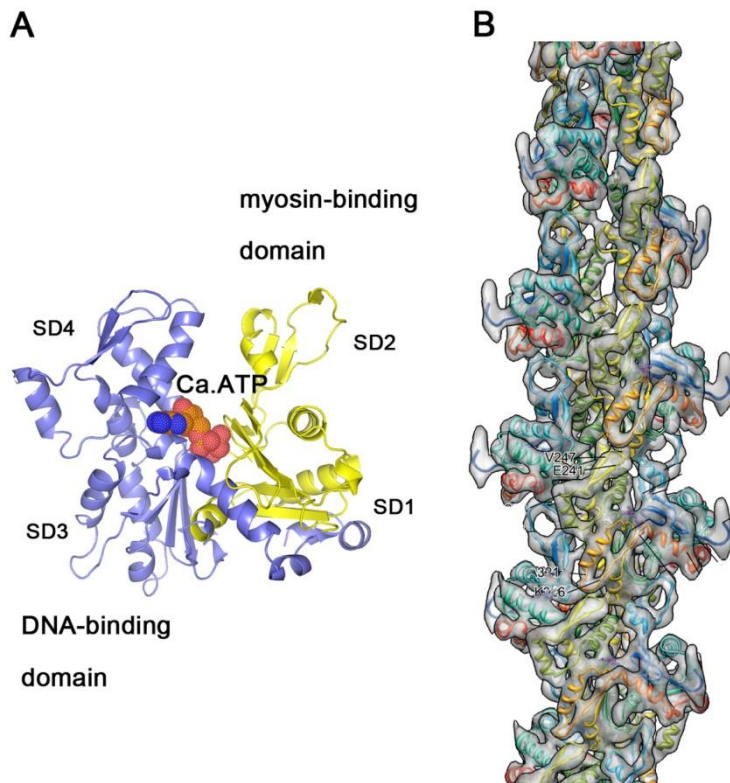

Figure 7. The structure of actin. (A) The crystal structure of G-actin. The myosin-binding domain (yellow) consists of subdomains (SD) 1 and 2, while the DNA-binding domain (blue) is made up of SD3 and SD4. (PDB code: 1ATN) **(B)The EM map-based atomic model of F-actin.** G-actin crystals are rainbow colored with ribbon representation, while the refined EM-map is transparent gray. The turn of the helical actin filament repeats every 36 nm, rises 2.75 nm/G-actin and contains 13 monomers. Each monomer interacts with four neighboring monomers. Figure was modified on the basis of [89].

The name actin comes from its effect on myosin, as it is the allosteric **act**ivator prote**in** of myosin. By actin binding to myosin, it increases myosin's basal ATPase activity (enzyme activity in the absence of actin) by several orders of magnitude.

The Structure of the Catalytical Domain of Myosin II

The first resolved atomic structure of myosin was chicken fast skeletal myosin S1 [91]. It revealed important insights into the mechanism of the actomyosin cycle. It possessed an extended carboxy-terminal tail, which looked like a lever-arm, assuming the first evidence for the swinging lever-arm hypothesis (**Figure 8.**). Moreover, this tail showed a correct orientation and position to function as a lever [92].
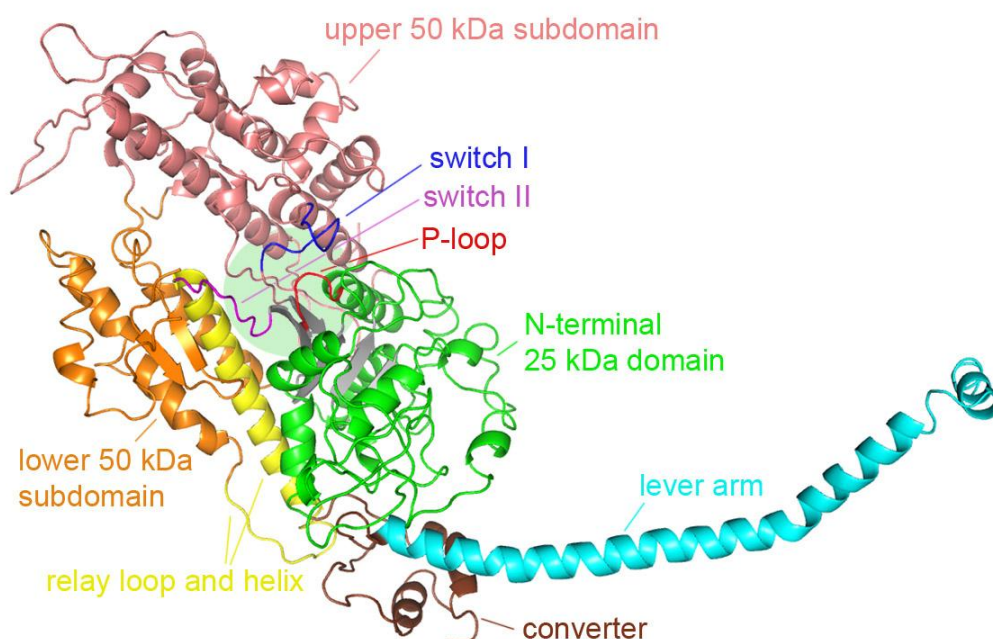
Figure 8. The atomic structure of chicken skeletal myosin S1. A deep cleft separates the 50 kDa domain into upper (pink) and lower (orange) 50 kDa subdomains, forming the actin binding interface. Between the 50 kDa and the N-terminal 25 kDa (green) domain lies the nucleotide-binding site (green shadowed area), containing P-loop (red), switch I (dark blue) and switch II (magenta). The relay (yellow) is part of the lower 50 kDa subdomain stretching to the C-terminal 20 kDa subdomain, the converter (brown). This serves as the basis for the lever (light blue) (PDB code: 2MYS).

The other remarkable feature was that its elongated head was separated by a deep cleft that runs from the actin-binding site to the nucleotide-binding pocket. It was suggested, that this cleft closes upon actin-binding, which was later supported indirectly by electron microscopy combined with image reconstruction and experimentally, by fluorescent probes located in the cleft [93-95]. The motor domain of the chicken skeletal myosin S1 contains a central seven-stranded β-sheet and α-helices that form the deep cleft at one end. This cleft divides the 50 kDa domain into upper and lower 50 kDa subdomains, which contain the *actin binding interface* of myosin, including several surface loops involved in actin-binding. In the presented structure, the cleft is in a prominent open conformation.

The *nucleotide-binding site* lies close to the apex of the actin-binding cleft. It consists of a P-loop, as well as switch I and switch II loops. All three structural elements also found in G-proteins, kinesins or dyneins. This suggests their common mode of sensing the different hydrolyzed forms of the nucleotide. The consensus sequence of the P-loop (Gly-XXXX-Gly-Lys-Thr/Ser) can be found in all P-loop NTPases, which form a very ancient group. The highly conserved P-loop is involved in the coordination of the Pi of the nucleotide. The switches are

also structurally and sequentially conserved loops in myosins, surrounding the nucleotide-binding pocket. Structural comparisons of different states of myosins and transient kinetic experiments revealed several conformations of the switches, but mainly we describe them as being open or closed. Switch I coordinates the γPi of ATP and the Mg^{2+} in the nucleotide pocket. Its conserved arginine forms salt bridge interaction with the glutamate of switch II, creating the closed conformation of the switches. Switch II coordinates the Mg^{2+} of the nucleotide binding pocket, and also catalysis the hydrolysis of ATP. Switch I 'switching' between its structural states seems to influence the closure of the actin-binding cleft, through interactions with the 7-stranded central β-sheet, while switch II movement is coupled to the movement of the lever-arm, through interactions with the 'relay' region.

The *relay* region structurally connects the actin- and nucleotide-binding sites with the basis of the lever-arm. The relay helix is a flexible structure, transmitting switch II movements through hydrophobic interactions to its C-terminal region, which is structurally connected with the 'converter'. The *converter*, located at the basis of the lever-arm, together with the relay can amplify movements originated at the nucleotide- or actin-binding sites. The continuation of the converter is the *lever*, or neck region, containing the binding sites of light chains.

The myosin state presented in Figure 8 structurally resembles the state after step 1 of the Lymn-Taylor cycle (**Figure 9**). Although it contains no bound nucleotide, it has a magnesium-sulfate ion in its nucleotide-binding pocket (derived from the purification of the protein) and
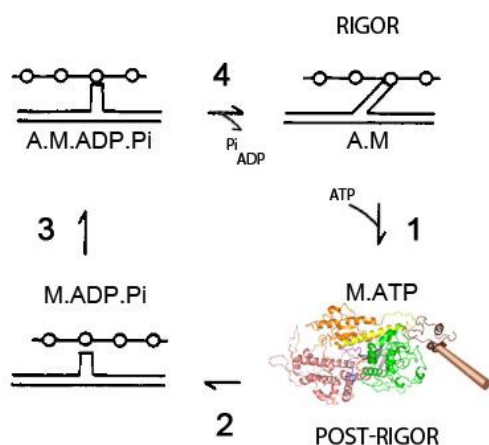

Figure 9. Structural states in the Lymn-Taylor cycle – the post-rigor state. The structure of the post-rigor state fits well into the chemomechanical cycle of the Lymn-Taylor model. The lever of the motor domain is represented as a brown rod.

has a lever in down orientation. Because of the lack of nucleotides, first it was thought to be close to the end state of the powerstroke, the rigor state. However, it was later recognized as a weak actin-binding, post-rigor state, which is formed after ATP bound to myosin at the end of the powerstroke and myosin is rapidly released from actin [96]. As this structure is formed after the rigor structure, it is further referred to as the *post-rigor* state. Later, with the help of ATP analogues and ADP, further post-rigor structures have

been revealed e.g. *Dictyostelium* myosin II (1MMD), chicken myosin Va (1W7J), squid myosin II (3I5F) [97-99].

Structural Features of Post-rigor and Pre-powerstroke States

Constructs lacking the lever, such as the motor domain, often crystallize more easily than the full-length crossbridge. Therefore, many structures of different states of *Dictyostelium* myosin II motor domains have been determined. Also, they can be easily expressed in plasmids and conveniently sequence manipulated [81]. Recombinant *Dictyostelium* motor domain usually consists of the first 761 amino acid residues, eliminating the whole lever, but 'keeping' the converter. This functional core of the enzyme is similar in all myosins (shown by sequence comparisons [15]). Shorter constructs that damage the converter seem to have unusual ATPase properties [100], while the 761 construct has the same kinetic properties as S1 or the complete myosin. *Dictyostelium* motor domains have been crystallized with various bound nucleotides e.g. ATP analogues as $ADP.BeF_3^-$, or ADP.Pi analogues such as $ADP.VO_4^{3-}$ or $ADP.AlF_4^-$. These analogs stabilize myosin in specific states that would be inaccessible for crystallization in the presence of ATP, as ATP is immediately hydrolyzed by myosin and the result is a highly inhomogeneous population of myosin structures. Upon the comparison of the structure of the $Mg.ADP.VO_4^{3-}$-bound myosin motor domain [101] with the post-rigor state, there are considerable differences between them (**Figure 10.**).
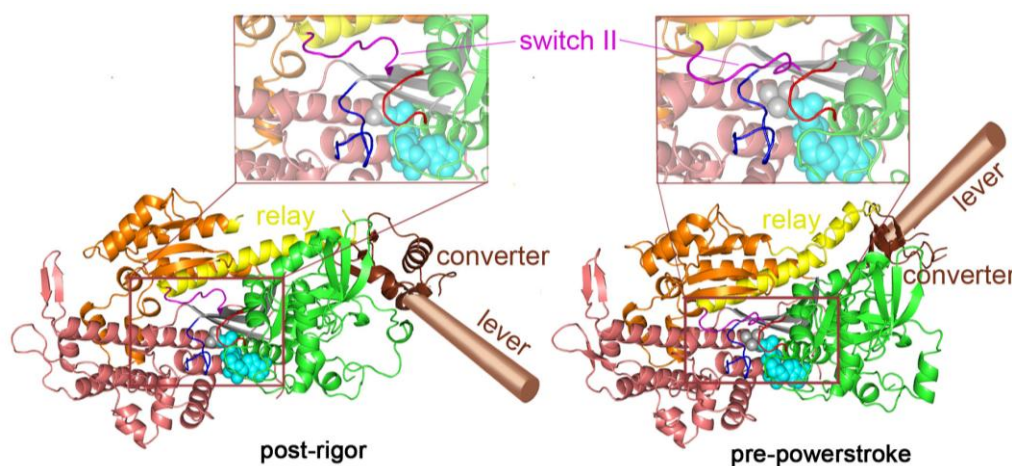

Figure 10. Post-rigor and pre-powerstroke states of *Dictyostelium* myosin II motor domains. Differences mainly affect the position of the lever (represented as a brown rod), switch II loop (magenta) and the relay (yellow). Both structures possess a closed switch I (dark blue), down-oriented P-loop (red), open actin-binding cleft and an untwisted β-sheet (gray). Other regions are also color-coded: upper 50 kDa is pink, lower 50 kDa is orange, converter is brown, the N-terminal domain is green. $Mg.ADP.BeF_3^-$ of the post-rigor state and $Mg.ADP.VO_4^{3-}$ of the pre-powerstroke state are colored light blue. The nucleotide binding pockets are enlarged in the insets (PDB codes: 1MMD, post-rigor; 1VOM, pre-powerstroke).

Most importantly, the position of the converter in the $Mg.ADP.VO_4^{3-}$-bound state reveals an alternative conformation of the lever, accompanied by a 'kinked' relay helix, representing an 'up' conformation of the lever. Additionally, the switch II of the $Mg.ADP.VO_4^{3-}$-bound myosin

is in a closed conformation compared to the post-rigor state. As the former structure is also actin-unbound, and has an up-lever conformation, it resembles the state after step 2 of the Lymn-Taylor cycle, before powerstroke takes place. Therefore it is named the *pre-powerstroke* state (**Figures 10 and 11**).

ADP.Pi analogues promoted the solving of other pre-powerstroke structures as well, e.g. chicken smooth muscle myosin II (1BR2), *Dictyostelium* myosin II (1MND) or scallop myosin S1 (1DFL) [97, 102, 103]
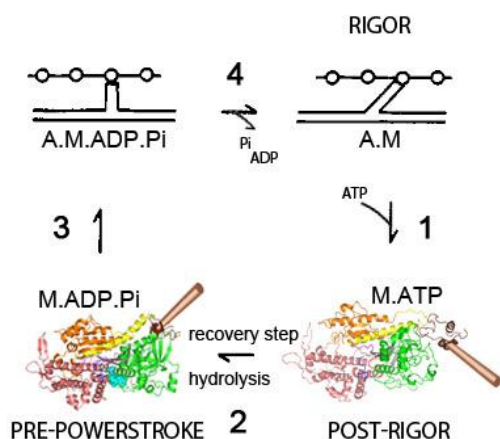

Figure 11. Structural states of the Lymn-Taylor cycle – the pre-powerstroke state. The pre-powerstroke structure resembles that of the sate after step 2 of the Lymn-Taylor cycle.

The Mechanism of the Recovery Stroke

Upon comparison, going from post-rigor to pre-powerstroke state, the most striking event is the down-to-up transition of the lever, which is the priming of the lever, also called *recovery stroke*. In post-rigor state, the switch II is ~5Å away from the γPi of the ATP, therefore it has an open conformation. Its switch I has already closed on the γPi, and this closed conformation of switch I together with P-loop promotes the closure of switch II as well. *In silico* simulations suggested a 2-phase 'seesaw-like' mechanism of the closure of switch II coupled to the priming of the lever (**Figure 12.**) [104, 105].

As switch II closes, it pulls the N terminal region of the relay through H-bond interactions. The relay pivots on a phenylalanine cluster (a fulcrum), like a seesaw, and the movement of its C-terminal to the opposite direction starts to rotate the converter and lever to an up position. The complete priming of the lever is finished after the second phase, when the interaction between P-loop and switch 2 is formed, pulling switch II towards the P-loop. This triggers a pull on the wedge loop, which pushes the SH1 helix, inducing a further movement of the converter. The conformational rearrangements of the second phase cause the kink in the relay, by the break of an intra-helical H-bond. The result is an up-lever, pre-powerstroke state myosin.
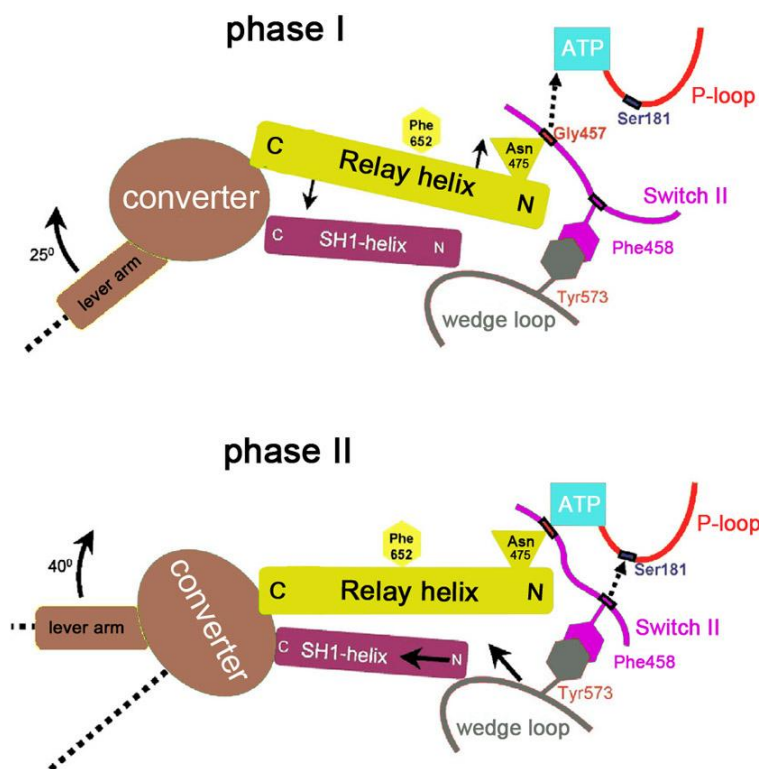
Figure 12. The structural mechanism of the recovery stroke. In the first phase, Gly457 of switch II loop (magenta) moves towards ATP. Thereby, it pulls the relay (yellow) through an H-bond with Asn475. The relay pivots around the fulcrum formed by Phe652 and other phenylalanines. This triggers the motion of the converter (brown), initiating the recovery of the lever. In the second phase, an H-bond interaction is formed between Ser181 of P-loop (red) and the backbone of switch II, pulling switch II closer to P-loop. This also pulls the wedge loop (grey) through the Tyr573-Phe458 interaction with switch II. Motion of the wedge loop pushes SH1-helix (purple), which induces the further priming of the lever. The figure is modified based on [93].

Upon the recovery of the lever, the myosin head activates its ATPase function by the closure of the nucleotide-binding pocket. The tight coupling between the motions of the converter and switch II is essential to avoid unproductive ATP hydrolysis. If switch II closes without the priming of the lever, it would result in a wasteful cycle [106]. The seesaw mechanism of the recovery-stroke was also experimentally supported by mutating the phenylalanines of the fulcrum (e.g.Phe652A) in *Dictyostelium* myosin II [107]. These mutations, affecting their supporting function for the relay, structurally decouple the C-terminal part of the relay from motions originating in the nucleotide-binding site. Thereby, switch II closure is not accompanied with lever priming. Interestingly, the fulcrum mutants could hydrolyze ATP despite having the equilibrium pushed towards the down-lever state. As they possess a closed switch II, this phenomenon further confirmed that closed switch II is needed for effective hydrolysis. In this study it was also suggested, that the reversal of the seesaw-like

movement may occur upon powerstroke. During powerstroke, there is a closure of the actin-binding cleft. This closure may somehow push the N-terminal of the relay, destabilizing the kinked conformation of the helix and rotating the converter back to a down-lever orientation. However, a direct communication pathway between the actin-binding region and the converter domain has not been revealed yet.

The majority of the crystal structures solved so far possess either an up or a down state of the lever. The converter can rotate its position by 60º, thereby rotating the lever too, as it is attached rather firmly to the converter. In the case of myosin II, this rotation creates a 10 nm change at the end of the lever, also referred to as *step size* of the myosin. The step size is proportional to the length of the myosin [108, 109], although different myosins can have different step sizes for the same length of the lever-arm [110]. The 'stepping'of the myosin, the powerstroke begins in a pre-powerstroke, up lever state, that is already bound to actin. Other crystal structures of squid [99] or myosin V [98] have been solved in the absence of nucleotides possessing a closed actin-binding cleft that resembles a closer state to the rigor, strong actin-binding actomyosin than the post-rigor state. Therefore, they are called *rigor-like* structures, and represent a better model for the end state of the powerstroke.

Rigor and Rigor-like Structures of Myosin

As there are no actomyosin crystal structures to date, neither the initial nor the end-state myosin structures of the powerstroke are known (before and after step 4 of the Lymn-Taylor cycle). Thus, other methods, e.g. electron microscopic data must also be taken into account in actomyosin structural studies. Rigor actomyosin can be generated by incubating actin filaments with isolated myosin motor domains/S1 without ATP, known as *decorated actin*. Cryo-electron microscopic image analysis of the decorated actin provides a model system to study the strong actin-binding state of myosin. Though, these data are limited in resolution (8-12 Å) and can be better interpreted if combined with high-resolution crystal structures of the actin-unbound myosin. X-ray structures of myosin and actin can be fit *in silico* into the three dimensional reconstruction of the electron density map (EM map) of the decorated actin filaments obtained from cryo-electron microscopy (**Figure 13.**). As a result, the upper 50 kDa domain of several fitted myosin crystal structures protruded out from the EM map, and serious torsions of the structures had to be applied for the best fit into the envelope [92, 93, 111]. All of these crystal structures represented weak actin-binding myosin states, with open actin-binding clefts. The first myosin crystal structure with the actin-binding region perfectly fitting into the EM map of decorated actin, was a myosin V nucleotide-free crossbridge [112]. It had a closed actin-

binding cleft, suggesting a strong actin-binding state. This led to the discovery of the third group of myosin crystals, the *rigor-like* structures e.g. chicken myosin Va (1OE9), squid myosin II (2OVK, 3I5G) or *Dictyostelium* myosin IE (1LKX) and [98, 99, 113], resembling the rigor state (**Figures 13 and 14**.).
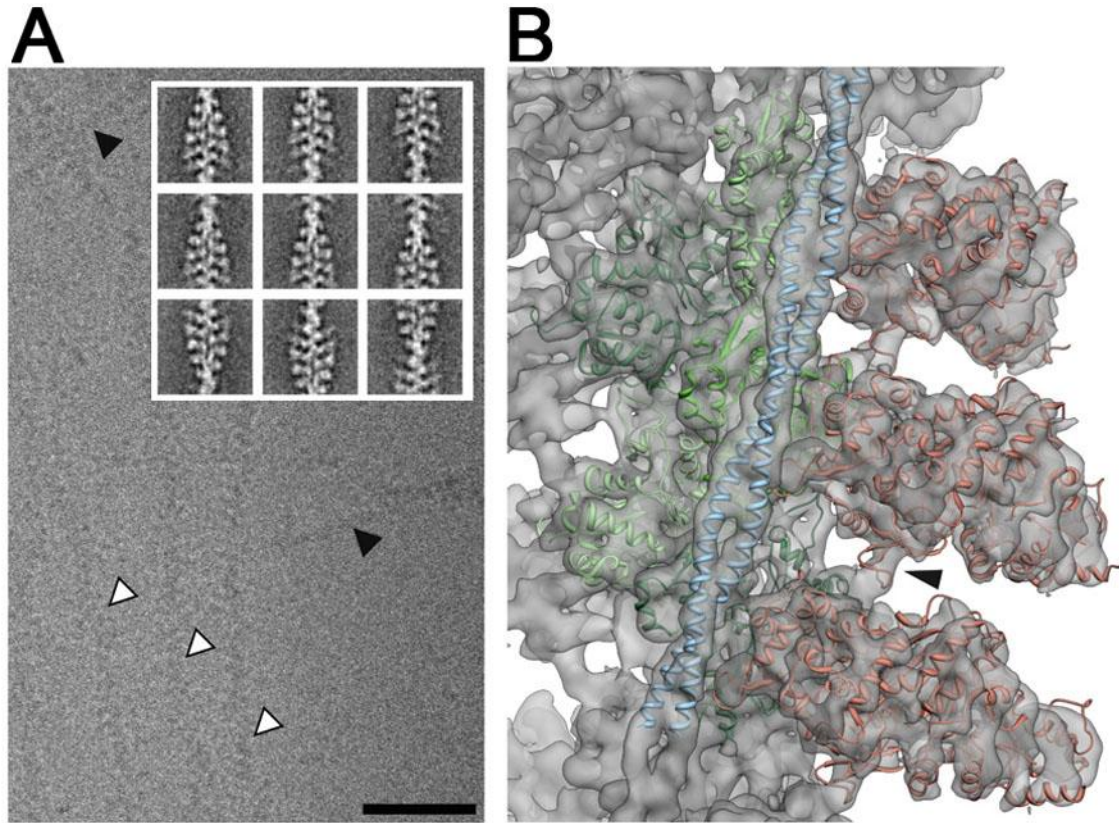

Figure 13. Fitting crystal structures into the EM map of decorated actin filaments. (A)Unprocessed electron micrographic image of F-actin. Decorated actin filaments are marked with white arrowheads, while undecorated filaments are marked by black arrowheads. Scalebar: 50 nm. Inset: average images of decorated actin filaments. **(B) Fits of atomic structures into the electron density map of the decorated actin.** Crystal structure of myosin IE in rigor-like state (PDB code:1LKX) and models of actin and tropomyosin are red, green and blue, respectively. Scalebar: 5 nm. The figure is based on a recently published paper, which reports the highest EM resolution obtained from decorated actin filaments so far, 8 Å [117].

Interestingly, the rigor-like conformation is accessible to a variety of myosin classes, even in the absence of actin. Most strikingly, compared to the previously described post-rigor or pre-powerstroke states, the rigor-like structures – as already mentioned − have a closed actin-binding cleft (**Figure 14.**). The cleft closure is carried out by the movement of the upper 50 kDa domain relative to the N-terminal subdomain. The movement of the upper 50 kDa domain is accompanied with switch I moving away from the γPi, thereby opening the nucleotide-binding pocket. Furthermore, the central β-sheet is twisted[1], associated with the

---

[1] We should note, that the twisted form of the β-sheet is the relaxed, unstrained form, as powerstroke is the relaxation of a 'primed' structure. Thus, 'untwisting' the β-sheet needs energy input, from the binding of ATP.

opening of switch II and a large movement in P-loop as well. Partial closure of the actin-binding cleft and a similar twist of the β-sheet could also be seen in the nucleotide-free structure of a *Dictyostelium* myosin II (1Q5G) [114], for this reason it can be placed rather among the rigor-like structures than anywhere else, but usually it is referred to as an apo structure. The rigor-like structure has a straight relay helix and a down-lever conformation. The orientation of the lower 50 kDa subdomain is similar to that of the pre-powerstroke state.
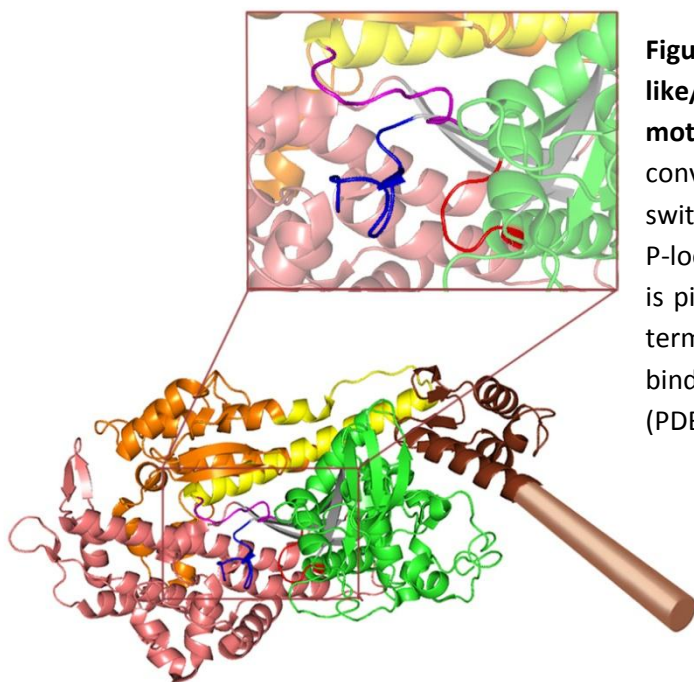
Figure 14. The nucleotide-free rigor-like/apo state of *Dictyostelium* myosin II motor domain. The lever and the converter are brown, the relay is yellow, switch II loop is magenta, switch I is blue, P-loop is red, β-sheet is gray, upper 50 kDa is pink, lower 50 kDa is orange and the N-terminal domain is green. The nucleotide binding pocket is enlarged in the inset. (PDB code: 1Q5G)

Structural features of pre-powerstroke, post-rigor and rigor-like structures are summarized in **Table 1**.

element state	switch I	switch II	P-loop	β-sheet	actin-binding cleft	relay helix	converter /lever
post-rigor (M.ATP)	*closed*	*open*	*down*	*untwisted*	*open*	*straight*	*down*
pre-powerstroke (M.ADP.Pi)	*closed*	*closed₁*	*down*	*untwisted*	*open*	*kinked*	*up*
rigor-like (M_apo)	*open*	*closed₂/open*	*up*	*twisted*	*closed*	*straight*	*down*

Table 1. Positions of the main flexible elements of myosin in its different structural states. Closed₁ and closed₂ are different closed conformations of switch II. The type of nucleotide bound to myosin in the different states is indicated in parentheses. Apo state of myosin (M_apo) does not bound any nucleotides.

The Actomyosin Interface

Flexible fitting of myosin and G-actin crystal structures into the EM map of decorated actin filaments is used to create atomic structural models of the rigor actomyosin complex. The

first three-dimensional atomic model of rigor actomyosin was presented by Schroder *et al* [115]. Recently, further atomic structural models of the rigor actomyosin complex have been presented based on high resolution electron microscopy [111, 116-118]. By analyzing the actomyosin interface derived from these models, it was seen that two actin monomers interact with the upper and lower 50 kDa subdomains of myosin [116, 119] (**Figure 15**.). Kinetic analysis of myosins carrying mutations in these regions also helped to identify specific loops that are involved in actin-binding. It was revealed that loops in the lower subdomain (loop 3, H-loop, helix-loop-helix motif, parts of loop 2) interact with actin both in weak and strong actin-binding states [120-122], whereas the upper subdomain (cardiomyopathy or CM loop, loop 4, parts of loop 2) creates interactions mainly in the strong actin-binding state [123-125]. Three actin monomers are sufficient to create rigor actomyosin models: the first (AC1) and the third (AC3) actin form secondary interactions with myosin, and the second actin (AC2) positions the other two actin monomers. Recent models involve five actin monomers as well [116].
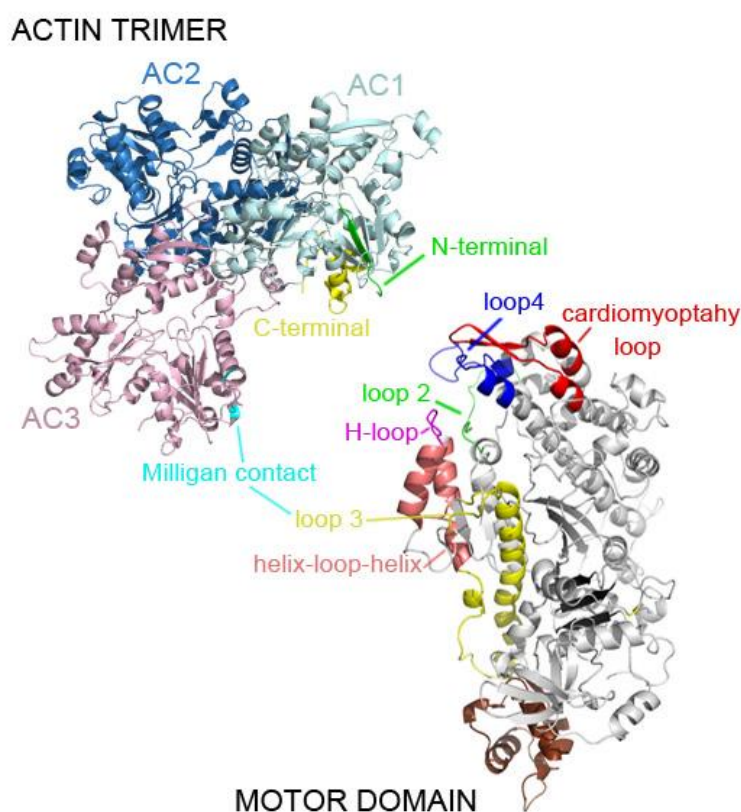
Figure 15. The actomyosin binding elements. The myosin-binding sites of a model of the actin trimer (AC1, AC2, AC3) [98] and the actin-binding sites of *Dictyostelium* motor domain (PDB code:1VOM) are highlighted. The relay and the converter are also indicated with yellow and brown, respectively.

AC3 helps to stabilize the forming interactions between AC1 and myosin by creating mainly H-bond interactions with loop 3 of myosin. This interaction is named the Milligan contact [126]. *In silico* docking of myosin and actin crystal structures indicate, that loop 2, and areas of the lower 50 kDa, the helix-loop-helix motif including H-loop initiate several electrostatic interactions with the N-terminal region of AC1 in weak actin-binding of myosin [127]. The

binding area of the helix-loop-helix motif is extended by hydrophobic interactions (through a hydrophobic triplet and a proline-rich loop) with AC1, while loop 2 forms new salt bridge interactions with the C-terminal of actin as well [127]. It was proposed, that these interactions, together with the initial actin-binding of CM loop, are essential for the weak-to-strong actin-binding transition of myosin. As actin-binding strengthens, loop 4 and the CM loop also create electrostatic and hydrophobic interactions mainly with the C-terminal regions of AC1 [111, 116, 117]. Main actomyosin interactions revealed from structural models of rigor actomyosin complexes [111, 116] are summarized in **Table 2**.
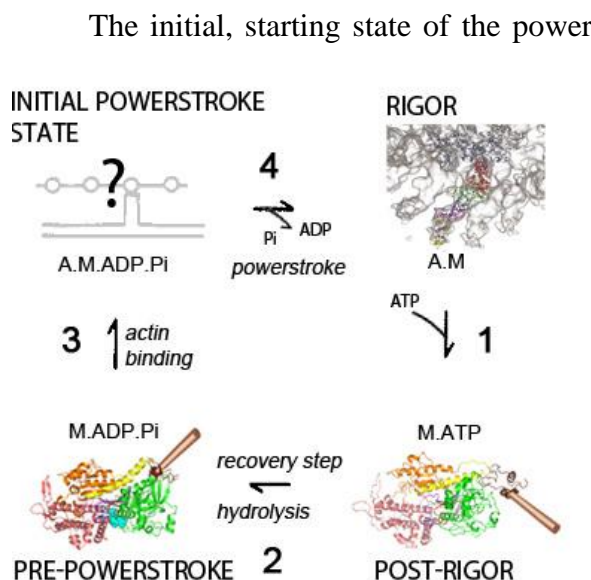
upper 50 kDa subdomain			*lower 50 kDa subdomain*		
Loop 2 – AC1	Loop 4 – AC1	CM loop – AC1	H-L-H – AC1	H-loop – AC1	Loop 3 – AC3
Glu629 – Arg28 /Asp24 Lys640 – Asp25 Lys642 – Glu334 Gly635 – Asp24 Lys637 – Gly23 /Ser348 Gly638 – Gly23 Lys642 – Glu334 Gly643 – Ser145	Arg371 – Asp311 /Lys328 /Gln314 /Ile329 Glu372 – Lys328 /Arg335 Glu373 – Arg147 Arg371 –	Asn410 – Tyr337 /Arg28 Glu411 – Lys336	Pro529 – Thr351	Lys544 – Glu167 **H-loop – AC3** Asn552 – Lys50 Lys553 – Gly46 /Gly48 Ser549 – Gln49	Glu576 – Arg95 /Lys50 Lys569 – Glu99 Pro570 – Arg95 Ala575 – Arg95 Lys572 – Arg95 Ala571 – Tyr91

Table 2. Myosin–actin interactions in strong-binding actomyosin state. The interacting residues (chicken skeletal myosin numbering) are determined by analyzing the actomyosin interacting surface of rigor actomyosin models created based on electron-micrography. H-L-H is helix-loop-helix motif of myosin. In strong-binding actomyosin, both the upper and lower 50 kDa subdomains form H-bond or electrostatic interactions with actin.

The CM loop, besides interacting with actin, also creates an intramolecular salt bridge with loop 2. Mutating this amino acid (R403Q) results in severe hypertrophic cardiomyopathy, reducing myosin's actin activated ATPase and actin binding affinity [128]. It seems that the function of the interaction of CM loop with loop 2 is to stabilize the conformation of the CM loop. Further mutations of ionic or hydrophobic actin-binding surface loops resulted in reduced ATPase activities of the constructs, affecting weak and/or strong actin-binding affinities of myosin [120, 122, 129]. Mutations in the CM loop, loop 2 and a hydrophobic triplet in the helix-loop-helix region also resulted in reduced actin activated ATPase activity of chicken HMM, hindering the motility of the constructs as well [121]. As a conclusion of these experiments, it has been stated that actin activation and motility are coupled, and are related to the closure of the actin-binding cleft. However, there is experimental evidence disproving this idea, in which actin activated ATPase is decoupled from motility [130]. In these experiments, the negatively charged N-terminal residues of actin were either neutralized or deleted. The activation of S1 ATPase with the mutant actins was very low. On the other hand, at low ionic strength S1 could move mutant actin filaments with similar velocities to that of the wild type. In actomyosin covalent cross-linking studies, two myosin regions are found to interact with the

N-terminal segment of actin, one of which is identified to be loop 2, whereas the second interacting myosin region remained ambiguous [131, 132].

Coupling of the Conformational Changes of the Nucleotide-binding site, Actin-binding Cleft and Relay Region during Powerstroke

The initial, starting state of the powerstroke, which is an up lever, M.ADP.Pi weakly binding to actin, is challenging to determine experimentally. It has a low proportion and a very short lifetime in equilibrium and steady-state systems, respectively. So far, we have very limited structural information on this state (**Figure 16.**). Its structure is only guessed by an extrapolation of the features of the adjoining structures, or experiments based on detecting signals on a transient kinetic scale. Additionally, the EM-based rigor structural models are also only attempts to approach the structure of the rigor complex (**Figure 16**). Although rigor actomyosin models are considered as the end states of the powerstroke, they cannot represent such state, since powerstroke ends in a nucleotide-bound state (A.M.ADP)[2].

Figure 16. Structural states of the Lymn-Taylor cycle – rigor and the initial state of the powerstroke. EM-based strong-binding actomyosin structural models using rigor-like myosin states may represent the rigor state in the Lymn-Taylor model. The structure of the actin-bound pre-powerstroke myosin state, which is the initial state of the powerstroke is unrevealed. EM map of actin is transparent grey.

When superimposing the pre-powerstroke state on the rigor-like structure, a model of the events of powerstroke can be generated. It is seen, that there are three main events happening between pre-powerstroke and rigor-like states, which must be harmonized after the binding of actin: the up-to-down lever swing, the actin-binding cleft closure and the release of the hydrolyzed products.

A model of the powerstroke has been suggested by combining several structural data of rigor-like and pre-powerstroke crystal structures (**Figure 17.**) [118]. We have seen that in the

---

[2] A further down lever movement coupled with ADP release has been revealed in brush border myosin I and smooth muscle myosin that may also be considered as a second part of the powerstroke [133.   Jontes, J.D., E.M. Wilson-Kubalek, and R.A. Milligan, *A 32 degree tail swing in brush border myosin I on ADP release.* Nature, 1995. **378**(6558): p. 751-3.] [134. Whittaker, M., et al., *A 35-A movement of smooth muscle myosin on ADP release.* Nature, 1995. **378**(6558): p. 748-51.].

recovery stroke, switch II closure was accompanied by the kinking of the relay helix, thereby priming the lever to the up position. A presumption has been made, that pre-powerstroke-state myosin binding to actin reverses this process, and removes the kink of the relay, so the lever can relax, and rotate back 60° to its down position. This could be accomplished by the opening of switch II. However, these authors stated that the rigor-like structure (looking at nucleotide-free myosin V) has a switch II in different, but still near-closed conformation compared to the closed switch II of the pre-powerstroke state. They suggest that, as the rigor-like myosin has a twisted β-sheet, the strain can be released from the relay by bending the β-sheet and leaving switch II in a closed conformation, causing its small repositioning towards the P-loop. Thereby, the coupling of the conformational movements of switch II with the relay/converter movements might be different in actin-attached powerstroke and actin-detached recovery stroke states. It turned out, that the unusual association of switch II to P-loop is unique for myosin V, caused by a steric hindrance of a large Tyr residue in switch II [99, 135]. By contrast, myosin II or VI have small residues in this position (Ala, Ser) creating no such steric effect on switch II loop. In these classes, it seems that the torsion of the β-sheet does open the switch II loop, which movement is strongly coupled to the up-to-down lever swing.

The second aspect of powerstroke is the closure of the actin-binding cleft. Closing the actin-binding cleft opens switch I which opens the nucleotide-binding pocket. According to crystal structures and fluorescence kinetic studies, switch I movements seem to be important in the strong negative linkage of myosin binding to actin and nucleotides, having an allosteric route that links the different nucleotide states of myosin to their different extent of actin affinities. ADP-bound or nucleotide-free myosin, where the open-closed transition of switch I is pushed rather to the open form, myosin binds actin strongly [136]. The binding of ATP to rigor actomyosin reduces this strong affinity of myosin to actin, rapidly dissociating the actomyosin complex, as the post-rigor state of myosin is formed. As switch I closes, the affinity of myosin to ATP increases. A myosin state, where the γPi site is occupied (ATP, ADP.Pi or their analogues) has the equilibrium of the open-closed transition of switch I pushed towards the closed conformation. Such closed switch I conformation of myosin have a weak actin-binding affinity [136]. The rebinding of myosin to actin with the hydrolysis products in its nucleotide-binding pocket reduces the affinity to the hydrolyzed products, leading to Pi dissociation first, then ADP release from myosin. This is possible, because actin-binding causes the opening of switch I (or switch I opening is coupled to the closure of the actin-binding cleft) [94, 95, 136]. Regarding the extent and location of the actin-binding cleft closure, differences occur among the rigor-like structures. In the case of myosin V, the outer cleft is tightly closed, supported by a network of H-bonds and salt bridges running along the two sides of the strut.

The strut is a semi-flexible connection between the upper and lower 50 kDa subdomains, whose variable positions are associated with the different extent of the closure of the outer cleft. In the case of *Dictyostelium* myosin II, the outer cleft is rather open, as the salt bridges are partially broken of the strut region.
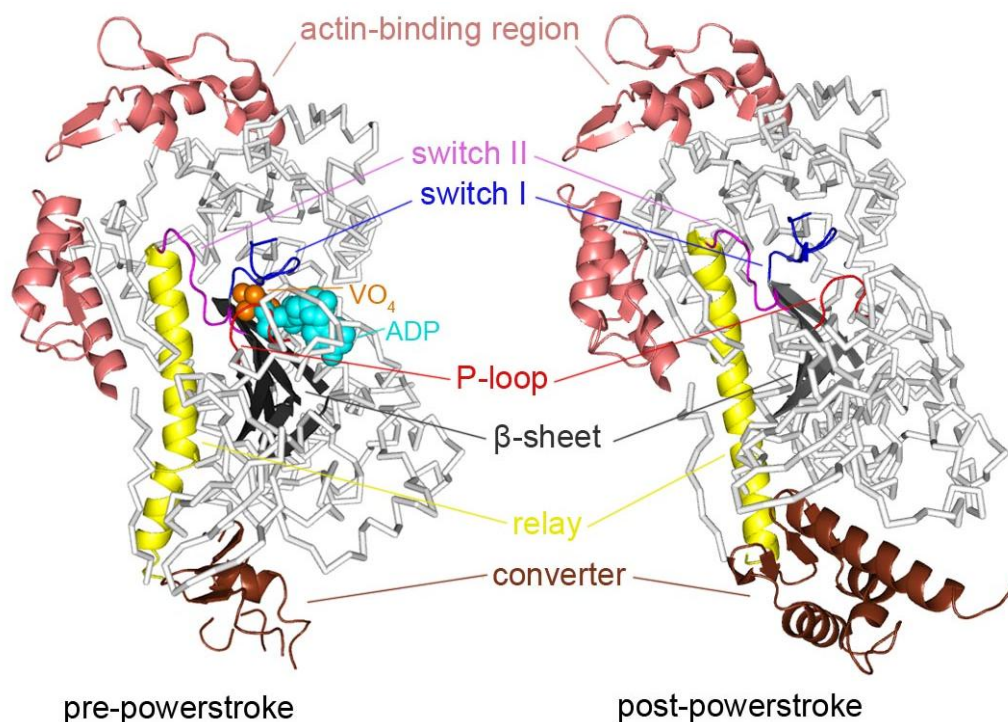
Figure 17. Structural movements of myosin during powerstroke. The up-lever, M.ADP.Pi weak actin-binding state is used to mimic the initial state of the powerstroke (pre-powerstroke), whereas the down-lever , strong actin-binding rigor-like state mimics the end state of the powerstroke (post-powerstroke). The main structural differences between the two myosin states (gray, ribbon representation) are highlighted with colors and cartoon representation. The actin-binding cleft sorrounded by the actin-binding region closes (pink), while switch I opens (blue), P-loop moves to an up position (red) and switch II repositions (magenta). The changes in the nucleotide-binding pocket are coupled to the twisting of the β-sheet (dark gray) and the straightening of the relay helix (yellow). The movement of the relay is accompanied with the movement of the converter (brown), resulting in the up-to-down lever swing (PDB codes: 1VOM, pre-powerstroke; 1Q5G, rigor-like)

Pi can only 'escape' from the nucleotide-binding pocket through an alternative route, different from entering into it, as ADP blocks its way through the 'front door'. A *backdoor mechanism* was proposed for the release of Pi, speculating the escape route through a rear opening situated in the tube of the actin-binding cleft [137]. According to molecular dynamic simulations, Pi release into the actin-binding cleft can alter the affinity of myosin to actin by inducing conformational changes in myosin, thus strengthening its actin-binding [138]. According to these simulations, it is more likely though, that the opening of switch I breaks its

salt bridge interactions with other residues in the pocket, forming a 'trapdoor', through which Pi can be released.

Another remarkable effect is that the P-loop moves upwards, destroying the nucleotide-binding pocket, and as structurally being linked with the β-sheet, creates a twist at the distal part of it. If the closure of the actin-binding cleft leads to the mandatory twisting of the β-sheet, then the binding of actin is the initiator of the powerstroke. There is no explanation though, for the closure of the cleft, or how the products are released. There are fluorescence-based transient kinetic experiments providing evidence, that cleft movement is coupled to actin and nucleotide binding [95], but the pathway of communication is unrevealed.

What structural changes are induced in myosin by the initial actin binding? What is the key, or is there a key element in myosin that initiates the powerstroke at the beginning of actin binding? These questions arise every time, when a model is being proposed for the powerstroke. There are many atomic structural models of the rigor actomyosin complex, but there is none of the pre-powerstroke state– actin complex, which is the real initial state of the powerstroke. As lacking such structure, every model of the powerstroke assume that actin-binding does not influence the structure of myosin before powerstroke takes place.

Although, the three-dimensional atomic structures of different states of myosin are crucial to understand the actomyosin cycle, they represent static points in the dynamic process of the myosin enzyme cycle. The comparison of the structures does not give indications for the sequence of events. Therefore, kinetic measurements are a great help to reveal yet unidentified structural states, detect the sequence of events and correlate existing crystal structures to appropriate states of the actomyosin cycle.

Kinetic Insights into the Myosin's ATPase Cycle on a Transient Scale

The Enzyme Cycle of Myosin in the Absence of Actin

Interestingly, the first detailed kinetic model of mysoin's ATPase in the absence of actin was presented without any knowledge of the mysoin atomic structure. It was established few years after the publication of the Lymn-Taylor cycle by Bagshaw and Trentham [139, 140]. They used the intrinsic tryptophan (Trp) fluorescence of rabbit skeletal muscle myosin II S1, as a sensor of the conformational changes that occur during its ATPase (**Scheme 1A**), which phenomena was previously shown by Werber *et al* [141]. In the aim of combining existing atomic structural states to the kinetic cycle of myosin and reveal states, that cannot be crystallized due to their rare appearance within the cycle, the idea of the intrinsic fluorescence

method was further developed [142, 143]. Based on the atomic structure of *Dictyostelium* myosin II motor domain (further referred to as *Dd* MD), site-specific single Trp mutant constructs were produced. To obtain a better signal-to-noise ratio, the original Trp residues of the motor domain were mutated to Phe amino acids, only one Trp was kept at a position that detects lever arm movement (named W501+, *Dictyostelium* numbering). Inserting a single Trp amino acid at specific regions of a Trp-less motor domain enables to detect structural changes occurring at that specific region of the molecule, as Trp is extremely sensitive to conformational changes occurring in its surrounding. Furthermore, the fluorescence of Trp can be detected independently from other fluorescent residues (Tyr, Phe). It was an important criterion, that the insertion of site-specific fluorophores into the motor domain should not affect its enzyme-kinetic features, in order to interpret the results directly by comparing them to the wild type enzyme. Using the single-Trp construct W501+ *Dd* MD, the Bagshaw-Trentham kinetic scheme was refined (**Scheme 1B**) [142, 143].

Scheme 1. The ATPase cycle of the myosin head in the absence of actin. (A)The Bagshaw-Trentham kinetic scheme of myosin ATPAse. The different conformational states of myosin rabbit S1 in the cycle can be distinguished by their enhanced (one asterisk) or further enhanced (two asterisks) intrinsic fluorescence compared to the apo myosin state. K is the equilibrium constant of the reaction step. **(B) The extended Bagshaw-Trentham model.** K is the equilibrium constant of the reaction step. The relative magnitude of the on and off rate constants are indicated by the length of the upper and lower arrows, respectively. W501+ *Dd* MD states possessing lower or higher fluorescence intensities than the apo state myosin are marked with daggar and star symbols, respectively. The structural names for a given state are indicated in parenthesis.

The ATPase cycle of myosin is a complex reaction, including several steps. The binding of ATP to myosin is a two-step process: after the formation of the collision complex (1) there is a

conformational transition of M.ATP (2). This second step is practically irreversible, which results in a very strong binding of ATP to myosin. This conformational change is accompanied by a Trp fluorescence enhancement (M*) in the case of rabbit skeletal muscle S1, while the fluorescence of the site-specific Trp in *Dictyostelium* decreases (M†)[3]. After this, ATP hydrolysis occurs (3), resulting in a further enhanced fluorescent state of myosin (M**) in the Bagshaw-Trentham scheme. ATP hydrolysis is much slower than the steps before, accompanied by a small free energy change, being a freely reversible step, in contrast to step 2, which is irreversible with a high free energy decrease. In the Bagshaw-Trentham scheme a large conformational change was proposed within step 3, which corresponds to the 'priming' of myosin (also presented in step 2 of the Lymn-Taylor cycle). This conformational change was separated from the hydrolysis step in the modified Bagshaw-Trentham scheme by using the W501+ *Dd* MD construct (Scheme 1B, steps 3a and 3b), which provided a much more sensitive and specific detection of the enzymatic steps compared to those of detected by rabbit S1. This was the first experimental evidence, that the priming of myosin (K_{3a}, recovery step) precedes the hydrolysis (K_{3b}). The conformational change in the recovery step is also accompanied by the open-closed transition of switch II. As both 3a and 3b steps are reversible, they confirm the reversibility of step 3 of the Bagshaw-Trentham model as well. The priming of myosin lever is relaxed by the *reverse recovery step* (K4), the actin-unbound up-to-down lever swing, and the sequential dissociation of the products (steps 4, 5, 6, 7). In the presence of actin, the relaxation of the lever is coupled to an actin-bound lever swing, resulting in sarcomere contraction (step 4 in the Lymn-Taylor cycle). Due to the much weaker binding of the hydrolysis products to myosin than ATP to myosin (e.g. in *Dd* MD: K_d,ADP=5-10 µM, K_d,Pi=10-50 mM, K_d,ATP=0,5-1 µM), the cycle is driven by the difference in the free energy between the different myosin-nucleotide complexes, and not the ATP hydrolysis step itself. This phenomenon is true for all ATPase motors.

Recent work of our research group showed that the rate-limiting step of the myosin II enzyme cycle in the absence of actin is the reverse recovery step [145] (step 4 of Scheme 1B). It was demonstrated, that Pi release and ADP release steps are several orders of magnitude faster than the rate-limiting reverse recovery step. Additionally, reverse recovery step occurs in M.ADP.Pi state, before the dissociation of Pi that is only possible from the down lever state of

---

[3] Nucleotide-binding (both ATP and ADP) on a transient scale induces an initial fluorescence quenching of W501 in *Dictyostelium*, whereas the fluorescence increase of rabbit S1 upon nucleotide binding is due to the fluorescence increase of W113 and W131 located at the entrance of its nucleotide-binding pocket, which tryptophans are not present in *Dictyostelium* at all [144.   Malnasi-Csizmadia, A., et al., *The dynamics of the relay loop tryptophan residue in the Dictyostelium myosin motor domain and the origin of spectroscopic signals.* J Biol Chem, 2001. **276**(22): p. 19483-90.].

myosin. Thus, in steady-state conditions and in the absence of actin, myosin is populated in the up lever, M.ADP.Pi pre-powerstroke state.

How Does Actin Activation Occur?

As the rate-limiting step of the enzyme cycle is the reverse recovery step in the absence of actin, actin activation is the acceleration of this up-to-down conformational change [145]. As the slowest step of the cycle (k_4=0.05 s^{-1}), it determines the overall basal steady-state cycling of myosin ($k_{basal=}$0.05 s^{-1}) in the absence of actin (**Scheme 2**). Previous studies showed that actin-binding causes relatively small changes in the rate constants of the ligand binding/dissociation (including ATP, ADP and Pi) and the recovery step [145, 146]. Thus, the largest effect of actin-binding is on the rate-limiting up-to-down lever swing, accelerating it by almost two orders of magnitude (k_4'>~5 s^{-1})[4], until another step of the enzyme cycle becomes the rate-limiting step, determining the actin activated ATPase activity of myosin ($k_{activated}$~5 s^{-1}). In some myosin isoforms, the rate-limiting step in the presence of actin has been determined to be the ADP release[5] from the actomyosin complex [28, 135, 148]. If we assume that the rate constant of the reversal of the reverse recovery stroke (k_{-4}) and the reversal of the powerstroke (k_{-4}') are equal (k_{-4}= k_{-4}'=0.15 s^{-1}), then the equilibrium constant for the lever arm movement increases from K_4=0.33 (K_4=k_4/k_{-4}=0.33) to K4'=25 upon actin activation. This represents a $\Delta\Delta G^o$=11 KJ/mol difference in free energy change (from $\Delta G^0_{reverse\ recovery}$=2.7 KJ/mol to $\Delta G^0_{powerstroke}$= -8 KJ/mol)[6], meaning that actin pushes the equilibrium towards the down-lever, post-powerstroke conformation (A.M†ADP.Pi). This free energy change is paid for the strengthening of actin-binding of myosin, as the actomyosin dissociation constant from the initial pre-powerstroke state (A.M*ADP.Pi, K_d=57 μM) decreases to K_d=0.7 μM after the lever swing, to K_d=0.12 μM after Pi release and to K_d=0.03 μM after ADP release steps [145]. As actin-binding strengthens, it pulls the reaction through the weak actin-binding state, so the main flux of the reaction is through the actin-attached states of myosin, even at low concentrations of actin.

---

[4] depending on salt concentration

[5] Fiber studies also demonstrated, that ADP release is the rate-limiting step under isometric conditions, although reducing the strain and allowing the fibers to shorten makes the Pi release step the rate-limiting step of contraction (147.   Dantzig, J.A., et al., *Reversal of the cross-bridge force-generating transition by photogeneration of phosphate in rabbit psoas muscle fibres.* J Physiol, 1992. **451**: p. 247-78.)

[6] Calculated on the basis of ΔG^o=-RTlnK.
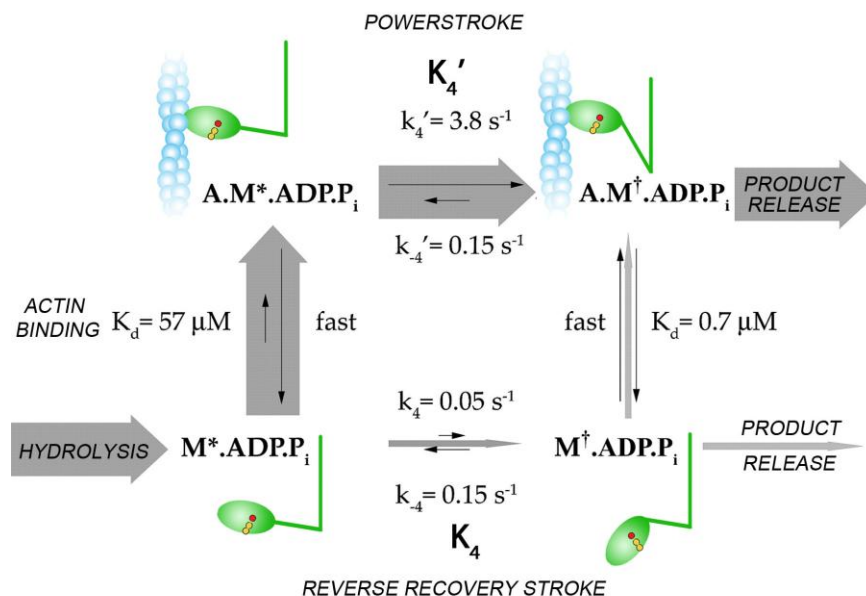
Scheme 2. Actin activation of myosin . Different *Dictyostelium* W501+MD states of the cycle possessing lower or higher fluorescence intensities than the apo state myosin are marked with daggar and star symbols, respectively. The value of k_{-4}' is based on the thermodynamic requirements. The route of the flux of the reaction is indicated by the width of the gray arrows. The relative value of the on and off rate constants are indicated by the length of the thin black arrows. Figure was modified based on [145].

There is an argument in the field whether Pi release or the up-to-down lever swing occurs first within the event of powerstroke. In the above presented scheme, the up-to-down lever swing is preferred to happen first, which is followed by the release of the hydrolyzed products. Physiological studies have also demonstrated that tension generation precedes the Pi release [147, 149, 150]. Other interpretations indicate that the powerstroke might occur after Pi release [151, 152]. Furthermore, Scheme 2 also suggests, that force-generation can be initiated from a weak-actin binding state. The weak-to strong actin-binding transition does not necessarily precede the lever swing, but they might be concurrent processes. This idea was in contrast to previous studies that suggested the weak-to-strong actin-binding transition to be essential for force-generation [149, 153, 154]. Moreover, the weak actin-binding myosin states represent higher free energy states compared to the actin-detached states, which can also be utilized upon the powerstroke.

A recently published, elegant experimental work by Muretta *et al* indicates, that the up-to-down lever swing upon actin-binding precedes the Pi release in *Dictyostelium* myosin II [155]. They engineered two cysteines (Cys) into a Cys-less S1at specific positions and labeled them with FRET pairs to detect the bending of the relay helix. The straightening of the relay helix is coupled to the up-to-down swing of the lever during powerstroke. They demonstrate that actin-binding to the myosin.ADP.Pi complex straightens the relay helix before the

dissociation of phosphate, which they followed simultaneously. This actin-activated relay helix straightening is reversible, but phosphate irreversibly dissociates from the post-powerstroke state, preventing reversal of the powerstroke. Thus, relay helix straightening gates phosphate dissociation, whereas phosphate dissociation provides the thermodynamic driving force underlying force production.

Powerstroke, the Effective Route for Myosin

Kinetic pathway selection is used in cases when the system has to choose the efficient, though thermodynamically unfavorable route instead of the futile, non-efficient but thermodynamically favorable one (**Box 1**) [156].

Box 1. As recently described, biochemical reactions can happen through *thermodynamic* or *kinetic pathway selection* mechanisms [156]. Thermodynamic pathway selection occurs, when a reaction follows the lowest free energy path. The kinetic pathway can only be chosen in non-equilibrium conditions, where the flux through the lowest energy route is hindered kinetically to such an extent that another, kinetically much favorable (although thermodynamically not favorable) higher energy route opens instead (**Figure 18.**). Kinetic pathway selection is only possible, if the rate of the step before the hindered step is much greater (water flowing in on **Figure 18.**) than that of the hindered step (lower narrow outlet), populating the state before the hindered step (accumulation of water).
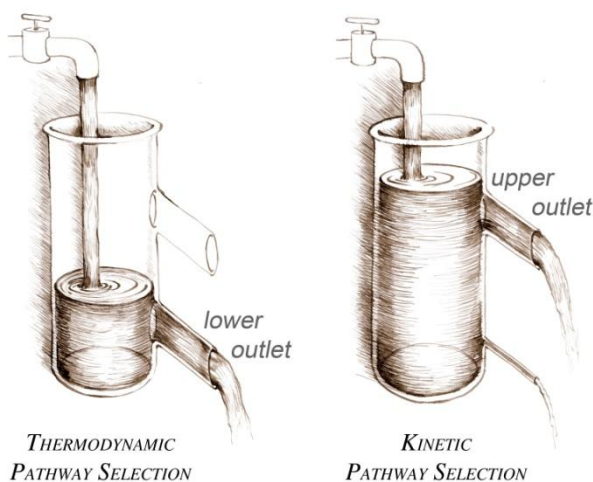
Figure 18. The two pathway selection mechanisms. In this water flow analogy, the heights of the water levels represent free energies and the widths of the outlets of the tank represent the magnitudes of the rate constants. If this outlet is wide enough, water flows through without accumulation (thermodynamic pathway selection). If the outlet is small compared to the amount of water flowing in, water accumulates and 'escapes' through another, kinetically much favorable alternative route (kinetic pathway selection). Figure modified based on [156].

In actomyosin systems (**Figure 19.**), the reverse recovery step is the rate-limiting, hindered step of the cycle in the absence of actin. When actin is present, the accumulated up-lever weak actin-binding M.ADP.Pi population escapes through the higher energy-containing actomyosin complexes, because actin accelerates the hindered step. In this way, though actin

binding is thermodynamically unfavorable, the subsequent much faster powerstroke step (and the strengthening of actin-binding) pulls the flux of the reaction through the accelerated actin-attached pathway. This is the effective route of the system, the pathway when up-to-down lever movement occurs in the actin-attached myosin state. When myosin heads cycle through the actin-detached reverse recovery step, they create futile cycles. So, as described by Scheme 2, the binding and the concentration of actin determines the ratio of the effectively/futilely cycling myosins.

Figure 19. The actomyosin enzyme cycle. Powerstroke occurs through the actin-bound effective route, while unlikely reaction routes are indicated with faded colors. The magnitudes of the gray arrows refer to the flux of the reaction. The lengths of the black arrows represent the relative magnitude of the rate constants of that step of the enzyme cycle. The existing atomic structure of each state is in italics, except for the initial state of the powerstroke, of which structure we have no knowledge.

The mechanism, with which actin accelerates the lever swing also demonstrates that powerstroke is not the reversal of the recovery step. Although both the pre-recovery and pre-powerstroke states represent weak actin-binding states, recovery stroke occurs through actin detached, while powerstroke takes place through actin-attached myosin states. Actin does not bind to weak actin-binding pre-recovery states, because recovery stroke is a fast process, and actin has no effect on this step [146], therefore kinetic pathway selection mechanism does not exist here. Thus, the flux through actin attached recovery is not favorable. Furthermore, actin does not initiate binding to myosin states after the lever swing e.g. strong actin-binding down lever M.ADP – although M.ADP has a higher affinity for actin than up-lever M.ADP.Pi pre-powerstroke state – , because the flux through this state is also unfavorable and would lead to futile cycles.

The Parallel Powerstroke Pathways

As we have seen, effective force generation can only occur, if the myosin head is bound to actin while performing the up-to-down lever swing. However, there are more than one

possible pathways to create efficient powerstroke (**Figure 20.**) [156]. The different pathways determine different energetic profiles of the actomyosin system, influencing its mechanical performance that may have functional relevance in different myosins. Thus, it would be important to determine the kinetic fluxes of the parallel powerstroke pathways.

The events that lead to powerstroke are: actin-binding, actin-binding cleft closure and lever swing. Recent findings indicate that cleft closure and lever swing can occur while Pi is still bound to myosin (**Figure 20.**) [155].
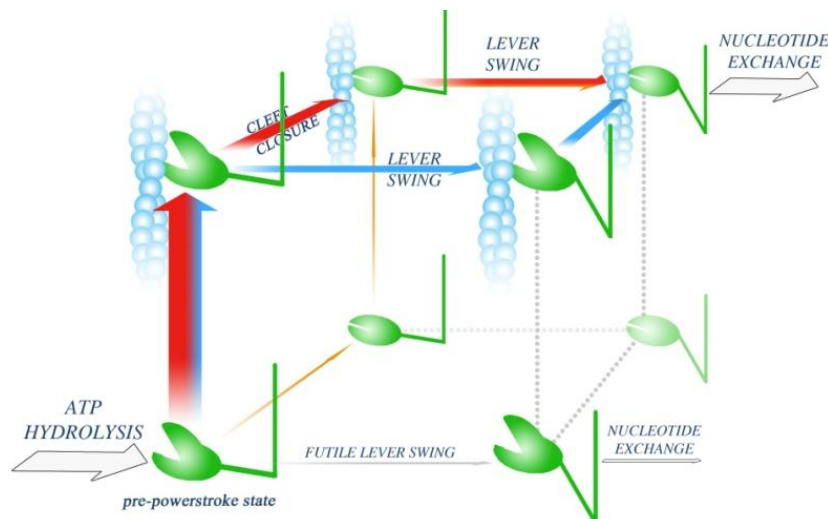
Figure 20. Parallel pathways within the actomyosin enzyme cycle – a mechanistic model of powerstroke. The effective lever swing pathways, which lead to powerstroke, thus force generation, are the orange, blue and red pathways. The futile pathway is indicated with thin grey arrow. The widths of the arrows represent the relative fluxes of the pathways. Figure modified based on [156].

After ATP binding and hydrolysis, we arrive to the weak actin-binding (but actin unbound), up lever M.ADP.Pi pre-powerstroke state. At this point of the enzyme cycle, there are three possible effective routes for myosin to follow, all of which involve actin-binding before lever swing (orange, blue and red pathways). The flux through the futile lever swing pathway (thin grey arrow) is prevented by the kinetic pathway selection mechanism.

On the orange pathway, the actin-binding cleft closes first then the strong actin-binding myosin state binds to actin, which is followed by the lever swing. However, the flux through this pathway is very low, because the first step, the open-closed transition of the actin-binding cleft in the actin-detached myosin state is kinetically very unfavorable in *Dictyostelium* myosin II (K<0,01), therefore hindered [136]. We note, that in other types of myosins (that have a larger equilibrium constant for the open-closed transition of the actin-binding cleft than *Dictyostelium* myosin II) this pathway might be more favorable.

The blue and the red pathways both start with the actin-binding of the prepowerstroke state. After this actin-binding either strengthens (cleft closes), followed by the lever swing (red arrows), or the lever swing occurs while myosin is still weakly bound to actin and the subsequent closure of the cleft stabilizes the powerstroke intermediate state (blue arrows). In

the latter case, cleft closure must be faster than actin detachment from the down-lever but still weak actin-binding myosin state [157]. Nevertheless, both blue and red pathways convey considerable fluxes according to available kinetic and thermodynamic data [145, 150]. This demonstrates that powerstroke events probably proceed through parallel pathways. We should note, that the flux of theses pathways were analyzed without having any external load on the lever of the myosin heads. It is possible, that external load influences the relative fluxes of the powerstroke pathways compared to each other.

This mechanistic model also suggests, that the ratio of the futile and the productive powerstroke pathways is regulated by the allosteric activation of the lever swing by actin. However, motility and contraction can still occur in the absence of actin activation, driven by occasional strokes of actin-bound myosin heads. This effect was demonstrated by Miller *et al*, where actin mutants that could not activate myosin ATPase activity were still motile in *in vitro* motility assays [130]. In summary, the model suggests that at low actin activation, most myosins hydrolyze ATP without effective lever swings (low ratio of effective cycle/hydrolyzed ATP), whereas at high actin activation, most myosins are channeled to the effective powerstroke pathways (high ratio of effective cycle/hydrolyzed ATP). Consequently, low actin activation in a muscle would result in low productivity, hence mechanical weakness of contraction of the muscle.

An Experimentally Discovered State of the Parallel Powerstroke Pathways

Blebbistatin is widely used in myosin research, as the only available myosin II specific small-molecule inhibitor [158-161]. Blebbistatin blocks myosin in a weak actin-binding state, slowing down Pi release from the M.ADP.Pi complex. The atomic structure of the M.ADP.VO$_4^{3-}$.blebbistatin complex resembles a well characterized state of the chemomechanical cycle of actomyosin: the up-lever, post-hydrolytic weak actin-binding pre-powerstroke state of myosin [162]. In contrast, it was demonstrated recently that in the presence of ADP, blebbistatin induces a structure of myosin with closed switch II, up-lever orientation but the switch 1 closed-open equilibrium pushed towards the open state with high actin-binding affinity [163]. This state might resemble a previously inaccessible state of the powerstroke, where actin-binding cleft closure has already taken place, but lever swing has not yet occurred. The authors emphasized the structure to resemble a strongly actin-bound state, with up-lever conformation, which they called the 'start-of-powerstroke' state (**Figure 21.**), although the structure was obtained in the absence of actin. This start-of-powerstroke state is difficult to characterize due to its low abundance and short lifetime in the working cycle of
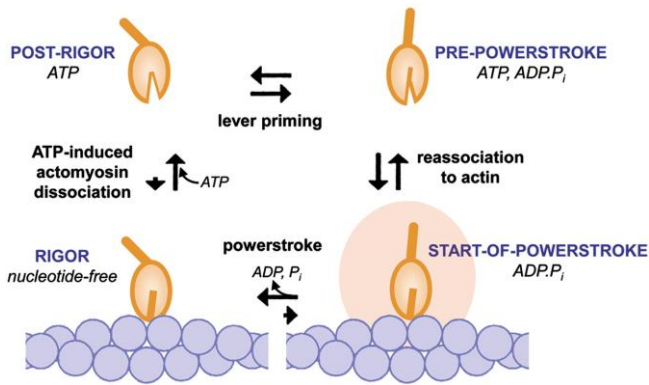
Figure 21. M.ADP.Bleb resembling the start-of-powerstroke state [163].

myosin. This structure in fact exists in the modified mechanistic model of the parallel powerstroke pathways, as a strong actin-binding (possessing a closed actin-binding cleft but not actin-bound), up-lever myosin state (**Figure 22**). This intermediate state of the parallel powerstroke pathways, with its yet unrevealed atomic structure, can be important in the understanding of the events of the powerstroke, and may further support the mechanistic model of myosin's enzymatic cycle.
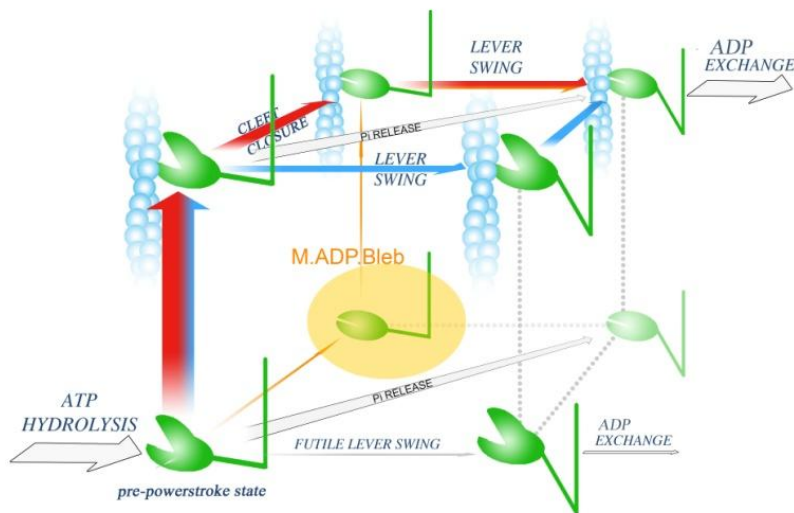
Figure 22. The experimentally detected strong actin-binding, up-lever state state of myosin. The blebbistatin-bound myosin structure in the presence of ADP (M.ADP.Bleb) resembles a state where actin-binding cleft closure has already occurred, but lever swing has not yet taken place (orange). This is a very low populated state of the cycle with low blebbistatin affinity to the M.ADP complex as well. Figure modified based on [156].

General Aspects of Activation of Motor Proteins

Besides the different routes of the sequence of events occurring during powerstroke, we have limited knowledge of the molecular mechanism of actin activation. What are the structural details of actin activation that influence the mechanical performance of the actomyosin systems? The importance of such question extends muscle function, as the activation of various NTPases exerting motor and signaling functions (e.g. microtubule based kinesins, GEFs and G protein, kinase-scaffold complexes) resemble similar activation mechanisms as described for actomyosin [164-167]. Besides the evolutionary conserved P-loop and switches of the nucleotide-binding site among P-loop NTPases, the core of the proteins diverged from a common ancestor, and functional specialization was enabled by later insertions to the core.

Allosteric activation was a common mechanistic principle applied during the evolution of these diverse enzymes [168]. Kinetic selection pathway mechanism is likely to be important in such systems as well, although specific modulations of the allosteric activation mechanisms determine the different functional properties of individual NTPases.

IV. Scientific Questions and Aims

The aim of this study is to reveal insights into the mechanism of actin activation of myosin. The rate limiting step of the myosin enzyme cycle in the absence of actin is the up-to-down lever swing i.e. the reverse recovery step, determining the basal steady-state ATPase activity of myosin. Actin accelerates the reverse recovery step, thereby enabling other steps of the myosin enzyme cycle to become rate-limiting in the presence of actin. As a result, myosin's steady-state ATPase activity increases by several orders of magnitude. Actin activation is carried out by actin binding weakly to myosin in its pre-powerstroke state, creating the initial powerstroke state of the myosin enzyme cycle. During powerstroke, which is the actin-attached up-to-down lever swing, actin-binding strengthens and Pi is released from the actomyosin complex. Actin activation channels myosin heads into the effective route of the myosin enzyme cycle by the kinetic selection pathway mechanism, leading through the powerstroke step. Although actin activation is a common mechanism among myosins, its structural background has been undiscovered, due to the lack of structural information of the initial, end or intermediate states of the powerstroke. Even the structural element of myosin specifically responsible for actin activation is unrevealed. Therefore, the following question have been raised:

Is there a key structural element in myosin responsible for its actin activation?

In spite of intense investigations of myosin by site-specific mutations, whether there is a structural element specifically responsible for actin activation has been unknown. All mutations of myosin affecting actin activation significantly influence other parameters of the myosin enzyme cycle as well, such as actin-binding or *in vitro* motility. The mechanistic model and kinetic pathway selection mechanism predicts that the lack of actin activation of myosin is not coupled to the abolishment of its *in vitro* motility. In fact, there are N-terminal mutants of actin that cannot activate myosin but retain *in vitro* motilities similar to wild type actin. There is a yet unidentified region of myosin interacting with actin N-terminal segment besides loop 2. Mutations in loop 2 affect actin activated ATPase activity of myosin − as they weaken actin-binding − and they also alter other parameters of the myosin ATPase cycle. Therefore loop 2 is not specific for the actin activation of myosin. The unidentified region of myosin interacting with actin N-terminal region may be a strong candidate for the specific actin activation of myosin. It leads us to a further question:

What are the myosin residues that interact with the N-terminal segment of actin?

We[7] examined the answers to these questions by conducting *in silico* and *in vitro* experiments. *In silico* preparation of myosin crystal structures and actin trimer models (extending actin structure with its N-terminal region), docking and molecular dynamic relaxation of the actomyosin complexes were carried out in order to identify the interacting myosin partner residues of actin N-terminal region. *In vitro* experiments were performed using recombinant *Dictyostelium discoideum* myosin II motor domain (*Dd* MD) and its site-specific mutants to verify the existence of interaction and examine its specific role in actin activation of myosin. Steady-state and transient kinetic properties of the wild type and mutant *Dd* MDs were investigated by applying fluorescence spectroscopy-based techniques e.g. stopped-flow and *in vitro* motility assays. In order to explore the role of myosin–actin N-terminus interaction in processive myosins, we investigated steady-state ATPase activities of *Mus musculus* myosin V S1 and its mutant, containing a mutation homolog to that of *Dictyostelium* myosin II.

What is the role of actin activation in vivo?

As no mutation has been identified to specifically affect actin activation until now, the lack of actin activation could not be examined solely *in vivo*. After identifying the structural element of myosin specifically responsible for the actin activation of myosin, we investigated the role of actin activation by applying transgenic *Caenorhabditis elegans* (*C. elegans*) strains, which contained wild type and mutant body-wall myosins and quantified the motile functions and force-generating capability of the animals.

What is the structure of the initial state of the powerstroke?

After investigating the role of actin activation *in vivo*, we were interested in the mechanism of actin activation, especially the structural rearrangements occurring upon actin-binding to myosin pre-powerstroke state. As the initial state of the powerstroke has a short life-time and low abundance in the enzymatic cycle of actomyosin, its structure is experimentally challenging to determine. Therefore, we created the actomyosin structural model of the initial state of the powerstroke by *in silico* docking and long-time molecular dynamic relaxations. We analyzed the structural changes that occurred upon actin-binding to myosin pre-powerstroke state.

---

[7] I intend to use plural for the presentation of this study, to honor the colleagues who I worked with or who contributed to this work in any aspects. All experiments have been carried out by myself unless otherwise stated.

What is the structure of M.ADP.Bleb complex?

With the knowledge of structures of different states of the powerstroke, the order of events and structural rearrangements happening within powerstroke could be mapped. The M.ADP.Bleb complex has been identified as the 'start-of-powerstroke' state, or rather an intermediate state of the parallel powerstroke pathways. As blebbistatin has a low affinity to the M.ADP complex, its crystallization has been hindered. Our aim was to covalently cross-link M.ADP and blebbistatin, thereby enabling the crystallization of the complex.

By revealing the structures of the initial state of the powerstroke or the M.ADP.Bleb complex, we will be one step closer to map the complex network of structural states within the parallel powerstroke pathways. Experimental identification of the structural element responsible for actin activation enables us to focus the *in silico* analysis of the structural changes occurring in myosin upon actin-binding around the identified actin-binding region, as well as discover the communication pathways from the actin-binding site to the nucleotide-binding pocket and relay/converter region.

V. Results

1. A Novel Actomyosin Interaction Responsible for Actin Activation and *In Vivo* Force Generation[8]

Revealing a Novel Actomyosin Interaction

The N-terminal region of actin is conserved, regarding the existence of at least two, maximum four negatively charged amino acids (Glu or Asp) [169, 170]. None of the crystal structures do not contain the highly flexible N-terminal region of actin, consequently its functional studies were hindered due to its lack from EM-based actomyosin structural models [111, 116, 118]. Therefore, we constructed a new *in silico* model of actomyosin, in strong and weak actin-binding states [171]. In these models, the actin subunits of an actin trimer model [111] were extended by their missing N-terminal residues including the acetylation of the N-terminus (Acetyl-Asp_1-Glu-Asp-Glu_4-). The actin trimer was docked to three different myosin states i.e. the weak actin-binding, up-lever (pre-powerstroke), the weak actin-binding down lever (post-rigor) and the strong actin-binding (rigor-like) myosin states. These docked complexes were then relaxed by a 15-ns-long molecular dynamics simulation. As the actin-binding cleft of *Dictyostelium* apo structure (1Q5G) is not fully-closed, we also obtained a rigor-like structure of *Doryteuthis pealeii* (squid) S1. The average actomyosin structures of the last few nanoseconds of the simulations are presented in **Figure 23**.

In all three states, the N-terminal region of AC1 of the actin trimer forms salt bridge interactions with the Arg or Lys of a yet uncharacterized loop, located in the helix-loop-helix motif, in the upper relay region of myosin. In the three different states, the interaction profile of the N-terminal actin segment with myosin is different, involving two or three negatively-charged residues forming salt bridges with one positively charged residue in myosin. It suggests, that this interaction is dynamic within the actomyosin enzyme cycle. We named this novel actin-binding loop of myosin activation loop, for reasons described later in Result 1.

---

[8] *In silico* experiments were carried out by my colleague, Zhenhui Yang, EDC cross-linking experiments were performed by András Málnási-Csizmadia and transmission electron microscopy was carried out by Attila L. Kovács. Results of this section of the study are published [Várkuti, Boglárka H., et al. "A novel actin binding site of myosin required for effective muscle contraction." Nature structural & molecular biology 19.3 (2012): 299-306].
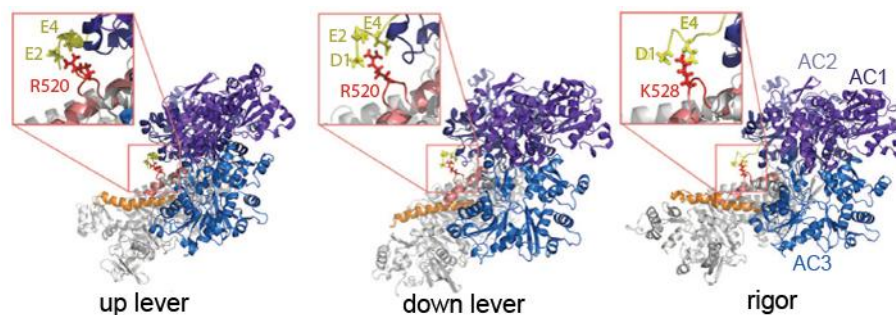
Figure 23. Actomyosin structural models revealing the interaction of actin N-terminal region with activation loop of myosin. *Dd* MD in its pre-powerstroke and post-rigor states and rigor-like squid S1 (grey) were docked to and relaxed with an actin trimer (AC1, AC2 and AC3), resulting in up lever, down lever and rigor actomyosin structures, respectively. The interaction of the negatively charged N-terminal region of actin (yellow) with the positively charged activation loop (red) of the upper relay region (pink) of myosin was formed spontaneously in the docking phase and remained stable in the entire molecular dynamics. The interaction is enlarged in the insets. (PDB codes: 1VOM, pre-powerstroke; 1MMD, post-rigor; 2OVK, rigor-like)

Activation loop is structurally conserved among myosins (**Figure 24**). Based on sequence comparison, the 5-10-residue-long loop exists in almost all myosin isoforms, and contains at least one positively-charged residue (Arg or Lys) in the same position. This charged residue points towards the solvent in the available myosin structures, and its interaction with other sidechains of myosin residues is highly unlikely. In smooth muscle or non-muscle myosin isoforms, activation loop is usually longer, containing a few additional Pro residues, which may have functional relations.

Figure 24. Sequence and structure comparison of activation loop among myosin isoforms. On the left panel, myosin classes are followed by abbreviations of their common names. Sequence numbering refers to its myosin type sequence numbering. The position of the positively charged amino acid of the upper relay loop is highlighted with light orange. Sequences of some myosin isoforms are color-coded and their structure of the upper relay with activation loop is visualized on the right panel.

We have found four myosin isoforms in the myosin family out of 143 which do not have positively charged aminoacid in this loop (www.mrc-lmb.cam.ac.uk/myosin/trees/txalign.html). Three of them are myosin I (*Mm* Brain IB, *Rn* Myr IA, *Mm* IA). Nevertheless, these three ones have a NNTN sequence in the activation loop which may form stabile H-bond(s) with the N-terminal peptide of actin, as we found similar interaction between *Dd* MD Gln521 and actin. We speculate that hydrogen bonds may substitute the salt bridge in these myosin I isoforms. For the fourth myosin isoform (Ce hum-2 – myosin V) we have not found relevant publications, even its motor function is questionable.

Experimental Evidence for the Activation Loop – Actin N-terminal Region Interaction

In order to obtain direct experimental evidence of the interaction between the upper relay loop and actin N-terminal region, we carried out cross-linking experiments of the actomyosin complex. We used a zero-length cross-linker, 1-ethyl-3-(3-dimethylaminopropyl) carbodiimide (EDC), which specifically creates covalent cross-links between Lys and Asp/Glu sidechains. A zero-length cross-linker has the advantage of avoiding unwanted, additional cross-links that may have been created due to length of the linker. EDC reacts with carboxyl groups creating an active intermediate, then easily displaced by a nucleophilic attack from primary amino groups. The primary amine forms an amide bond with the original carboxyl group, and an EDC by-product is released. By this, a covalent cross-link is only formed between Lys-Asp/Lys-Glu residues that are in close proximity.

By the covalent cross-linking of wild type *Dd* MD (*Dd* MD$_{wt}$) and actin with EDC, we detected one cross-linked actomyosin product. As *Dd* MD$_{wt}$ contains an Arg in its activation loop, this cross-linked product could not be the result of a covalent cross-link between them, but between some other Lys-Asp/Glu interactions. When we replaced the Arg with Lys (*Dd* MD$_{R520K}$), we detected the original cross-linked product, and an additional higher molecular mass covalent actomyosin complex (**Figure 25**.).
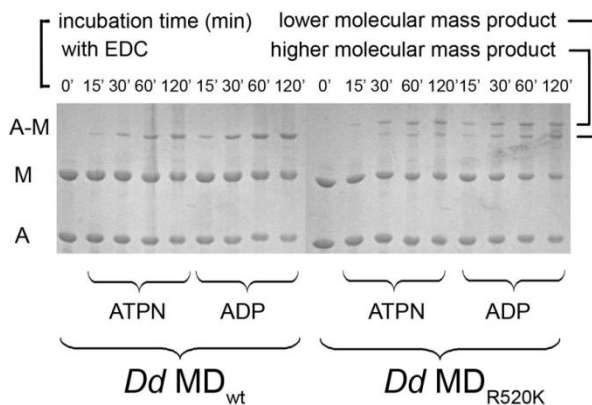
Figure 25. Zero-length cross-linking of actomyosin. SDS-PAGE visualization of actin (A), myosin (M) and the covalent actomyosin product (A-M) with increasing time of EDC incubation and in the presence of different nucleotides. *Dd* MD$_{wt}$ produced one, whereas the mutant *Dd* MD$_{R520K}$ produced a higher and a lower molecular mass actomyosin product.

This result was similar to results obtained from previous experiments, by the covalent cross-linking of rabbit skeletal muscle myosin and actin [132, 172]. That myosin isoform contains a Lys in the position homologous to Arg520 in *Dictyostelium*. In these previous experiments, the lower molecular mass actomyosin product was determined to be the result of the interaction of loop 2 and actin, whereas the interacting regions of the higher molecular mass product remained ambiguous [131]. In our experiments, a single Arg520Lys mutation in activation loop created the higher molecular mass product, indicating that the Lys residue in position 520 interacts with actin. The cross-linking reactions were carried out in the absence and presence of different nucleotides representing different states of myosin: the up lever state (in the presence of ATPN, a non-hydrolysable ATP analogue), the down-lever state (in the presence of ADP) and rigor (in the absence of nucleotide). All reactions proceeded to the same extent in all conditions.

We conclude that the sequentially and structurally conserved activation loop in the upper relay region of myosin creates interactions with actin in the weak actin-binding up and down lever, as well as in rigor states, which is in accordance with our simulation results. Furthermore, our *in silico* docking and molecular dynamics reveal that this myosin loop creates interactions with the N-terminal region of actin.

The Effect of the Upper-relay Loop Mutations on the Kinetic Properties of Nucleotide- and Actin-binding

To selectively interrupt the interaction between the activation loop and actin N-terminal peptide, we carried out site-specific mutations of activation loop. First, we designed and expressed a mutant in *Dd* MD in which we deleted the whole loop by removing the amino acids Gly_{519}-Arg-Gln-Pro-Pro_{523} (*Dd* $MD_{\Delta519-523}$). Upon the deletion of the loop, the upper relay helix does not suffer any torsion, and forms a continuous helical structure as predicted by our structural simulations (**Figure 26**). The program used for deleting activation loop is based on a neural network principle that can offer a protein a secondary structure prediction from its primary sequence [173]. It offers a three-state prediction which provides probabilities for residues to be in loop, helix or strand. After deleting the loop Gly_{519}-Arg-Gln-Pro-Pro_{523}, the prediction results showed that the down-stream part of upper relay helix will connect with the up-stream part, forming a 15 residues long helix.
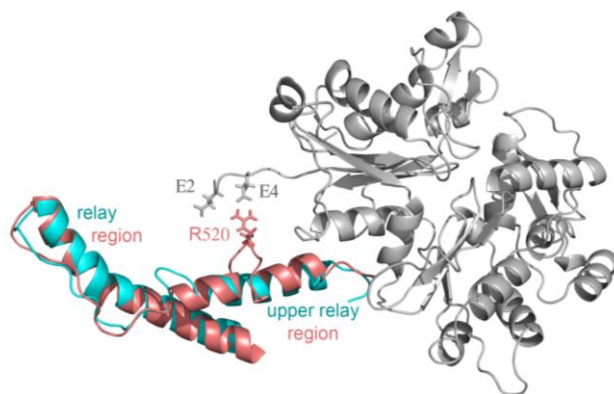
Figure 26. Structural representation of the wild type and loop-deleted upper relay region of myosin. The interacting residues of the wild type *Dd* MD (pink) after docking and molecular dynamics with actin (gray) N-terminus are shown, while the mutant *Dd* MD$_{\Delta519-523}$ (cyan) has no contacts with actin. Elimination of Gly$_{519}$-Arg-Gln-Pro-Pro$_{523}$ does not break the helical structure of the upper relay helix, making no further torsions in other regions of the myosin structure.

We also changed the R520 amino acid interacting with actin N-terminal region to neutral glutamine (MD$_{R520Q}$) or negatively charged glutamate (MD$_{R520E}$).

We performed thorough kinetic characterization of the mutant MDs and compared their kinetic properties to the wild type. We studied their ADP-, ATP- and actin-binding, ATP hydrolysis and actomyosin dissociation by using stopped-flow transient kinetic method (**Table 3**).

Nucleotide binding properties – rate and equilibrium constants in the absence of actin					
	ADP binding[a]			ATP binding[b]	ATP hydrolysis[b]
	k_{on} $(s^{-1}\mu M^{-1})$	k_{off} (s^{-1})	K_d (μM)	k_{on} $(s^{-1}\mu M^{-1})$	$k_{hydrolysis}$ (s^{-1})
Dd MD$_{wt}$	0.7 ± 0.14	7.2 ± 1.5	10.1 ± 3.0	1.2 ± 0.02	31 ± 1.2
Dd MD$_{R520E}$	0.69 ± 0.12	7.6 ± 2.1	10.9 ± 3.6	1.2 ± 0.02	34 ± 0.8
Dd MD$_{\Delta519-523}$	0.90 ± 0.22	7.1 ± 4.2	7.8 ± 5.0	1.3 ± 0.02	18 ± 1.4

Actin-binding properties – rate and equilibrium constants in the absence or presence of nucleotides							
	actin binding in apo state [c]			actin binding in ADP-bound state [c]			actin-binding in the presence of ATP	actomyosin dissociation by ATP [c]
	k_{on} $(s^{-1}\mu M^{-1})$	k_{off} (s^{-1})	$K_{d,apo}$ (μM)	k_{on} $(s^{-1}\mu M^{-1})$	k_{off} (s^{-1})	$K_{d,ADP}$ (μM)	$K_{d,ATP}$ (μM)	$k_{actin\ dissoc}$ (s^{-1})
Dd MD$_{wt}$	1.7 ± 0.16	0.54 ± 0.33	0.32 ± 0.21	0.28 ± 0.02	0.34 ± 0.05	1.2 ± 0.3	26 ± 9.7	97 ± 8
Dd MD$_{R520E}$	0.40 ± 0.16	0.44 ± 0.07	1.1 ± 0.61	0.043 ± 0.02	0.22 ± 0.05	5.2 ± 2.3	17 ± 5.7	186 ± 4
Dd MD$_{\Delta519-523}$	0.22 ± 0.03	0.27 ± 0.07	1.2 ± 0.46	0.030 ± 0.02	0.20 ± 0.05	6.5 ± 6.0	20 ± 6.8	195 ± 11

Table 3. Nucleotide- and actin-binding properties of wild type and mutant *Dd* MDs. The means ± s.d. values of at least three independent experiments are presented. K_d values were calculated from the appropriate rate constants, except for $K_{d,ATP}$, which was determined from a fitted hyperbola to the experimental data obtained from actomyosin co-sedimentation experiments (also see Fig. 28). Values were determined based on changes in [a]mant-dADP fluorescence, [b]intrinsic Trp fluorescence or [c]pyrene-actin fluorescence.

We found no significant difference between the mutants and the wild type [143] in any of the steps in the absence of actin, except for the hydrolysis of one of the mutants, where the change was within an order of magnitude. Actin-binding properties of wild type and mutant *Dd* MDs were characterized in strong actin-binding apo and ADP-bound states, as well as in the presence of excess of ATP, populating the weak actin-binding state of *Dictyostelium* myosin (**Table 3, Figure 27**).
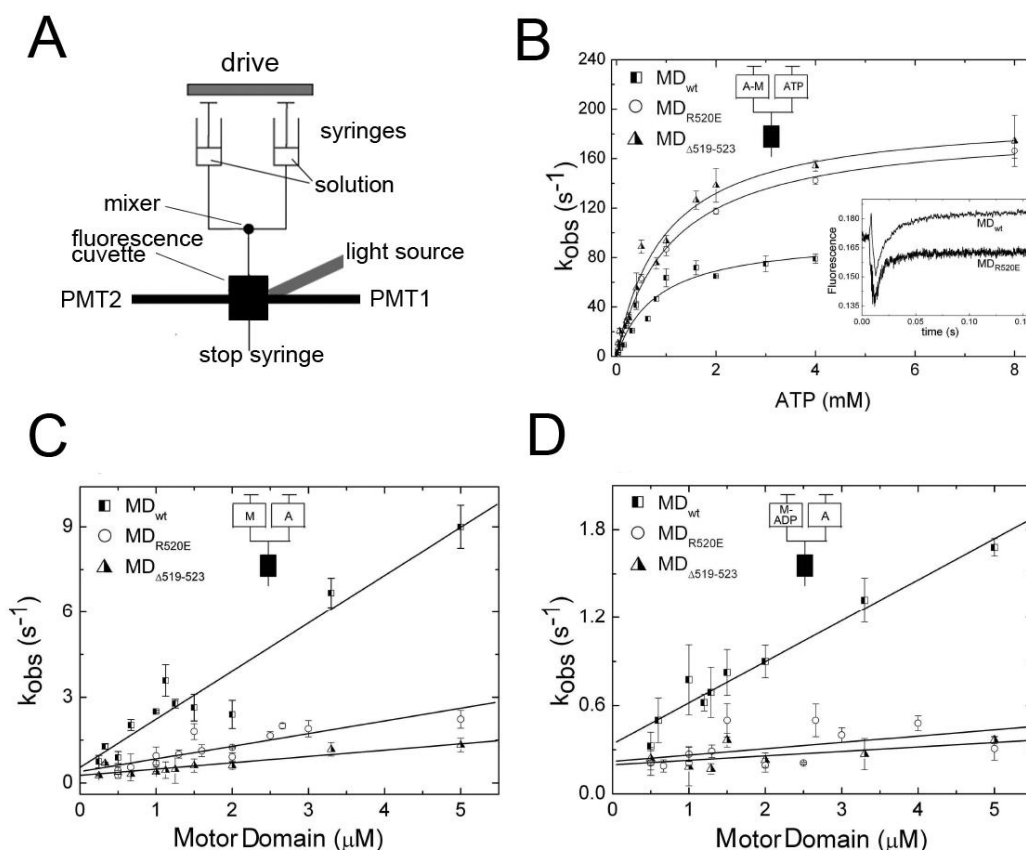
Figure 27. Transient kinetic properties of actin-binding of the wild type and mutant *Dd* MDs. A) The scheme of a stopped-flow. The principle of detecting fluorescence/light scattering changes on a transient scale is achieved by rapid mixing of two reactant solutions, then detecting the changes by the two photomultipliers (PMT) in line with the fluorescence cuvette and perpendicular to the source of excitation. **B) Actomyosin dissociation induced by ATP.** The observed rate constants (k_{obs}) for actomyosin dissociation of the wild type (MD$_{wt}$) and mutant (MD$_{R520E}$, MD$_{\Delta519-523}$) motor domains are plotted in the function of increasing ATP concentration. The fitted hyperbole determines the maximal value of k_{obs} ($k_{actin\ dissoc}$). Inset: pyrene-labelled F-actin in complex with myosin motor domain is mixed with ATP and the absolute fluorescence increase of pyrene is monitored in time. **C,D) The actin-binding of the wild type and mutant *Dd* MDs in apo and ADP-bound states.** The observed rate constants of the motor domain binding to pyrene-actin is presented in the function of increasing motor domain concentration in the absence (C) and presence of ADP (D). The gradient of the fitted linear function determines the binding rate constant (k_{on}), while the y-intercept gives the dissociation rate constant (k_{off}). Small diagrams depict the components of the rapid mix in each stopped-flow experiment (A-M= actomyosin, M=myosin, A=actin). All data presented are the means ± s.d. of at least three independent experiments.

The actin-binding properties of the mutant constructs were slightly different from those of the wild type. K_d values of actin-binding of the mutant *Dd* MD constructs in apo and in ADP-bound states increased four-five times compared to the wild type values. Importantly, the coupling ratio of actin-binding in apo and ADP-bound states ($K_{d,apo}/K_{d,ADP}$) of the mutant *Dd* MDs remained unaffected. The mutations caused a modest increase in the ATP-induced actomyosin dissociation rate constants ($k_{actin\ dissoc}$). The weak actin-binding of the mutants were similar to that of the wild type ($K_{d,ATP}$) (**Table 3, Figure 28**). For detailed data analysis see Materials and Methods.
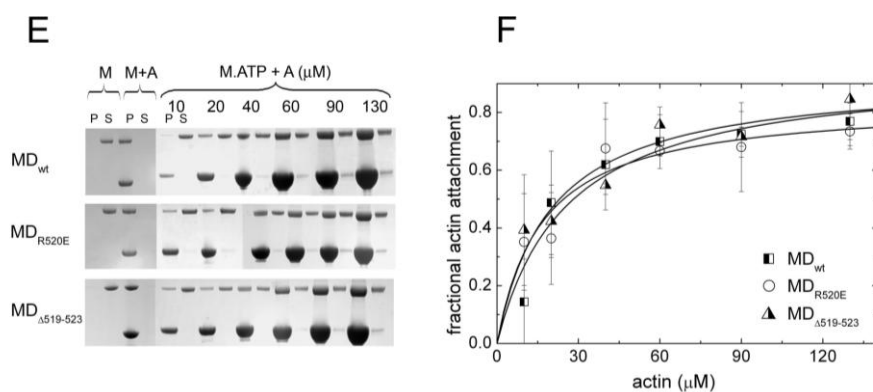
Figure 28. Actomyosin co-sedimentation assays to determine the weak actin-binding of the wild type and mutant *Dd* MDs. A) After ultracentrifugation, the pellets (P) and supernatants (S) of mixtures of myosin in the presence of ATP (M.ATP) and increasing concentrations of actin (A) were visualized by Coomassie Brilliant-blue staining of SDS-gel after electrophoresis. Myosin (M) and actomyosin (M+A) in the absence of ATP serve as controls for the experiment. **B)** Fractional actin attachments of wild-type and mutant motor domains - determined following the densitometry of SDS-gels - were plotted in the function of increasing actin concentration. $K_{d,ATP}$ was determined from the fitted hyperbole to the experimental data (see **Table 3**).

In summary, mutations that disrupt the interaction between the N-terminal region of actin and the upper-relay loop of myosin did not alter the kinetic properties of the motor domain in the absence of actin. The perturbations associated with actin-binding of mutant *Dd* MDs confirm the existence of such interaction, verifying the *in silico* simulations as well as the cross-linking experiments.

Activation Loop and the Uncoupling of Actin Activation from Actomyosin Motility

We also studied the basal and actin activated Mg-ATPase activities of the mutant and wild type *Dd* MD constructs. In addition, we applied the mutant construct MD_{R520K} as a further control, in which the positive charge of R520 was replaced by another positively charged amino acid. F-actin increased the basal ATPase activity (0 µM actin) of the MD_{wt} as well as

the MD$_{R520K}$ control mutant by almost two orders of magnitude (**Figure 29A, Table 4**). Remarkably, the basal ATPase activities of the loop-mutant constructs increased only by two-four folds even at very high concentrations of actin. In order to test this phenomena for processive myosins as well, we created a myosin V S1 containing the Lys502Glu mutation (*Mus musculus* numbering), which position is homolog to the *Dictyostelium* Arg520. Notably, we observed a similar effect upon comparing the actin activation of the mutant (myoV$_{K502E}$) and wild type myosin V (myoV$_{wt}$) (**Figure 29B, Table 4**). These results indicate, that the loop in the upper relay region of myosin is specifically responsible for the actin activation of myosin, therefore we named it activation loop.
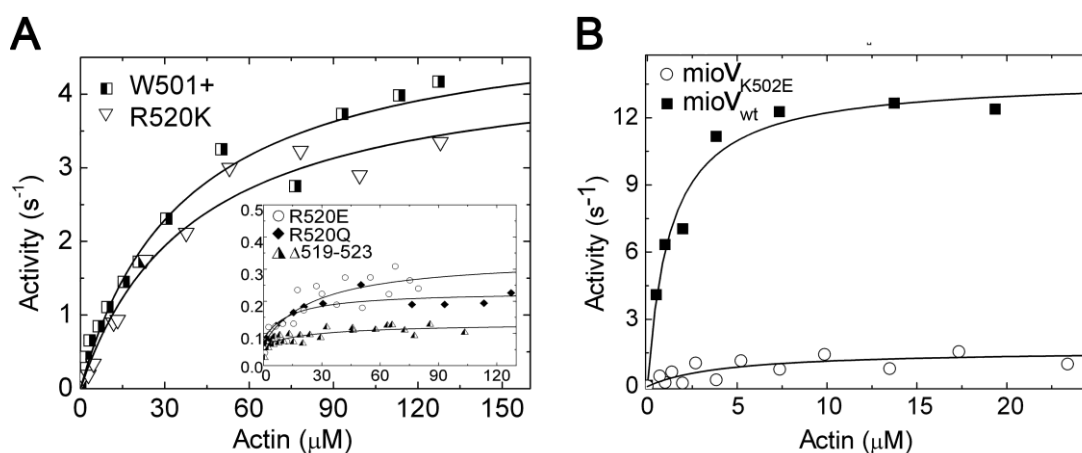
Figure 29. Activation loop mutations suppress the actin activated ATPase activity of myosin. A) Steady-state actin activated ATPase activities of MD$_{wt}$ and mutant *Dd* MD constructs are plotted in the function of increasing actin concentration. Inset: the saturation of the ATPase activities of MD$_{R520E}$, MD$_{Δ519-523}$, and MD$_{R520Q}$ is shown in a y-axis-upscaled graph. **B)** Steady-state actin activated ATPase activities of myo-5$_{wt}$ and the activation loop mutant myo-5$_{K502E}$ S1 constructs presented in the function of increasing actin concentration. Data of three independent experiments are shown

The basal ATPase activities of the activation loop mutant myosins were not affected, and their increase was not significant even at high concentrations of actin, in contrast to the wild type.

The mechanistic model (see Introduction) predicts that *in vitro* motility is not hindered by the lack of actin activation of myosin. The velocity of motility is not determined by the steady-state ATPase activity, but by other steps e.g. the rate of detachment of the actin filaments after powerstroke induced by ATP-binding [174-176], ADP release [135, 177]or ATP hydrolysis [178, 179]. The velocity controlling step in different myosin isoforms under different experimental conditions can be different. In order to test the mechanistic model, whether the activation loop mutation only affected actin activation and left the mechanism of contraction intact, although with a low productivity (low ratio of effective cycles/hydrolyzed
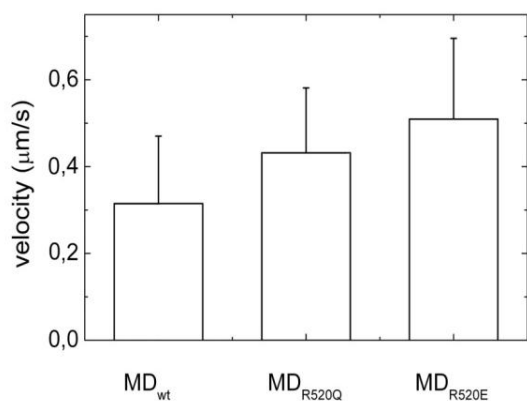
Figure 30. *In vitro* velocities of wild type and mutant *Dd* MDs. Error bars represent s.d. of at least three independent experiments.

ATP), we carried out *in vitro* motility assays with the wild type and activation loop *Dd* MD constructs (**Figure 30, Table 4).**

The average velocities of actin filament movement by the wild type and activation loop mutant motor domains were very similar to each other. Additionally, the average filament sliding speed for the wild type *Dd* MD was similar to previously published values [180]. Thus, the interruption of the interaction between activation loop and actin's N-terminus can decouple actin activation and motility. By reducing the actin activated ATPase activity of *Dd* MD, its capability of moving actin filaments *in vitro* is unaffected.

	activitity				velocity
	V_{basal}^{a} (s^{-1})	V_{max}^{b} (s^{-1})	K_{actin}^{b} (µM)	Acceleration	v (µm/s)
Dd MD$_{wt}$	0.067 ± 0.011	5.1 ± 0.37	36.9 ± 7.0	66x	0.32 ± 0.15
Dd MD$_{R520Q}$	0.070 ± 0.014	0.15 ± 0.01	13.3 ± 5.0	1.9x	0.43 ± 0.15
Dd MD$_{R520E}$	0.068 ± 0.013	0.27 ± 0.05	26.8 ± 14.0	3.5x	0.51 ± 0.18
Dd MD$_{\Delta519-523}$	0.064 ± 0.010	0.13 ± 0.01	26.6 ± 14.0	1.8x	
Dd MD$_{R520K}$	0.070 ± 0.017	4.5 ± 0.38	39.8 ± 8.3	52x	
Mm myo-5$_{wt}$	0.038 ± 0.004	13.8 ± 0.59	1.3 ± 0.2	690x	
Mm myo-5$_{K502E}$	0.029 ± 0.011	1.6 ± 0.33	4.4 ± 2.7	76x	

Table 4. Basal and actin-activated ATPase activities and sliding velocities of wild type and activation loop mutant *Dd* MD constructs. V_{basal} = basal ATPase activity, V_{max} = maximal actin-activated ATPase activity, K_{actin} = actin concentration at half of V_{max}, v = velocity. [a]Determined from NADH-coupled assay. [b]Determined from the fitted hyperbole to experimental data. Mean values ± s.d. are from at least three independent experiments.

Interestingly, for the mutant *Dd* MDs, a higher concentration of myosin had to be applied at the coating of the coverslips used for the motility assays in order to evoke motion of the actin filaments. This aspect further support the mechanistic model, as by increasing the concentration of the myosin heads in a low productivity system, the number of the effectively cycling heads increase, thus the probability of effective powerstrokes increase. When there is no or very low actin activation, the number of heads that go through the effective powerstroke pathway is determined only by the actin-binding affinity of myosin and the concentration of actin. As the binding of myosin to actin in the pre-powerstroke state is weak, the frequency of powerstrokes

is low. When the concentration of the activation loop mutant myosin heads is increased, the frequency of powerstroke events is also increased, thus motility becomes detectable. Due to the unloaded conditions of such motility assays, the few heads that grab and move actin filaments do it with speeds identical to the wild type, as no other kinetic parameters of the activation loop mutant myosins has been affected, including ADP release which mainly determines the velocity of the actin filaments. In case of the wild type, where there is actin activation, almost all heads are channeled into the effective powerstroke pathway. In summary, the ratio of effective versus futile cycles of myosins is determined by the extent of actin activation, which is enabled by activation loop− actin interaction.

How Does Activation Loop Regulate Mechanical Performance *In Vivo*?

Due to the specificity of the activation loop mutation in *Dd* MD, its singular effect can be explored *in vivo* by model organisms. We generated transgenic *C. elegans* strains carrying wild type or activation loop mutant body-wall myosins. With the help of these transgenic strains, we were interested in the worm's motile functions and mechanical properties.

Four types of myosin II are coded in the *C. elegans* genome and expressed by the animal: *myo-1* and *myo-2* in the pharynx, *myo-3* and *myo-4* in the body-wall. *Myo-3* − as the minor isoform in muscle − has a role in the thick filament assembly [181], whereas *myo-4* − encoding the major isoform − is the main component of the body-wall muscle, responsible for body motion [182]. *Myo-4*, also called *unc-54*, codes the protein UNC-54. UNC-54 deficient *C. elegans* strains have an 'uncoordinated' phenotype, and their speed of movement is approximately 20 % of the wild type. A successful, but not complete rescue of the motion and speed of UNC-54 deficient animals was reported previously by introducing the wild type body-wall myosin into them [183]. This UNC-54 deficient strain is an *unc-54*− null mutant, carrying a substitution in its *e1092* allele, resulting in the lack of myosin heavy chain expression [184]. This strain was applied for our further experiments.

We introduced the wild type body wall myosin gene, *unc-54* fused with C-terminal GFP (expressing UNC-54::GFP chimera protein) into the *unc-54*− null mutant strain (Δ*unc-54*) by microparticle bombardment, creating the Δ*unc-54;unc-54::gfp* transgenic strain. We also introduced the GFP-fused activation loop mutant body-wall myosin gene *unc-54$_{K525E}$::gfp* into Δ*unc-54* strain, generating the Δ*unc-54;unc-54$_{K525E}$::gfp* transgenic strain (expressing UNC-54$_{K525E}$::GFP) **(Figure 31.)**. The Lys525 position in *C. elegans* UNC-54 myosin II is homologous to the position Arg520 in *Dictyostelium* myosin II.
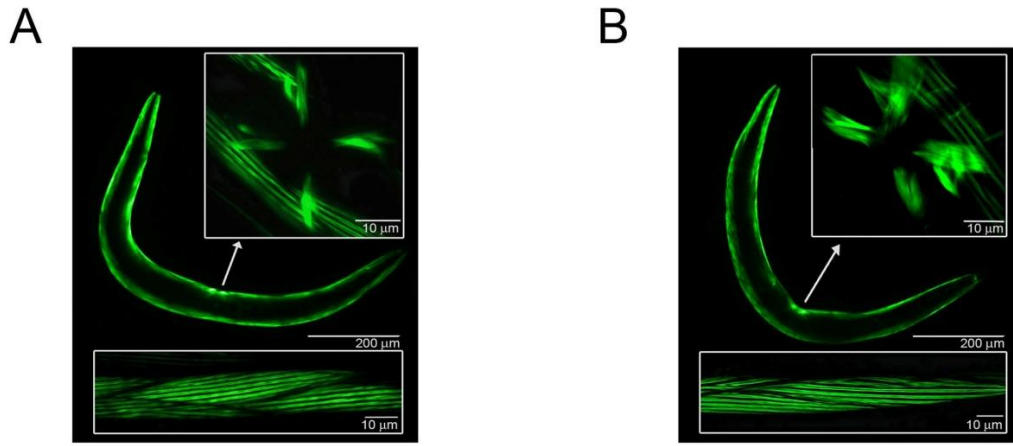
Figure 31. Fluorescence confocal microscopic images of transgenic *C. elegans* strains expressing GFP-fused body-wall myosin. A) A representative of the Δ*unc-54;unc-54$_{K525E}$::gfp* strain. **B)** An animal of the Δ*unc-54;unc-54::gfp* strain. UNC-54::GFP and UNC-54$_{K525E}$::GFP are expressed along the body as well as in the vulval muscle cells (upper insets). Parallel A bands of spindle-shaped muscle cells are also visualized (lower insets).

We compared the physiological properties of the two transgenic strains to N2 wild type and Δ*unc-54* strains. Body size, morphology, larval development and lifespan (**Figure 32A)** were similar in each strain. As presented, UNC-54 is also expressed in the vulval muscles. Therefore, egg-production of the Δ*unc-54* strain was rather defective, resulting in larvae hatching within the mother animal, causing its death. The egg-production of the two transgenic strains was between the values of Δ*unc-54* and wild type strains (**Figure 32B**).
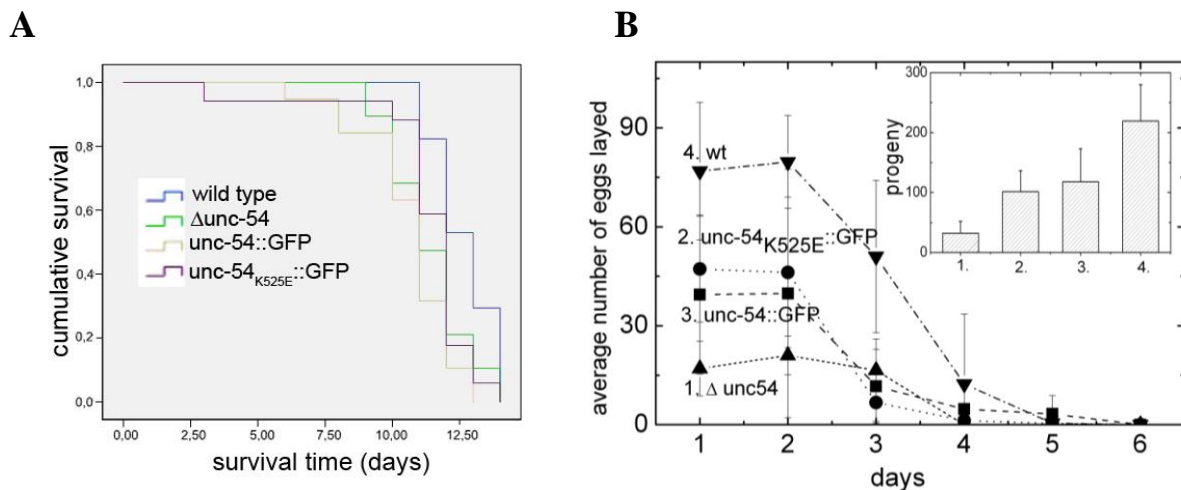
Figure 32. Vial parameters of the four *C. elegans* strains. A) Keplen-Meier survival curve depicting the lifespan of the four strains, showing their cumulative survival in time. Also see Appendix, Table A1 and A2. **B)** Egg-production of the strains, showing the total number of eggs layed for each strain in time. Inset: total progeny produced by the strains. Mean values ± s.d. (n=20) are presented.

Lifespan assays were carried out on plates that contained floxuridine (FUDR), preventing egg-production of the strains, thus defective egg-laying could not influence the survival of the strains.

C-terminal GFP fusion of the body-wall myosin did not disrupt the sarcomere structure of the transgenic *C. elegans* strains. They showed intact structures of obliquely striated muscles along their body (**Figure 31 and Figure 33**). In contrast, Δ*unc-54* animals had a stunted, disorganized body musculature as they lacked the major isoform of the muscle, UNC-54.
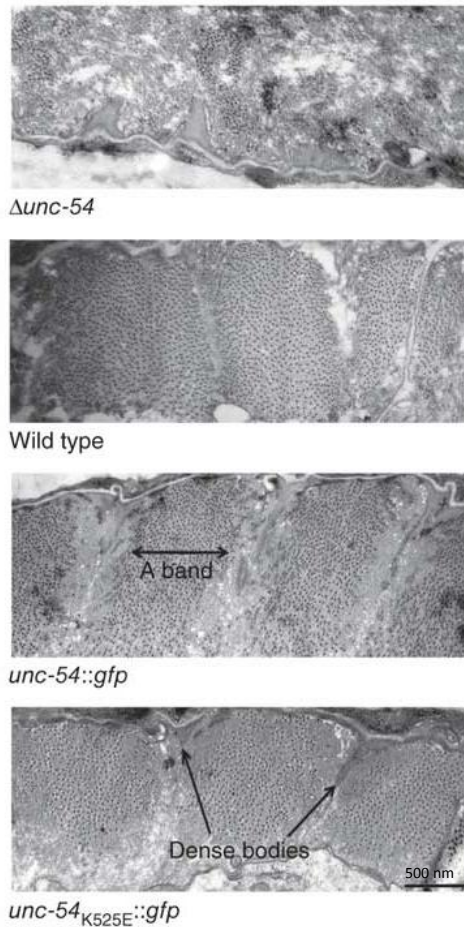
Figure 33. Transmission electron microscopy of the cross-sections of *C. elegans* strains. The body-wall myosin null-mutant Δ*unc-54* has a disorganized muscle ultrastructure compared to wild type animals. The transgenic Δ*unc-54;unc-54::gfp* (shortly *unc-54::gfp*) and Δ*unc-54;unc-54$_{K525E}$::gfp* (shortly *unc-54$_{K525E}$::gfp*) strains expressing UNC-54::GFP and UNC-54$_{K525E}$::GFP could restore the wild-type structure of the muscle of the animals.

After proving that the muscle structure of the two transgenic strains are re-established, and alike, we investigated the motile function of each strain, by measuring the velocities of the animals under standardized conditions. Video recordings were taken from their movement, which were processed by a custom-written real-time automatic movement analyzer software (δVision). As expected, movement of the Δ*unc-54* was ~20% of the speed of the wild type (**Figure 34, Table 5**). Additionally, mutation in activation-loop affected the speed of the worms. Most of the Δ*unc-54;unc-54$_{K525E}$::gfp* animals moved faster than those without the construct, but significantly slower than nematodes of Δ*unc-54;unc-54::gfp* genotype. Animals from Δ*unc-54;unc-54::gfp* strain could not restore fully the speed of the wild type animals (71%), as it was also seen previously [183]. There can be several reasons behind uncomplete restoration of function of transgenic strains containing wild type genes. These include the possibility of producing lower amounts of the transgenic protein than the original wild type protein, or that the transgenic protein incorporates with less efficiency into thick filaments than the wild type. Nevertheless, full recovery of wild type nematode motility could be detected

when transgenic Δ*unc-54;unc-54::gfp* animals were treated with FUDR (inset of **Figure 34, Table 5**), indicating that egg-production can have severe impact on long-term physical performance of transgenic strains. Notably, in the case of the other transgenic strain, Δ*unc-54;unc-54$_{K525E}$::gfp*, FUDR-treatment did not result in significant difference in the velocity values compared to the FUDR untreated animals.
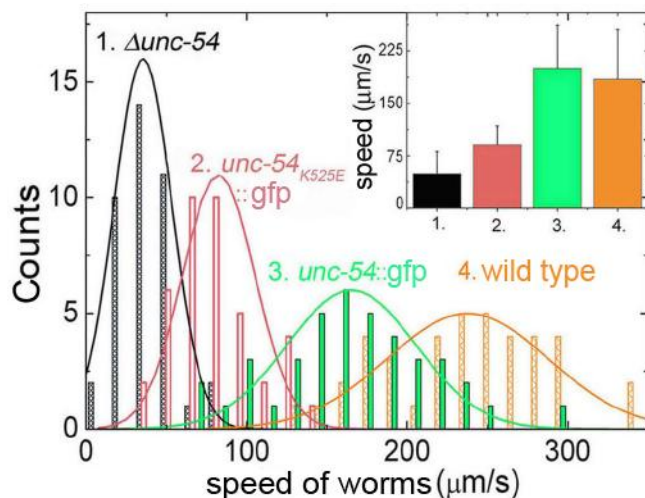
Figure 34. The distribution of speed of animals among the four *C. elegans* strains. The speed of animals from each strain (n=40) were measured and their distribution is presented. Inset: the mean velocity values ± s.d. of the FUDR-treated animals (n=20) of each strain are presented.

	speed	speed with FUDR-treatment
Δ*unc-54*	38.8 ± 16.4	49.0 ± 32.1
unc-54$_{K525E}$::gfp	82.5 ± 25.5	90.5 ± 27.5
unc-54::gfp	164.8 ± 49.5	200.4 ± 61.5
wild type	232.3 ± 51.1	184.5 ± 71.4

Table 5. Speed values of the *C. elegans* strains in the presence and absence of FUDR. Mean speed values ± s.d. are presented of the FUDR-untreated (n=40) and FUDR-treated (n=20) animals of each strain.

In order to exclude the possibility that the difference between the transgenic strains carrying wild type and activation loop mutant myosins arose from the different levels of their expression, we measured the expression levels of the transgenic proteins. We detected and measured the fluorescence of the GFP-fused body-wall myosin, and found no correlation between the increasing values of motility and the corresponding fluorescence in this range of protein expression (**Figure 35 and Table 6**).
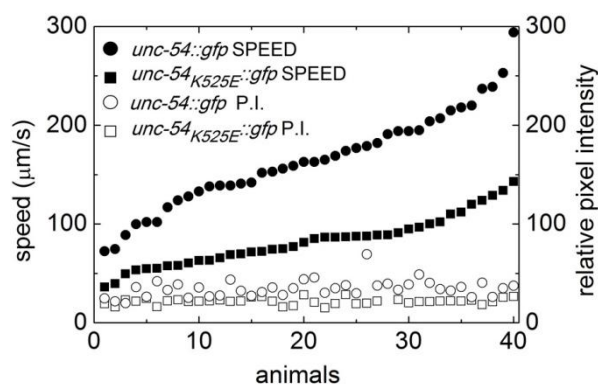
Figure 35. Speed and fluorescence of the transgenic strains. 40 animals of each transgenic strains are plotted in the order of increasing speed values (left y-axis), whereas the corresponding pixel intensities of the animals are also shown (right y-axis). P.I. = pixel intensity.

	speed (µm/s)	p.i.	speed/p.i.	Pearson's r.
unc-54::gfp	164.8 ± 49.5	34.74 ± 8.75	4.88 ± 1.35	0.29052
unc-54$_{K525E}$::gfp	82.50 ± 25.5	21.65 ± 2.99	3.88 ± 1.53	0.20638
p value	0.000	0.000	0.0008	

Table 6. Correlation of speed and the amount of expressed protein in the two transgenic strains. Mean values ± s.d. are listed. p.i.= pixel intensity, measured by detecting the GFP signal of expressed proteins in the whole body, resulting in a mean pixel intensity value for each animal. Pearson's r.= Pearson's correlation, reflecting the degree of linear relationship between speed and pixel intensity. *p* values are calculated for n=40.

We conclude that activation loop mutation in *C. elegans* nematodes reduces the speed of the animals, but does not abolish motion. Actin activation is low, but there are still some myosin heads that go through powerstroke and evoke contraction of the muscles. It is interesting to test how force generation of the activation loop mutant animals is affected. Therefore we designed a novel experimental approach to measure force generation of the animals by applying atomic force microscopy (AFM). Adult worms of similar size and body morphology were captured by lowering the cantilever of the AFM to a standardized level, then exerted force on them for a given time (**Figure 36**). Force generated by the animals as a response to pushing them with the cantilever was detected in time.
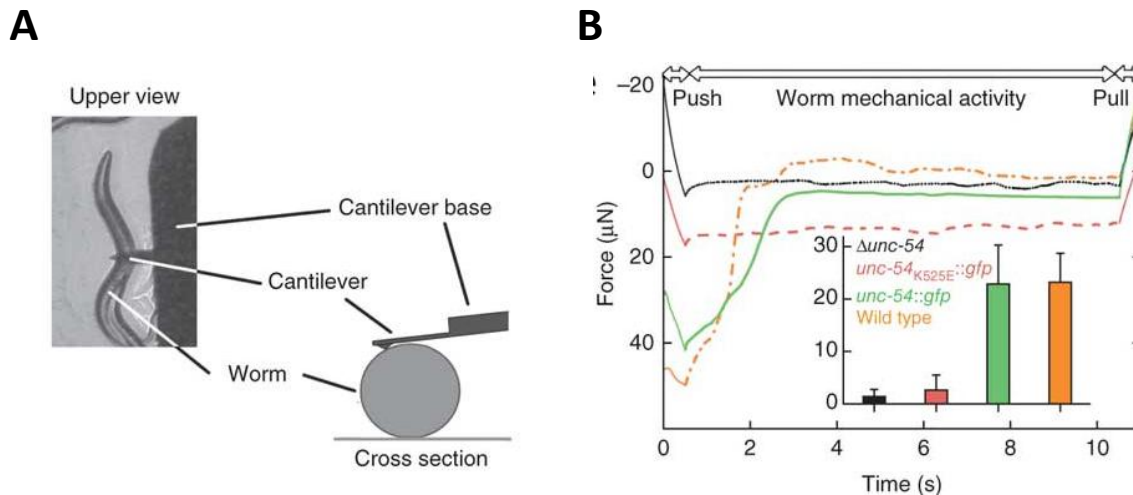
Figure 36. Force-measuring experiments on *C. elegans*. A) Schematic representation of measuring force response of worms evoked by the external load exerted by the cantilever of an AFM. **B)**. Typical force changes in time produced by the animals during force-measuring experiments. Worms were exposed to a deforming force (push) for the same periods of time. After the push phase, the mechanical response was detected, until the retraction of the cantilever. Average force productions ± s.d. (n=15-25 animals) of each strain is presented in the inset.

Perturbating the animals with external load on their musculature resulted in an escape response. This response consisted of oscillatory motions and in the case of wild type and *unc-54::gfp* animals it led to a final escape from underneath the cantilever. The mean force values of the

$\Delta unc\text{-}54$ and *unc-54$_{K525E}$::gfp* strains were ~20 times smaller than in the case of the wild type or *unc-54::gfp* animals (**Table 7**).

strain	force (μN)
Δunc-54	1.46 ± 1.25
unc-54$_{K525E}$::gfp	2.57 ± 2.90
unc-54::gfp	22.79 ± 7.53
wild type	23.26 ± 5.62

Table 7. Force generated by the four *C. elegans* strains. Mean values ± s.d. are listed (n=15-25). *unc-54$_{K525E}$::gfp* worms were only slightly stronger than *Δunc-54* animals (p=0.1563, n=24).

Mutational depletion of actin activation of myosin drastically weakens the force generated during muscle contraction *in vivo*, while motile functions are retained. The capability of the activation loop mutant worms to move is much less affected (2x less than wild type) compared to their force exerting mechanical performance (8.9x less than wild type). These results are in consistent with our *in vitro* motility results, which demonstrate that under no load, the motile functions are retained by the few effectively cycling heads. In case of a whole body of an animal, the effectively cycling few heads cannot be synchronized between the muscle cells. Additionally, the muscles of the animals are not unloaded, which results in the decreased *in vivo* motility of the worms. Applying additional external load on the animals resulted in their complete loss of force generating capability, indicating that for effective muscle performance activation loop-actin interaction is essential.

In summary, we characterized a novel interaction of myosin's activation loop and actin's N-terminal region, which is specifically responsible for actin activation. *In vitro* motility and *in vivo* results of the activation loop mutant myosin support the mechanical model, which predicts the uncoupling of actin activation and motility. Activation loop mutant myosin only differs from wild type by one parameter: it is incapable of being activated by actin. As a result, only few myosin heads go through powerstroke, but the ones that proceed do it with the same rate as the wild type, as it was seen in the unloaded *in vitro* motility assay. As soon as load is exerted on the system, the overall mechanical performance in muscle becomes weaker, as there are not enough effectively cycling heads to carry out contractions and generate force as sufficiently as wild type myosins in the muscle.

After discovering the key structural element – activation loop – behind actin activation, the question regarding the structural mechanism of actin activation still remains unanswered. We do not know the structural rearrangements that occur upon actin-binding, sensed by activation loop and transmitted towards other regions of myosin. The answer would lie in the knowledge of the structure of the initial state of the powerstroke.

2. A structural model of the initial state of the powerstroke: actin-binding induced 'extra' priming of myosin[9]

Structural Model of the Initial State of the Powerstroke

We resolved the atomic structural model of the weak-binding actomyosin complex (initial powerstroke state) and strong-binding actomyosin complexes (rigor) by *in silico* techniques, using protein-protein docking of myosin and actin structures and long-time molecular dynamics simulations of the complex. These simulations are different from the one presented at the beginning of the Results 1, as it uses a more recently published actin trimer for docking and a much longer molecular dynamics simulation, enabling the complete relaxation of the complexes. After completing the actin trimer [89], the pre-powerstroke, apo and rigor-like states of myosin II structures with their missing residues (**Table 8**), they were relaxed by molecular dynamics and docked to each other by using HADDOCK program. The docked actomyosin complexes and the uncomplexed actin and myosin structures were placed into explicit water boxes and relaxed by a 100-ns-long molecular dynamics. To validate the results of the structural simulations, we compared the created rigor structures ($_{rel}A.M_{rigor,Dd}$ and $_{rel}A.M_{rigor,sq}$) with an experimentally determined, EM map based rigor actomyosin model ($_{EM}A.M_{rigor,ch}$) [116].

structure (PDB code) state	M_{up} (1VOM) pre-powerstroke	$M_{apo,Dd}$ (1Q5G) apo	$M_{apo,sq}$ (2OVK) rigor-like	$_{EM}A.M_{rigor, ch}$[a] (model)
relaxed	$_{rel}M_{up}$	$_{rel}M_{apo,Dd}$	$_{rel}M_{apo,sq}$	
docked	$_{dock}A.M_{up}$	$_{dock}A.M_{rigor,Dd}$	$_{dock}A.M_{rigor,sq}$	
docked+relaxed state	$_{rel}A.M_{up}$ initial powerstroke	$_{rel}A.M_{rigor,Dd}$ rigor	$_{rel}A.M_{rigor,sq}$ rigor	rigor
nucleotide	ADP.Pi	no	no	no

Table 8. Myosin and actomyosin structures and the occupancy of their nucleotide binding sites. [a]Structural model of rigor actomyosin based on electron micrography (EM). 1VOM and 1Q5G are *Dd* myosin II MDs. 2OVK is *Doryteuthis pealeii*, squid (sq) myosin II S1. VO_4^{3-} at the active site of 1VOM was replaced by Pi. M=myosin, A=actin, A.M=actomyosin, up=up lever, dock=docked, rel=relaxed and ch=chicken (*Gallus gallus*) myosin.

The comparison validated the applied *in silico* procedures as the non-directed protein-protein docking and molecular dynamics simulations resulted in a highly similar structure to the

---

[9] *In silico* experiments were carried out by my collegue, Zhenhui Yang. Results of this section of the study are under submission [Várkuti, Boglárka H., et al. " A structural model of actomyosin in the prepowerstroke state: actin induced 'extra priming' of myosin "].

experimentally determined one. During the molecular dynamic relaxation, actin induced significant closure of the actin binding cleft of $_{dock}$A.M$_{rigor,Dd}$ and $_{dock}$A.M$_{rigor,sq}$ resulting in similarly closed clefts as in $_{EM}$A.M$_{rigor,ch}$. The actin binding cleft of the non-actin bound M$_{apo}$ did not change upon relaxation ($_{rel}$M$_{apo}$) (**Table 9**).

crystal/model	distance (Å)	crystal/model	distance (Å)	crystal/model	distance (Å)
M$_{up}$	21.1±1.5	M$_{apo,Dd}$	16.7±1.3	M$_{apo,sq}$	18.3±1.4
$_{rel}$M$_{up}$	21.7±1.4	$_{rel}$M$_{apo,Dd}$	16.7±1.2	$_{rel}$M$_{apo,sq}$	18.3±1.3
$_{rel}$A.M$_{up}$	20.6±1.6	$_{rel}$A.M$_{rigor,Dd}$	11.9±1.0	$_{rel}$A.M$_{rigor,sq}$	16.8±1.1
				$_{EM}$A.M$_{rigor, ch}$	17.2

Table 9. Extent of closure of the actin binding cleft of different myosin states and actomyosin complexes. Extent of closure was measured by the distance between the backbone Cα of Glu365 of the upper 50 kDa domain and Asn537 of the lower 50 kDa domain.

Furthermore, we found that the orientation of myosin relative to the actin filament in *Dd* and squid $_{dock}$A.M$_{rigor}$ did not match well with that of $_{EM}$A.M$_{rigor,ch,}$ while in the first 10 ns of the molecular dynamics myosin oriented to the experimentally determined position in both cases, similar to $_{EM}$A.M$_{rigor,ch}$. (**Figure 37**). Additionally, a further down lever movement occurred upon the relaxation of the $_{dock}$A.M$_{rigor,sq}$ complex, positioning its converter well buried into the EM map of $_{EM}$A.M$_{rigor,ch}$ (**Apendix, Table A3**).
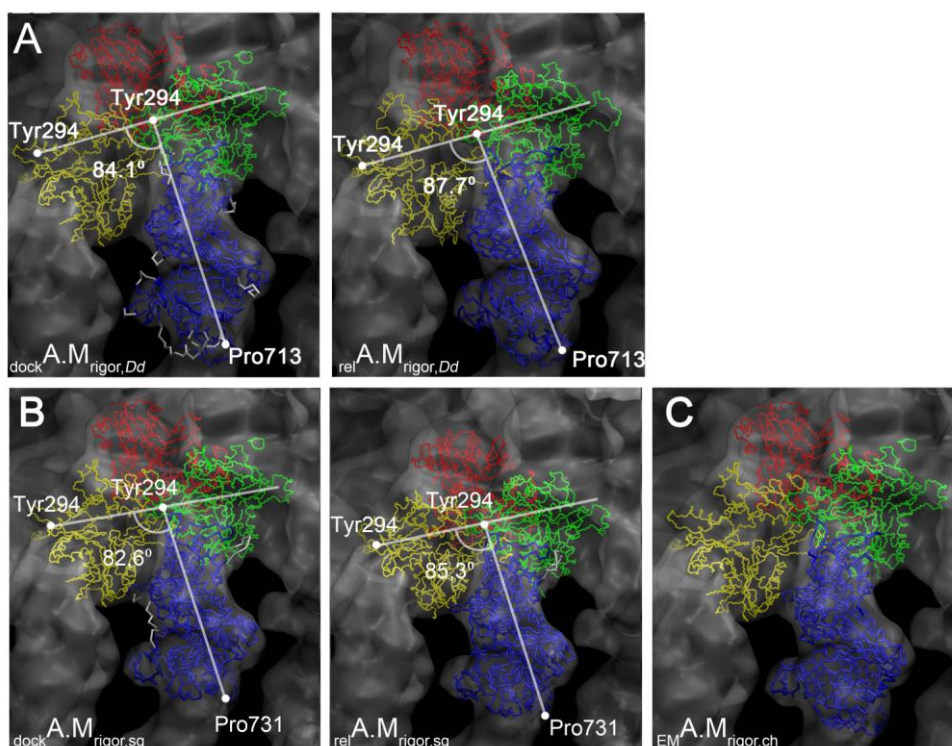
Figure 37. Fits of docked and relaxed *Dd* and squid actomyosin structures into the EM map of a chicken rigor structure. *Dd* rigor (A) and squid rigor (B) structures before and after relaxation were fitted into the electron density map (transparent gray) of $_{EM}$A.M$_{rigor,ch}$ (C) with their actin trimers (yellow-red-green) as best fits for the map. Myosin (blue) outside the EM map is colored white.

We further compared the binding free energies and calculated dissociation constants of the simulated actomyosin complexes with those obtained from *in vitro* experiments [124, 177] (**Table 10**, **Appendix Table A4**). The ratio of *in silico* determined dissociation constants of weak and strong actomyosin complexes is similar to that of experimentally determined values ($K_{d,weak}/K_{d,rigor} \approx 200$ or 400 and ≈ 200 or 1000, respectively). Nevertheless, the calculated binding free energies of all simulated actomyosin complexes are systematically smaller by ~2-3kcal/mol than those of the experimentally determined values.

	ΔG_{bind} (kcal/mol)	K_d (μM)	$_{EXP}\Delta G_{bind}$ (kcal/mol)	$_{EXP}K_d$ (μM)
$_{rel}A.M_{up}$	-7.6±0.8	2.8	-5.8	33
$_{rel}A.M_{rigor,Dd}$	-12.4±1.3	0.013	-9.6	0.03
$_{rel}A.M_{rigor,sq}$	-11.4±1.0	0.007	-9.2	0.19

Table 10. Binding free energies and dissociation constants of the relaxed actomyosin complexes. K_d values were calculated on the basis of ΔG_{bind}=-RTlnK. EXP=experimentally determined values.

Comparison of the Actomyosin Interface in Weak- and Strong-binding Actomyosin Complexes

The binding surface areas of myosin, the number of interacting amino acids of the docked actin and myosin structures before and after the relaxation, and the type of interactions were determined (**Table 11**). All actomyosin interactions are listed in **Appendix, Table A5**. The actin binding surface area of myosin expands during the weak-to-strong actin binding transition mainly due to the increasing contribution of loop 4 and cardiomyopathy loop in the binding (**Figure 38**).

structures	myosin		actin		surface area ($Å^2$)	number of H-bonds	number of salt bridges
	$^1I_{res}$	$^2I_{at}$	$^1I_{res}$	$^2I_{at}$			
$_{doc}A.M_{up}$	33	146	42	176	1478	13	4
$_{doc}A.M_{rigor,Dd}$	41	177	55	220	1753	19	12
$_{doc}A.M_{rigor,sq}$	40	133	50	164	1468	16	5
$_{rel}A.M_{up}$	46	216	61	235	1997	30	24
$_{rel}A.M_{rigor,Dd}$	51	238	62	271	2205	35	25
$_{rel}A.M_{rigor,sq}$	60	244	69	294	2707	40	24
$_{EM}A.M_{rigor, ch}$	57	230	65	271	2244	41	23

Table 11. Quantification of the interactions between actin and myosin in different actomyosin structural models. ^{1}Number of interacting residues. ^{2}Number of interacting atoms.
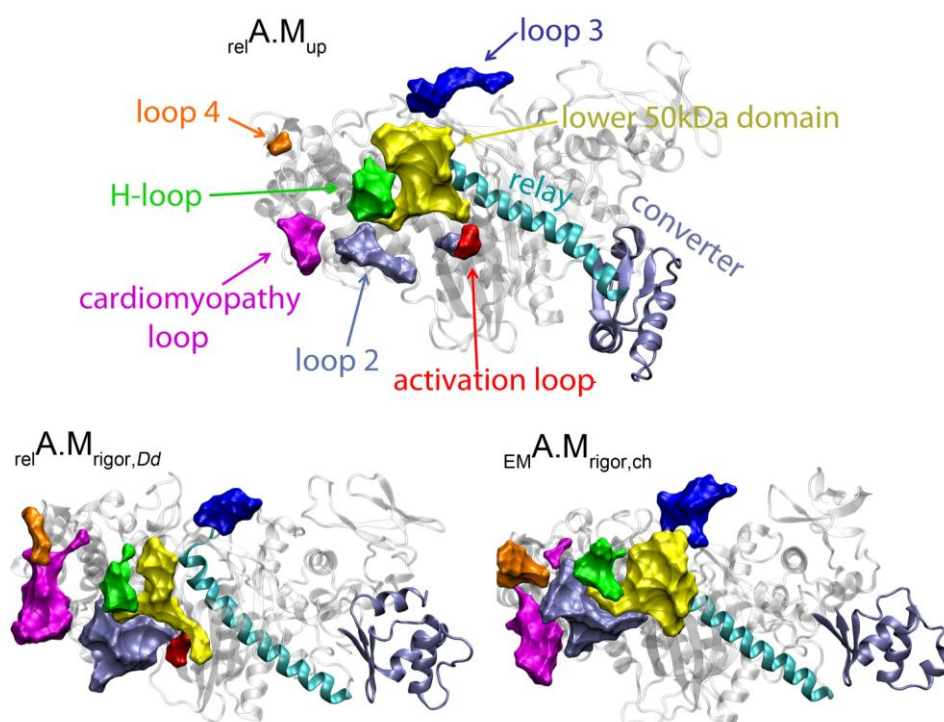
Figure 38. The actin-binding myosin interface of the relaxed actomyosin complexes. Myosin's (transparent grey, cartoon representation) actin-binding loops are highlighted. Loop 4 (orange), cardiomyopathy loop (purple) and loop 2 (light blue) of the upper 50 kDa domain have few interactions in the weak actin-binding state of myosin ($_{rel}$A.M$_{up}$), while loop 3 (blue), H-loop (green), activation loop (red) and residues of the lower 50 kDa domain (yellow) have extended interactions with actin both in weak and strong actin-binding states ($_{rel}$A.M$_{rigor,Dd}$, $_{EM}$A.M$_{rigor,ch}$).

The existence of the interaction between activation loop and the N terminal segment of actin was confirmed by the simulations. Arg520 (*Dd* MD) located in the activation loop interacted with the negatively charged N-terminal segment of actin in all relaxed actomyosin structures. This interaction was formed spontaneously in the first few nanoseconds of the molecular dynamics relaxations. In the $_{EM}$A.M$_{rigor,ch}$ model this interaction is missing since the actin crystal structure used for creating the model is lacking the N-terminal region of actin. In the weak-binding actomyosin structure, the conformation of activation loop is different from that of the rigor. Arg520 in $_{rel}$A.M$_{up}$ has a salt bridge interaction with Asp1 of actin while in $_{rel}$A.M$_{rigor}$ it forms a more extended salt bridge cluster with Asp3 and Glu4 (**Figure 39**). These interactions are stable as their occurrence is 95% throughout the whole molecular dynamics. During the weak-to-strong actin-binding transition, loop 2 also endures a large conformational change. In both weak and strong actin-binding states, there is a salt bridge between Lys622 of myosin and Asp25 of actin, while the C-terminal part of loop 2 (Lys 635) forms a salt bridge interaction with the actin N-terminal peptide in rigor.
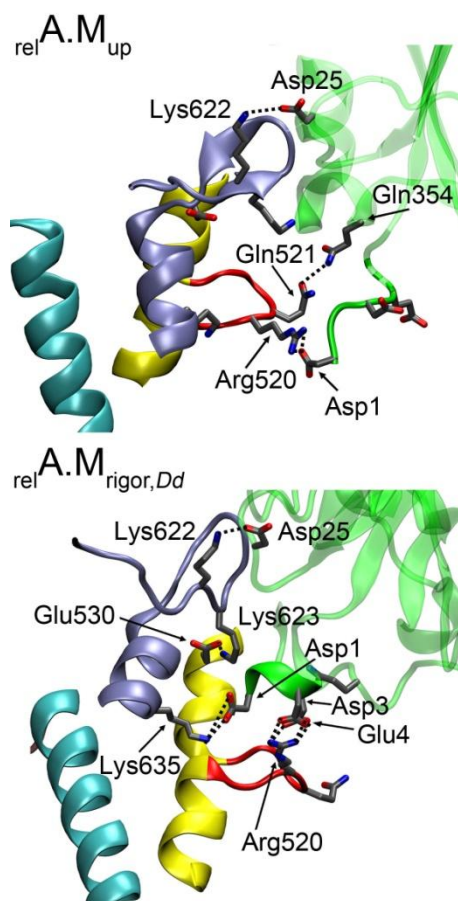
Figure 39. Interactions of loop 2 and activation loop in weak and strong actin-binding states of myosin. (A) In weak actin-binding state ($_{rel}$A.M$_{up}$) loop 2 (ice blue) interacts with Asp25 of actin (green), while activation loop (red) of the upper relay (yellow) has interactions with the N-terminal region of actin. **(B)** In strong actin-binding state ($_{rel}$A.M$_{rigor,Dd}$) the N-terminal part of actin positions between loop 2 and activation loop, creating interactions with both of them. The position of the relay (cyan) is also presented.

The helix-loop-helix element (residues 530-537) – structurally coupled to activation loop – has more hydrophobic interactions with residues 143-147 of actin in rigor than in weak actin-binding myosin state. It is in agreement with previous results describing expanding networks of hydrophobic interactions between actin and myosin during the weak-to-strong actin-binding transition [185]. Furthermore, the conformational rearrangements and altering interaction network of activation loop with actin N-terminal region upon the up-to-down lever movement and the weak–to-strong actin binding transition indicates that actin may directly affect the relay/converter/lever movement through its structural coupling to activation loop.

Structural Changes Caused by Actin-binding: 'extra priming' of myosin

Significant conformational relaxations appeared in the relay/converter and the nucleotide-binding pocket upon molecular dynamics of $_{dock}$A.M$_{up}$. All conformational relaxations were completed in the first 15 ns and remained stable in the following 90 ns of the simulations. The most striking effect induced by actin-binding was an 18° further up movement of the already up-positioned myosin lever (**Table 12, Figure 40A.**).

	angle (^{0})	lever state	switch 2− switch 1 distance (Å)	switch 2 position
M_{up} (1VOM)	122	up	10.4	closed
$_{rel}M_{up}$	123±3	up	10.3±0.2	closed
$_{rel}A.M_{up}$	105±3	further up	9.5±0.2	further closed
$_{rel}A.M_{up,R520Q}$	120±3	up	10.2±0.2	closed
$_{rel}A.M_{up,R562Q}$	111±3	further up	9.5±0.2	further closed
$_{rel}A.M_{up,K622Q/K623Q}$	113±2	further up	9.6±0.2	further closed

Table 12. Converter/lever and switch 2 positions of myosin and actomyosin structures upon molecular dynamics. Angles were measured between the C_α atom of residues Gly684 and Arg689 of SH1 helix and Ala748 of the converter domain. Lever positions of all other structures are presented in the **Appendix, Table A3.**

Interestingly, the further up movement of the lever was coupled to another conformational change occurring in the nucleotide binding pocket. The C-terminal part of switch 2 loop upon relaxation of the $_{doc}A.M_{up}$ moved to a further closed position (**Table 12, Figure 40A**). We call the myosin possessing a further up lever and a further closed switch II the 'extra primed' state of myosin, which is induced by the binding of actin. In order to investigate the role of activation loop-actin interaction in the detected conformational changes, Arg520 of $_{rel}A.M_{up}$ was mutated to Gln ($_{rel}A.M_{up,R520Q}$), interrupting the salt bridge interaction between activation loop and the N-terminal region of actin. The mutated actomyosin complex was relaxed by molecular dynamics for 100 ns. In the first 5 ns the lever moved back to the same up position as that of the actin detached myosin ($_{rel}M_{up}$) (**Table 12, Figure 40B**). This specific effect of the extra priming of myosin caused by activation loop− actin interaction is further supported by the fact that mutations in other actin binding regions (loop 2 or loop 3, $_{rel}A.M_{up,K622Q/K623Q}$ and $_{rel}A.M_{up,R562Q}$, respectively) caused only slight 'back-relaxations' and the lever remained mainly in the further up position (**Table 12, Figure 40B**). Similarly to the back-relaxation of the lever, upon mutating Arg520 of activation loop to Gln, switch 2 loop relaxed to the same position as that of the actin detached, closed conformation ($_{rel}M_{up}$) (**Figure 40B**). In the loop 3 and loop 2 mutants ($_{rel}A.M_{up,R562Q}$ and $_{rel}A.M_{up,K622Q/K623Q}$) switch 2 remained in the further closed position (**Figure 40B**). The effect of the mutation in activation loop indicates that activation loop has a key role in the extra priming of myosin.
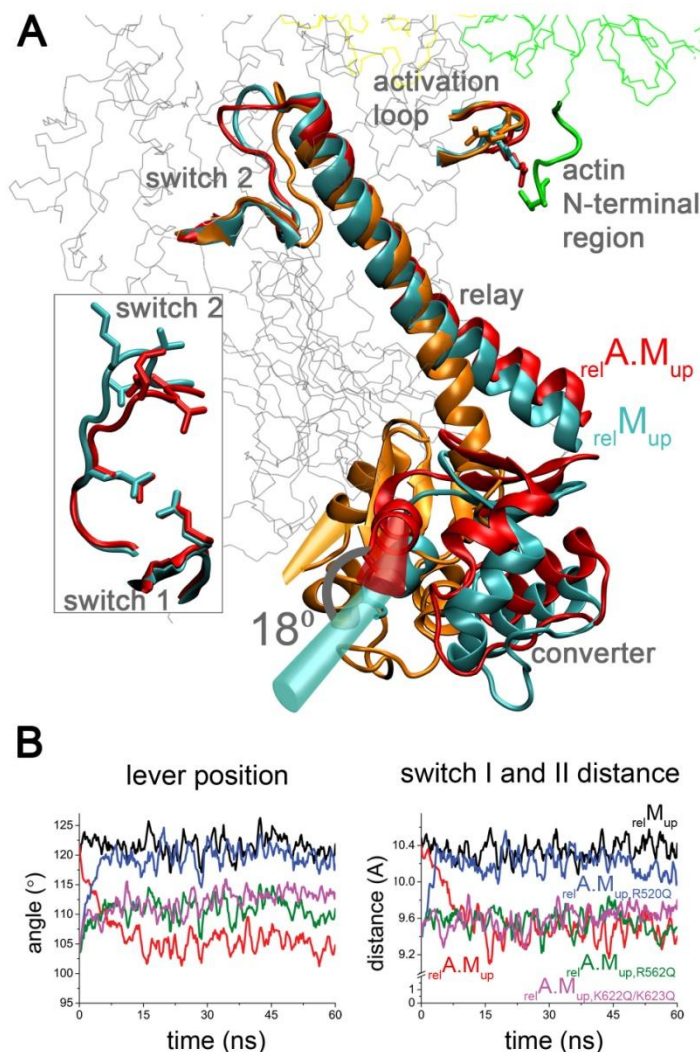
Figure 40. The extra primed state of the weak-binding actomyosin complex. (A) After docking and relaxation of myosin (gray) and actin (green-yellow), the $_{rel}$A.M$_{up}$ (red) possesses a further up lever and a further closed switch 2 compared to $_{rel}$M$_{up}$ (cyan) and the overlayed 1MMD down lever motor domain (orange) structures. Arbitrary extensions of the levers are represented by red, cyan and orange rods. Inset: positions of switch 2 and switch 1 in further up (red) and up (cyan) states of myosin. **(B)** Changes in the angle of the position of the lever (left panel) and the distance between switch 1 and switch 2 (right panel) throughout the molecular dynamic simulations of $_{doc}$A.M$_{up}$ (red), $_{rel}$A.M$_{up,R520Q}$ (blue) $_{rel}$A.M$_{up,R562Q}$ (green), $_{rel}$A.M$_{up,K622Q/K623Q}$ (pink) and as a control M$_{up}$ (black). Arg520Gln, Arg562Gln and Lys622Gln/Lys623Gln mutations interrupt the interactions of actin with activation loop, loop 3 and loop 2, respectively.

Transmission Pathways of Actin-binding Induced Conformational Changes: from activation loop to the nucleotide binding pocket and relay region

Upon analyzing the structural changes in myosin caused by actin-binding, we detected transmission pathways originating from activation loop and proceeding towards the nucleotide binding pocket and relay region through a central structural element, the wedge loop. When actin binds to myosin, the wedge loop forms interactions with the lower 50kDa helix-loop-helix (upper relay) region, the relay helix and the C-terminal region of switch 2 (**Figure 41**), structurally connecting these regions in the weak-binding actomyosin state. This connection between the upper relay and switch 2 does not exist in rigor state and in the absence of actin. When a salt bridge is formed between Asp1 of actin and Arg520 of activation loop in weak actomyosin state, Leu529 of the upper relay is positioned to be able to form a hydrophobic cluster with Trp584 of the wedge loop and Phe466 of the relay. Thereby, the repositioned Glu580 side chain of the wedge loop creates a salt bridge interaction with Lys462 of switch 2. This newly formed interaction pulls switch 2 to its further closed position. The relay helix is

reoriented and stabilized resulting in the further up position of the lever by the Leu529-Trp584-Phe466 hydrophobic cluster and the Glu580-K462 salt bridge. This reorientation of switch 2 and the relay does not occur in the activation loop mutant ($_{rel}$A.M$_{up,R520Q}$, **Figure 41**), while they remain in the same orientation in the loop 3   and loop 2 mutants ($_{rel}$A.M$_{up,R562Q}$ and $_{rel}$A.M$_{up,K622Q/K623Q}$, **Figure 41**). These results indicate that activation loop is a specific sensor of actin-binding and is responsible for transferring the information of actin-binding to the nucleotide-binding pocket and the relay/converter region.
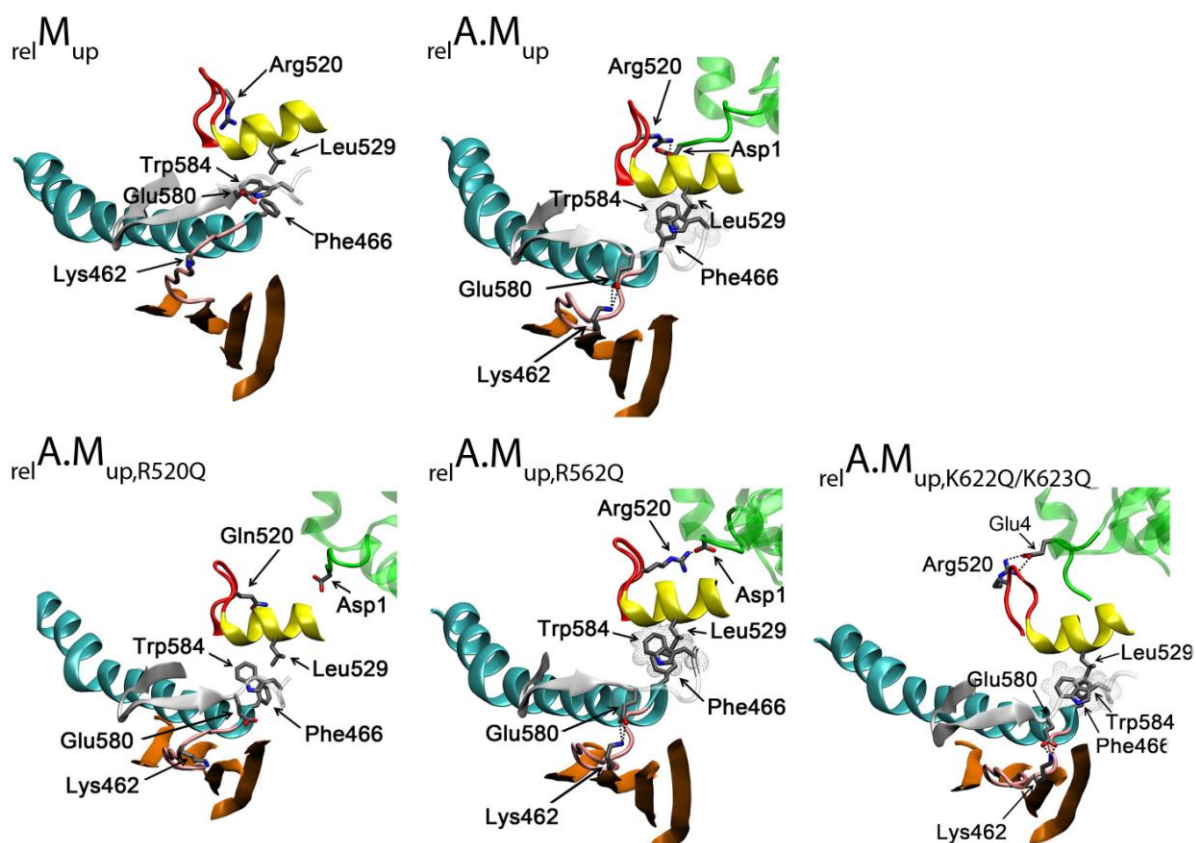
Figure 41. Transmission of structural changes from actin to the relay/converter and nucleotide-binding pocket. In the $_{rel}$M$_{up}$ structure, β-sheet (orange), switch 2 (pink) and the relay (cyan) are not connected through the wedge loop (gray) to the upper relay (yellow) and activation loop (red). As activation loop creates interaction with the N-terminal region of actin (green) in $_{rel}$A.M$_{up}$, a hydrophobic cluster (cloud) is formed between the upper relay, wedge loop and relay regions. Wedge loop is also repositioned, creating interaction with switch 2. In $_{rel}$A.M$_{up,R520Q}$ the hydrophobic cluster and wedge loop-switch 2 interactions could not form, while they are still present in $_{rel}$A.M$_{up,R562Q}$ and $_{rel}$A.M$_{up,K622Q/K623Q}$.

In summary, we have determined the atomic model of the weak actomyosin, up lever complex by *in silico* techniques. For the validation of the simulated weak actomyosin structure, rigor actomyosin complexes were also resolved and compared to experimentally determined rigor structures. We found that upon actin-binding, the closed switch 2 loop becomes more closed that is coupled to an 18 degree further up movement of the up positioned lever, resulting in an extra primed state of myosin. We also demonstrate the specific role of activation loop in the communication pathway between the actin binding site, the nucleotide binding pocket and

the converter domain. The presented extra primed weak-binding actomyosin model state, as the possible structure of the initial state of the powerstroke may lead to further experiments to reveal a more detailed reaction coordinate pathway of the powerstroke. Revealing the structures of further states of the powerstroke would help us to get closer to understand the mechanism of the powerstroke event.

3. Para-Azidoblebbistatin, the Tool for Cross-linking Myosin in its Different Structural States[10]

Modifying the Myosin II inhibitor Blebbistatin to 'Capture' an Intermediate State of the Powerstroke

As previously reported, blebbistatin could stabilize myosin in the presence of ADP in a
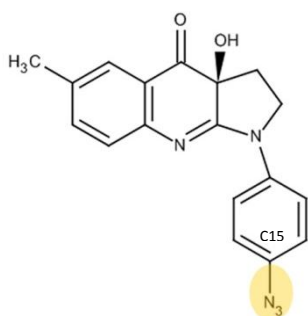
Figure 42. Para-azidoblebbistatin. The C15 of blebbistatin is substituted by an azido (N₃) group, at para position of blebbistatin's phenyl group.

yet unidentified structural state, that can be a possible starting point of the powerstroke [163], or an intermediate state of the parallel powerstroke pathways. Crystallization of myosin in the presence of ADP and blebbistatin has not been successful yet, due to the low affinity of blebbistatin to the M.ADP complex. We have synthesized the C15 substituted azido-derivative of blebbistatin, para-azidoblebbistatin (**Figure 42**) [186], which offers a solution to overcome this problem. The inhibitor was produced by a two-step reaction (**Appendix, Figure A1**).

Aryl azides are photo-inducible agents which enable covalent cross-linking to their targets upon irradiation. UV light irradiation induces the azido group to react with a nucleophile side-chain in close proximity (e.g. in the binding-pocket of its target molecule), as a result a covalent adduct is formed (**Figure 43**). This method proved to be successful in target identifications, receptor characterization and enzymatic studies [187]. By the help of para-azidoblebbistatin, the hurdle of the low affinity of blebbistatin to M.ADP can be overcome by saturating the enzyme through sequential covalent cross-linking with para-azidoblebbistatin in the presence of high excess of ADP.

---

[10] Synthesis of para-azidoblebbistatin, HPLC and LC-MS experiments were performed by my colleague, Miklós Képiró. Tryptic digestion of covalent myosin-azidoblebbistatin adducts were carried out by Prof. György Hegyi. Most results of this section of the study are published [Képiró, Miklós, et al. "Azidoblebbistatin, a photoreactive myosin inhibitor." Proceedings of the National Academy of Sciences 109.24 (2012): 9402-9407].
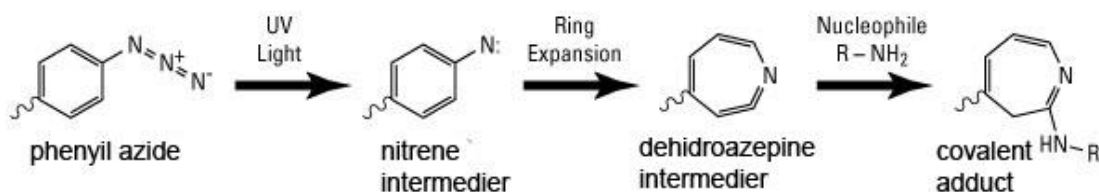
Figure 43. Photoactivation of aryl azides. Phenyil azide is activated by UV light to form a nitrene, then dehidroazepine intermediers. A nucleophile attacks the activated carbon of the expanded ring of the azepine intermedier and form a covalent adduct with it.

First, we investigated the spectral properties and photoreactivity of para-azidoblebbistatin, and applied 310 nm irradiation to activate the azido group. This wavelength caused a change in the absorption spectra of para-azidoblebbistatin (ABleb), but did not change the spectra of blebbistatin (Bleb) (**Figure 44**). Effective degradation of azidoblebbistatin at 310 nm was further validated by HPLC (**Appendix, Figure A2**).
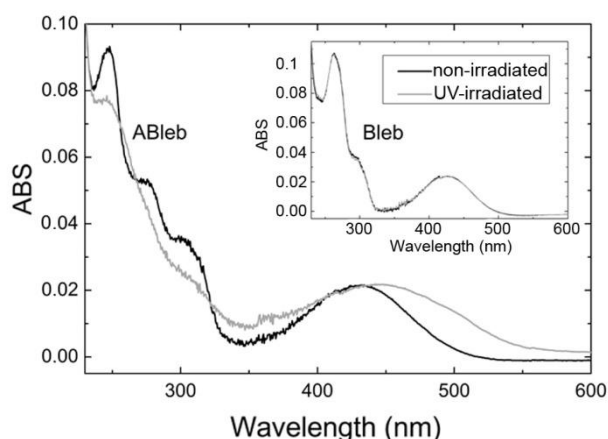
Figure 44. Spectral properties of para-azidoblebbistatin. The absorption spectra of ABleb was recorded before (black) and after (grey) irradiation. The spectra significantly changed after 310 nm irradiation, indicating the successful azide activation. Inset: absorption spectra of Bleb before and after UV irradiation, which spectra are practically the same.

Covalent Saturation of Myosin with ABleb in the Absence and Presence of ADP

We compared the inhibition of the basal steady-state ATPase activity of *Dd* MD by ABleb and Bleb in the absence of irradiation. The Bleb and ABleb concentrations at half of the maximal inhibition were similar ($IC_{50,Bleb}= 6.4 \pm 0.9$ µM and $IC_{50,ABleb}= 5.2 \pm 0.3$ µM), proving that the azido group did not influence the inhibitory properties of blebbistatin (**Figure 45**). Importantly, irradiation of ABleb before adding it to myosin completely abolished its inhibitory properties, while irradiation of Bleb did not have any effect on its inhibition (inset of **Figure 45**). Upon UV irradiation of the azido group, the phenyl ring suffers a ring-expansion, which completely destroys the structure of the molecule [188].
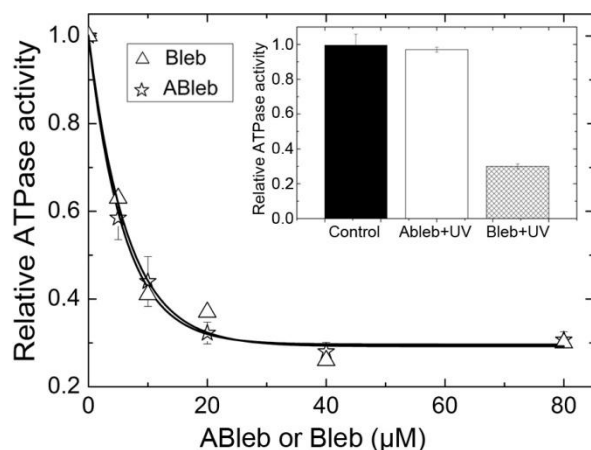
Figure 45. Inhibition of the basal ATPase activity of *Dd* MD in the absence of irradiation. Relative ATPase activities of *Dd* MD were measured at increasing ABleb or Bleb concentrations. Hyperbolic fit to experimental data yielded IC_{50} values of 6.4 ± 0.9 µM and 5.2 ± 0.3 µM for Bleb and ABleb, maximal inhibition was 71% and 70%, respectively. Inset: inhibitory effect of ABleb irradiated before addition to myosin (ABleb+UV) is abolished. Error bars represent ± s.d. of the mean values of at least three independent experiments.

Addition of ABleb to myosin and irradiation of the complex were performed sequentially several times, to saturate the enzyme with ABleb by covalent cross-linking (**Figure 46**). After each cycle, the inhibition of myosin's ATPase activity by ABleb was measured. Importantly, ATPase activity of myosin was only inhibited by the covalently cross-linked ABleb, as ABleb in solution was degraded completely. 310 nm irradiation of myosin in the same circumstances but in the absence of the inhibitor did not have any effect on the ATPase activity of the enzyme. After several cycles of ABleb addition and irradiation, saturation of inhibition of the ATPase activity of myosin was reached, where practically all myosin molecules were cross-linked to the inhibitor.
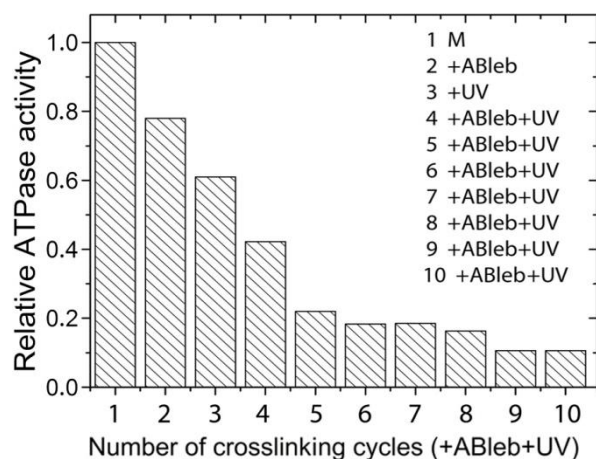
Figure 46. Inhibition of the basal ATPase activity of *Dd* MD in the presence of irradiation. Relative basal ATPase activity of *Dd* MD was measured after adding 10 µM ABleb to 8 µM myosin (2.), cross-linking with UV (3.) then repeating the cross-linking cycles by the addition of 10 µM ABleb and UV irradiation each time (4-10). Maximal inhibition of *Dd* MD ATPase was 90%. Inhibition was achieved only by the covalenly cross-linked ABleb, as ABleb in solution degraded completely.

We separated the covalent M.ABleb complex from the photodegraded ABleb in solution by using His-tag affinity chromatography. The His-tagged *Dd* MD coeluted with the covalently bound ABleb as a yellow-colored fraction (as ABleb and Bleb are yellow), providing further evidence for the covalent cross-link between them.

Covalent cross-linking of myosin with ABleb in the presence of excess of ADP (1mM) was achieved as described above. After saturating the extent of the inhibition of myosin (**Figure 47.**) by several cross-linking cycles, the M.ADP.ABleb complex was purified similarly to M.ABleb, but always in the presence of 1mM ADP.
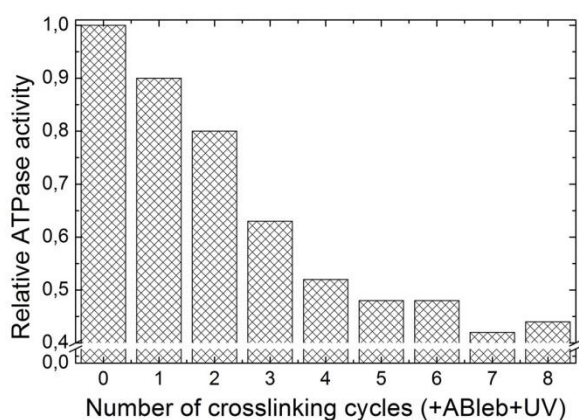
Figure 47. Covalent saturation of myosin with ABleb in the presence of ADP. Relative basal ATPase activites of *Dd* MD were measured after a series of crosslinking cycles with ABlebb in the presence of 1 mM ADP. 8 µM *Dd* MD was treated with 10 µM ABleb and 310 nm irradiation for the number of cycles indicated (1-8). Maximal inhibition of *Dd* MD ATPase in the presence of ADP was 57%.

Interestingly, the maximal extent of inhibition of myosin's ATPase by the covalently cross-linked ABleb in the presence of ADP was much less (57%) compared to the absence of nucleotide (90%).

For the crystallization of the M.ADP.ABleb, the purified complex was concentrated by centrifugation in concentrating tubes to 10 mg/ml protein concentration. The complex is being crystallized in collaboration with the laboratory of Anne Houdusse, Marie Curie Institute, Paris.

With the help of atomic structural information on one of the possible intermediate states of the powerstroke, we will be one step closer to understand the structural changes that occur during powerstroke. Until resolving the atomic structure of the M.ADP.ABleb complex, we were interested in whether ABleb has a similar binding-site on myosin in the presence of ADP as that of Bleb in the presence of $ADP.VO_4^{3-}$ revealed by the crystallization of the $M.ADP.VO_4^{3-}.Blebb$ complex [162].

Identifying the Myosin Binding-site of ABleb in the Presence of ADP

After purification of the M.ADP.ABleb complex (similarly to M.ABleb), we digested myosin with trypsin. The trypsin digested sample was analyzed by LC-MS, detecting the peptides at 260 nm and para-azidoblebbistatin at 410 nm. On-line detection revealed three peptides that had the mass of ABleb+peptide within 0.5 Da of difference compared to calculated values (**Table 13**). These were the peptides $_{419}DALVK_{423}$ or in the case of partial digestion $_{414}SSSSRDALVK_{423}$ and $_{588}NK_{589}$.

	measured mass (Da)	calculated mass (peptide + ABleb) (Da)	Δ mass (Da)
NK	566.000	261.156 + 305.115	0.271
DALVK	850.000	545.329 + 305.115	0.444
SSSSRDALVK	1355.000	1049.559 + 305.115	0.326

Table 13. Masses of the ABleb-bound peptides of *Dd* MD in the presence of ADP.

Identifying the peptides on the amino acid sequence of *Dd* MD, we determined the binding-site of ABleb in the presence of ADP (**Figure 48**). The binding peptides of ABleb in the presence of ADP are situated on the lower and upper, inner actin-binding cleft of the myosin molecule. We assume that the azido group of ABleb creates a covalent bond interaction with one of the lysines revealed in the binding peptides.
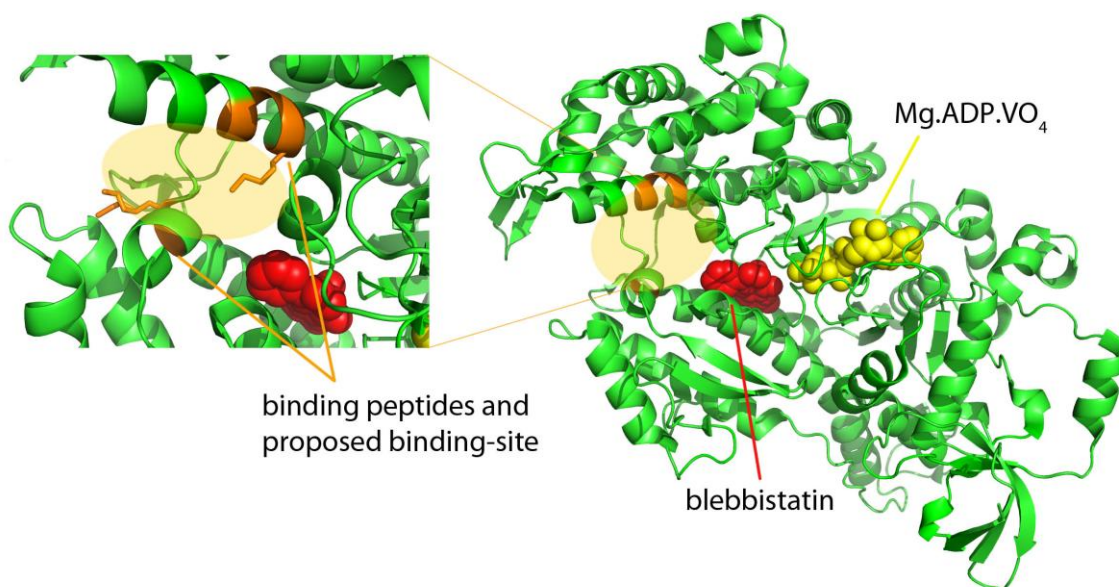
Figure 48. Binding site of ABleb on myosin in the presence of ADP. The ABleb binding peptides in myosin (orange) and the proposed binding-site (orange background) in the presence of ADP is presented in the M.ADP.VO$_4^{3-}$.Bleb crystal structure. The proposed binding-site of ABleb is enlarged in the inset, showing the Lys sidechains of the binding peptides (PDB code: 1YV3).

The binding-site of ABleb on myosin in the presence of ADP is very close to that revealed of Bleb in the presence of ADP.VO$_4^{3-}$ by crystallization the complex [162]. The blebbistatin binding site is in an aqueous cavity between the actin-binding cleft and switchI/switchII regions. Our results show the proposed binding site of ABleb to myosin in the presence of ADP to be closer to the actin-binding cleft, not so deeply buried as blebbistatin binding site in the M.ADP.VO$_4^{3-}$ structure. Before the crystallization of the M.ADP.VO$_4^{3-}$.Bleb complex, blind docking of blebbistatin to M.ADP.AlF$_4^-$ structure (1MND) resulted in localizing the binding site at a similar position as our proposed binding site in the presence of ADP [159].

Further validation of our results would be to covalently cross-link M.ABleb in the presence of ATP/ ADP.VO_4^{3-}, determine the binding site of ABleb and compare the results with that obtained from the crystal structure of M.ADP.VO_4^{3-}.Bleb. Additionally, the successful crystallization of the M.ADP.ABleb complex would reveal the binding site of ABleb to myosin in the presence of ADP, as well as offering insights into structural details of this intermediate state of the powerstroke.

In summary, we synthesized a new derivative of blebbistatin, para-azidoblebbistatin, which is able to covalently saturate low blebbistatin affinity states of myosin, such as M.ADP. Modification of blebbistatin by an azido group leaves the inhibitory properties of the molecule intact. The azido group can be activated by UV irradiation, thereby forming a covalent adduct with myosin. With the help of para-azidoblebbistatin, we proposed a binding site for ABleb on myosin in the presence of ADP. Our further aim is to reveal the atomic structure of M.ADP.ABleb, thereby also validating our proposed binding site.

VI. Discussion and Conclusions

In this chapter of the study, I would like to refer to the questions raised in the Scientific Questions and Aims section, thereby discussing our results.

Is there a key structural element in myosin responsible for its actin activation? What is the role of actin activation in vivo?

Activation Loop, specifically responsible for actin activation of myosin and in vivo force generation of muscles

In spite of decades of thorough investigations, the structural mechanism of actin activation and the functional role of it, tuning the efficiency of the actomyosin system, have been unrevealed. Here, we present a yet unidentified actin-binding loop of myosin, named activation loop, which interacts with the N-terminal segment of actin. We carried out thorough kinetic characterization of wild type and activation loop mutant *Dd* MDs, and revealed that activation loop is specifically responsible for actin activation of myosin. By abolishing the interaction between activation loop and actin, *in vitro* motility and actin activation of myosin could be uncoupled.

We examined the *in vivo* role of actin activation by applying transgenic *C. elegans* animals containing wild type and activation loop mutant body-wall myosin. The transgenic mutant animals retained the capability to move, although with a much slower speed compared to wild type or transgenic wild type worms. Additionally, activation loop body-wall myosin mutations almost completely abolished the force-generating capability of the animals. These results demonstrate, that force-generation of muscles *in vivo* is regulated by actin activation through activation loop-actin interaction, tuning the efficiency of the actomyosin system.

Activation loop is a conserved structural element, although its sequence and length varies among myosin isoforms, except for the positively charged amino acid at the tip of the loop found in all types of myosins. Actin activation can be tuned by the length of activation loop, as previously reported [120]. In that study, the proline-rich region of activation loop in chicken smooth muscle ($-Thr_{531}-Asn-Pro-Pro_{534}-$) was replaced by a single Met, leaving the conserved Arg529 of smooth muscle intact (homologue to Arg520 in *Dd*), thereby mimicking the activation loop of skeletal muscle myosin. Changing the sequence of activation loop from chicken smooth muscle to chicken fast skeletal muscle resulted in the increase of the actin activated ATPase (V_{max}) by 2-fold, while the unloaded *in vitro* motility also increased by 1.5-fold compared to the wild type. These results demonstrate that the ratio of working myosin

heads is tuned by activation loop to adapt different myosins to their different physiological functions.

Uncoupling actin activation and in vitro motility

The unique role of activation loop can be presented by comparing the effect of mutations in different actin-binding loops of myosin with activation loop mutations. The effect of the mutations on the actin activated ATPase activities and *in vitro* motility sliding speeds of myosin are summarized and presented below (**Table 14, Figure 49**).

wild type myosins and its mutations in actin-binding loops		actin activated ATPase, V_{max} (s^{-1})	relative actin activated ATPase[d]	*in vitro* motility (µm/s)	relative *in vitro* motility[d]
wild type[a]	–	1.78 ± 0.05	1	0.91 ± 0.20	1
Loop 2[a]	K652A	0.18 ± 0.02	0.10	0.45 ± 0.15	0.49
	K653A	0.59 ± 0.03	0.33	0.86 ± 0.16	0.95
	K652A/K653A	0	0	0	0
CM loop[a]	I407A	0.51 ± 0.03	0.29	0.7 ± 0.14	0.77
	V409A	2.04 ± 0.07	1.15	1.04 ± 0.2	1.14
	D412A	0.17 ± 0.01	0.1	0.27 ± 0.09	0.29
	V414A	0.66 ± 0.03	0.37	0.65 ± 0.13	0.71
H-loop[a]	W546A	0.114 ± 0.006	0.06	0.19 ± 0.07	0.21
	F547A/H	0	0	0	0
	P548A	0.046 ± 0.005	0.03	0.1 ± 0.08	0.11
wild type[b]	–	2.0 ± 0.1	1	0.41	1
Loop 3[b]	K576A/K578A	1.5 ± 0.1	0.75	0.38	0.93
H-loop[b]	W546A	0.12 ± 0.01	0.06	0	0
wild type[c]	–	5.1 ± 0.37	1	0.32 ± 0.15	1
activation loop[c]	R520Q	0.15 ± 0.01	0.029	0.43 ± 0.15	1.34
	R520E	0.27 ± 0.05	0.053	0.51 ± 0.18	1.59

Table 14. Actin activated ATPase activities and *in vitro* motilities of different wild type and actin-binding loop mutant myosins. Data was collected from studies on chicken gizzard smooth muscle myosin II [a]Onishi *et al* [121], [b]Kojima *et al* [120] and *Dictyostelium* myosin II [c]Várkuti et al [171]. [d]Values are relative to the wild type values of that study. Also see Figure 49.
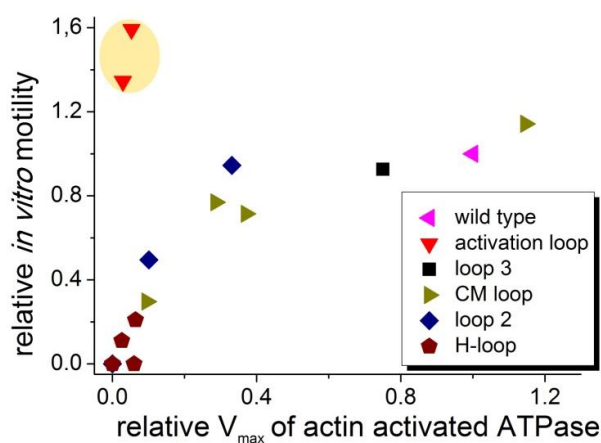
Figure 49. Relative actin activated ATPase activities and *in vitro* motility values of wild type and actin-binding loop mutant myosins. Relative values of *in vitro* motilities of actin-binding loop mutant myosins are plotted in the function of their relative V_{max} values of actin activated ATPase activities. All values presented are relative to the related wild type. Data is obtained from Table 14. Activation loop mutant myosins are highlighted with orange background.

A strong correlation can be detected upon plotting relative values of *in vitro* motilities of actin-binding loop mutant myosins in the function of the V_{max} of their actin activated ATPase activities (**Figure 49).** The different actin-binding loop mutations (except for activation loop mutation, red triangles) outline a hyperbole. Actin-binding loop mutant myosins at the saturation of the hyperbole move actin filaments in *in vitro* motility assays with similar velocities as that of the wild type, and can be activated by actin to different extents compared to the wild type value. There are two mutations outstanding from the curve depicted by other actin-binding loop mutant myosins, both of them are located in the activation loop (orange-shaded area). These activation loop mutations affecting the positively charged amino acid of the loop disrupt the salt bridge interaction with the N-terminal region of actin. As a result, activation loop mutant myosins are practically unable to be activated by actin, though fully retain the capability to move actin filaments *in vitro*. These activation loop mutations completely decouple actin activation of myosin from its capability to move actin filaments *in vitro*.

Rate-limiting steps of the actomyosin enzyme cycle

Steps of the actomyosin cycle different from the actin-attached up-to-down lever swing can be rate-limiting in the maximal actin activated ATPase activity and the unloaded actin sliding velocity. The rate-limiting steps can precede (e.g. hydrolysis step) or follow (e.g. ADP release) the powerstroke step (**Table 15**). Rate-limiting steps of the actomyosin cycle can also affect the processive features of myosins. In processive myosin V, phosphate release step coupled to the lever swing is the rate limiting process in the absence of actin, accelerated by actin to a much higher extent than the following ADP release step. Thus, in the presence of actin, the latter step becomes rate limiting. Therefore, if a mutation reduces ADP release of myosin V, its actin activated ATPase also decreases. Since ADP release directly determines velocity, sliding speed of actin filaments in *in vitro* motility assays also decreases [135, 177].

	rate-limiting steps of myosin enzyme cycle		
	in the absence of actin	in the presence of actin	in *in vitro* motility assays
Dictyostelium myosin II	up-to-down lever swing[a]	?[g]	ADP release[b]
myosin V	Pi release[c]	strong–weak-binding AM.ADP transition[d]/ADP release[e]	ADP release[f]

Table 15. Rate-limiting steps of the myosin enzyme cycle in two types of myosin under different conditions. Results obtained from [a]Gyimesi *et al* [145], [b] Murphy *et al* [189], [c] De La Cruz *et al* , [d]Jacobs *et al* [190], [e]De La Cruz *et al* [148] and [f]Nagy *et al* [135]. [g]There is no experimental evidence for the rate-limiting step in the enzyme cycle of *Dictyostelium* myosin II in the presence of actin.

If another mutation reduces the hydrolysis step below the rates of the actin-attached up-to-down lever swing (coupled to phosphate release) and ADP release, the actin activated ATPase activity will be limited by the hydrolysis step. However, since hydrolysis step takes place in an actin-detached state, its change does not influence the limiting step of motility – ADP release – , resulting in unchanged motility values [178, 179]. Thus, in this case velocity and steady-state actin activated ATPase activity will become uncoupled similarly to activation loop mutations, although for a different reason. We note that the network of biochemical pathways of myosin is very complex in actin attached states, as lever movement, actin binding cleft closure, weak-to-strong actin binding transition and products' releases occur in a coupled manner [156, 191]. These networks become even more complicated if we consider the different extents of load dependency of these steps. A major issue for future research is to reveal this complex pathway network and unravel the different coupling mechanisms that regulate the motor functions to adopt the myosin isoforms to their biological functions.

What are the myosin residues that interact with the N-terminal segment of actin?

The interacting partner of activation loop: the N-terminal region of actin

N-terminal mutants of actin acting on wild type myosin showed similar results in actin activated ATPase assays and *in vitro* motility tests as activation loop mutant myosins in complex with wild type actin. In one study, the two acidic residues of the N-terminus of yeast actin (Ac-Met_1-Asp-Ser-Glu_4-) were either neutralized (Ac-Met_1-Asn-Ser-Gln_4; DNEQ mutant) or the whole N-terminal segment was deleted (Δ-DSE) [130]. The actin mutants could not activate rabbit skeletal muscle myosin II S1, though retained similar sliding speeds to the wild type actin filaments. By covalent cross-linking of rabbit skeletal acto-S1 with dimethyl suberimidate (DMS), the ATPase activities of myosin with the mutant as well as wild type actin constructs increased (**Table 16**).

	maximal actin activated ATPase of myosin (s^{-1})	
	uncross-linked	cross-linked
wild type actin	0.1	0.8
DNEQ actin	0.05	0.4
Δ-DSE	0.05	0.5

Table 16. Myosin ATPase activities activated by wild type and N-terminal mutant actins. Uncross-linked ATPase of myosin activated by wild type and mutant actins elevated 8-10-fold upon cross-linking with DMS for the same length of time. Data obtained from [130].

The authors concluded that low actin activation of myosin by the mutant actin constructs was due to the decreased affinity of the mutant actins to myosin. However, the

ATPase activity values of myosin cross-linked to the mutant actin constructs were below the ATPase values of myosin cross-linked to the wild type actin, indicating that actin affinity alone cannot be the reason behind the low actin activation of myosin by the mutant actins. In the light of our study, their data supports that the lack of actin N-terminal-activation loop interaction hinders the efficient channeling of myosin heads by actin to the effective powerstroke pathway.

In another study, two additional negatively charged residues were engineered into yeast actin N-terminus, resulting in four acidic amino acids (4Ac mutant) [192]. 4Ac mutant actin construct elevated the ATPase activities of rabbit skeletal myosin S1 by two-fold, while retained *in vitro* motilities similar to the wild type. Cook *et al* possessed no knowledge of the myosin structural element interacting with the N-terminal region of actin, and could not explain the detected effects upon the manipulation of actin N-terminal region. However, their results can be explained by our observations. As myosin heads can be tunneled to the effective powerstroke pathway through the actin N-terminal segment–activation loop interaction, when the 4Ac mutant actin was applied to activate myosin, an increase could be detected in the overall steady-state ATPase activity of myosin. Nevertheless, in the *in vitro* motility assay they could only detect the results of the effective powerstrokes creating the sliding of the actin filaments. As the rate of the powerstroke did not increase and the motility of the filaments is limited by other steps of the enzyme cycle, they did not detect the increase of the sliding speeds of the actin filaments upon applying the 4Ac mutant actin to myosin.

What is the structure of the initial state of the powerstroke?

The actomyosin structural model of the initial state of the powerstroke

The mechanism of the powerstroke has been proposed on the basis of comparing pre-powerstroke crystal structures with pseudoatomic cryo-EM map-based atomic rigor models [111, 116-118], although the actomyosin structures of the initial or end states of the powerstroke are unknown. The pre-powerstroke state is an actin detached, up lever myosin head in complex with an ADP.Pi analogue (1MMD, 1VOM, 2V26), which cannot be considered as the initial state of the powerstroke, since effective powerstroke must start in an actin-attached state [156]. The major structural change induced by actin binding to pre-powerstroke state myosin was considered to be the closure of the actin-binding cleft [95], initiating rearrangements in the nucleotide binding pocket which leads to the powerstroke. As the initial powerstroke state, $A.M_{up}.ADP.Pi$, has a short lifetime and low abundance in transient kinetic and steady-state experiments, its structural investigation is highly challenging. Therefore, we created the atomic model of the initial state of the powerstroke, $A.M_{up}.ADP.Pi$

($_{rel}$A.M$_{up}$) by *in silico* techniques, representing the missing structure after step 3 of the Lymn-Taylor cycle (**Figure 50**). In addition, we also created rigor actomyosin models to validate our weak-binding actomyosin structure. We found, that actin-binding to pre-powerstroke state myosin induced the extra priming of myosin i.e. further up movement of the lever and further closure of switch II loop. We also revealed the structural communication pathway originating from the N-terminal region of actin through activation loop towards the nucleotide-binding pocket and relay/converter region. Actin-binding to *Dictyostelium* apo state induced the further closure of its half-way closed actin-binding cleft, and induced a further down movement of the lever of squid rigor-like state.
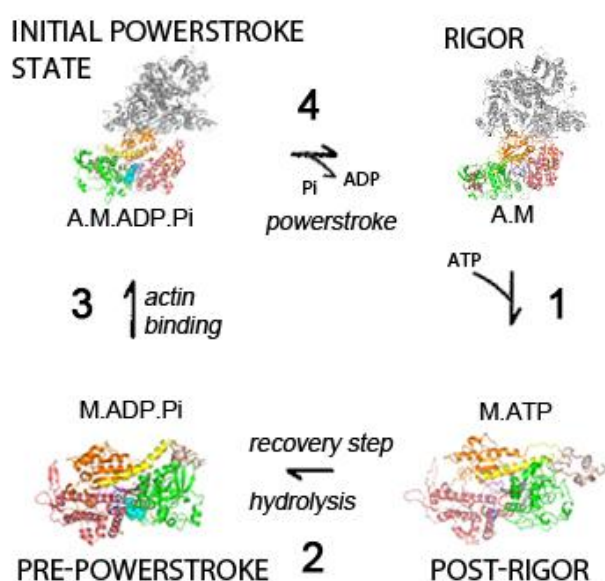
Figure 50. Structural states of the Lymn-Taylor cycle – creating the initial powerstroke state and rigor actomyosin atomic models. We have created an atomic structural model of weak-binding actomyosin, hitherto structurally unrevealed initial state of the powerstroke. We have created strong-binding rigor actomyosin models as well. Actin trimer is grey, while *Dd* MD colored accordingly.

Interactions of actomyosin and the role of activation loop in the formation of the extra primed state of myosin

We presented, that weak actin-binding of myosin is initiated by the lower 50 kDa subdomain, including loop 3, H-loop and activation loop. Loop 3 creates interactions with two actin monomers, as also presented in previous studies [114, 126]. Loop 2 seems to have a role in the weak-to-strong actin-binding transition, as indicated by structural and mutational studies depicting the dynamic interactions of loop 2 with different regions of actin in the different states of actomyosin [122, 193]. We also found, that loop 2 is positioned differently in rigor and weak actin-binding states. Within the weak-to-strong actin-binding transition of myosin, loop 2 competes with activation loop for the highly negatively charged N-terminal region of actin, while also interacting with other regions of actin (Asp24/25). Recently, the activation loop– actin N-terminal interaction was verified by a model of the rigor actin-myosinIE

complex, where a similar 'sandwich-like' pattern of charged residues was detected: actin (Asp_{24}-Asp_{25})– loop2 (Lys_{556}-Lys_{557})– actin N-terminal region (Asp_1-Glu-Asp-Glu_4)– activation loop (Lys_{450}-Lys_{451}, myoE numbering) [117]. Previous rigor models lack the N-terminal segment of the applied actin structure, missing the interaction of activation loop with actin [111, 116, 118].

Upon molecular dynamics of the weak actin-binding, up lever myosin structure we found that actin-binding causes the structural relaxation of the myosin structure. We note, that conformational relaxations are not hindered by free energy barriers, thus occur at the nanosecond timescale, therefore they must be distinguished from first order kinetic steps. The major structural rearrangements occurred in the relay/converter/lever region and the switch 2 loop: an 18° further up lever movement coupled with a further closure of the switch 2 loop. A minor actin binding cleft closure was also detected upon molecular dynamics relaxation. We demonstrated that activation loop has an essential role in the extra priming of myosin, since actin induced conformational changes are transmitted through activation loop towards the relay and the nucleotide-binding site. This structural finding explains the specific role of activation loop in actin activation of myosin, providing structural explanation for the mechanism of actin activation, which proceeds through an extra primed state of myosin. The disruption of activation loop–N-terminal actin interaction eliminates the extra primed state, which results in the lack of actin activation. These findings indicate, that powerstroke is not the reversal of the recovery stroke, the actin-detached priming of the lever. Actin-binding restructures the reaction coordinates and channels lever arm swing through a different route as that of found in the priming of the lever. Additionally, structural models of myosin VI indicate that powerstroke may occur after phosphate release [194, 195]. As according to experimental evidence, in the absence of actin lever swing precedes phosphate release [145], thereby it is suggested that besides accelerating the lever swing, actin-binding also restructures the sequence of events compared to the actin-detached reverse recovery stroke.

Intriguingly, myosin VI in the absence of actin, complexed with $ADP.VO_4^{3-}$ (2V26) is highly similar to myosin II in the presented structure of $_{rel}A.M_{up}$, possessing a further primed lever and a further closed switch II [194] (**Figure 51**). The resemblance of myosin VI structure to the extra primed myosin state of the initial actomyosin structure of the powerstroke indicates that myosin structures are highly dynamic and discover several possible structural states in equilibrium systems.
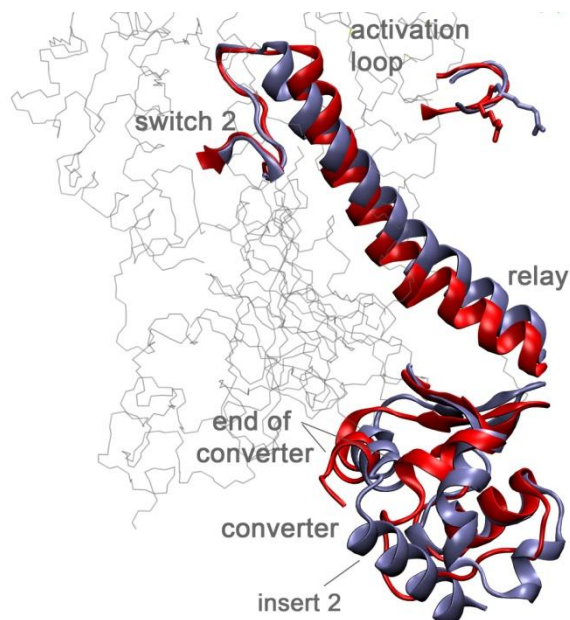
Figure 51. Comparison of the extra primed state of myosin II and myosin VI. Activation loop, switch 2, the relay and the converter region are highlighted from myosin (gray). Myosin VI pre-powerstroke state (2V26, blue) possesses a similar, or even more further primed lever and further closed switch 2 compared to $_{rel}$A.M$_{up}$ (red). The two myosin structures were aligned by their backbones. As myosin VI is a reverse motor, its converter is elongated by a structure named insert 2, which repositions its lever.

An experimental approach for the detection of the extra primed state in vitro

Although direct experimental investigation of the extra primed myosin state is challenging, it would provide experimental evidence for the results of our *in silico* simulations. Our future attempt is to detect the extra priming of the myosin lever *in vitro*, by the use of FRET (Förster Resonance Energy Transfer). The concept lies on an experimental design, which enables direct detection of the lever arm movement of myosin. In this approach, GFP is fused to the C-terminal of *Dd* MD, which acts as a lever (**Figure 52**). The connection can be either rigid, or flexible, by the introduction of glycines into the linker between GFP and myosin. The N-terminal of *Dd* MD is lengthened by the binding sequence of a FRET pair of GFP, FlAsH, AsCy3 or ReAsH biarsenical dyes [196-199]. Biarsenical dyes have been successfully used for intracellular localization of proteins and protein co-localization studies in intact cells [200-202], and their application for FRET-based structural studies of proteins has been recognized recently [203-205].
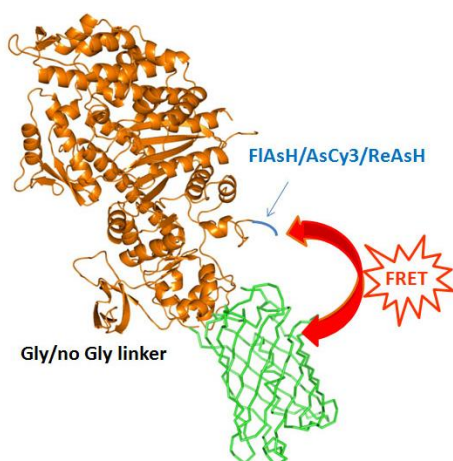
Figure 52. The concept of detecting lever movement directly. GFP (green) is fused to the C-terminal of *Dd* MD (orange). The N-terminal of *Dd* MD contains the binding sequence of a biarsenical dye (FlAsH, AsCy3 or ReAsH), which is a FRET pair of GFP. Movement of GFP, acting as a lever, could be monitored directly through the fluorescence change in FRET signals.

As the N-terminus of *Dd* Md is located next to the base of the lever (29.2 Å in pre-powerstroke, 32.7 Å in the extra primed and 23 Å in rigor states, measured between the Cα of Asn_2 and Arg_{747}), the movement of GFP can be detected by stopped-flow on a transient level by the fluorescence change in FRET signals. We have followed the down-to-up movement (recovery) of the lever upon ATP addition to *Dd* MD, simultaneously detecting the FRET-based fluorescence change of GFP and ReAsH, by exciting GFP (**Figure 53**).
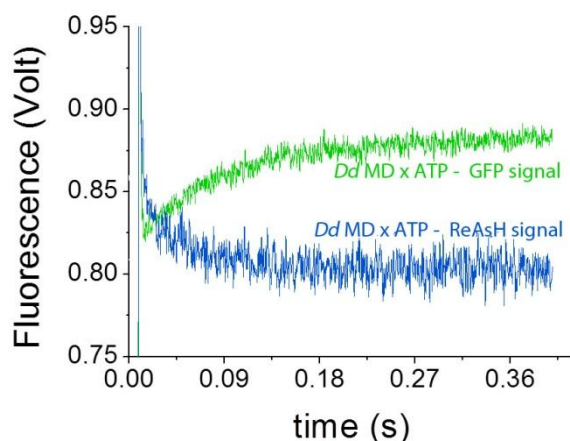
Figure 53. Detecting lever movement directly by FRET. *Dd* MD was mixed with 1 mM ATP, and the fluorescence change of the two fluorophores was detected in time by stopped-flow on 20°C. Excitation was accomplished by a 450±20 nm interference filter, while emissions were detected by a 500±10 nm (GFP signal) and 600±10 nm interference filters. The fitted exponentials to the curves yielded observed rate constants to be 15/s (GFP signal) and 19/s (ReAsH signal).

Lever movement has never been detected directly before, and we hope that by the help of this experimental approach, intriguing questions of the myosin enzyme cycle could be answered. Our main aim is to detect the extra priming of the lever in the initial state of the powerstroke, by performing double push experiments with stopped-flow, mixing myosin with ATP in single turnover conditions, then rapidly mixing the M.ADP.Pi complex with actin. Additionally, on the same concept, it would be possible to separate lever movement and Pi release upon actin-binding to myosin pre-powerstroke state. Such experiments would be closely related to a recently published study by Muretta *et al* [155]. They detected the bending of the relay (which is closely related to lever movement) by FRET and also Pi release upon actin-binding of M.ADP.Pi. They found that relay movement precedes Pi release in the powerstroke of *Dictyostelium* myosin II. It would be challenging to confirm or disprove their findings upon detecting the lever movement directly by our approach.

What is the structure of the M.ADP.Bleb complex?

Para-azidoblebbistatin, the photoreactive myosin II inhibitor enabling the crystallization of the M.ADP.Bleb complex

By synthesizing para-azidoblebbistatin, we were able to covalently cross-link myosin with blebbistatin in the presence of ADP and populate myosin with ABleb. The crystallization of the M.ADP.ABleb complex would reveal a yet unidentified structural state of the parallel

powerstroke pathways. We have identified a possible binding site of ABleb to myosin in the presence of ADP, in a similar position to that of blebbistatin in the presence of $ADP.VO_4^{3-}$.

Para-azidoblebbistatin is the first photo-inducible myosin inhibitor. Its advantage extends beyond the covalent saturation of low blebbistatin affinity structural states of myosin enabling the discovery of unknown states of the myosin enzyme cycle. Although blebbistatin is a myosin II specific inhibitor, it has other, weak-binding partner proteins as well. It was found, that besides myosin II, blebbistatin inhibits myosin II independent processes in wild type *Dictyostelium* cells e.g. macropinocytosis and phagocytosis [206]. They observed myosin II aggregates upon blebbistatin inhibition, which also formed when only inactive myosin II was expressed in cells, where macropinocytosis and phagocytosis was also inhibited. They concluded that myosin II aggregates indirectly inhibit myosin II independent processes. With the help of para-azidoblebbistatin, we were able to map all strong- and weak-binding partners of blebbistatin in *Dictyostelium* cells (**Table 17**) [186].

protein	myosin II	vacuolar H^+-ATPase A subunit and RNA-binding region RNP-1 domain-containing protein	Elongation factor 1α	hypothetical protein (DDB G0275045) and malate dehydrogenase
IC50 (µM)	5.1 ± 1.4	50 ± 31	>100	55 ± 17

Table 17. Strong and weak-binding proteins of para-azidoblebbistatin in *Dictyostelium* cells. Interacting partners of para-azidoblebbistatin were identified by cross-linking, SDS/PAGE and MS analysis of the fluorescent bands detected on SDS/PAGE. In two cases, MS revealed more than one type of azidoblebbistatin-protein complex in the band of the SDS/PAGE.

These results indicate, that blebbistatin at high concentrations (100 µM or 150 µM used in [206]) does interact with other proteins besides myosin II. Additionally, the aggregates detected in their study may be formed by blebbistatin, as it has a low solubility in aqueous buffers (at 25 °C it is 7.4 ±0.6 µM at 0.1% DMSO, and it increases linearly with DMSO concentration to 80 µM at 10% DMSO [186]). Thus, the azido substituted cross-linkable variant of blebbistatin could be effectively applied at low concentrations (using cross-linking cycles) to eliminate cellular effects arising from low-affinity interactions or from solubility problems of blebbistatin. Azidation technology may also provide a useful technique to determine all binding partners of small molecules together with their apparent binding constants as well [186].

In the absence of UV irradiation, para-azidoblebbistatin exhibits identical inhibitory properties as that of blebbistatin, proving that the C15 substituted azido group did not influence the effect profile of the inhibitor. Visualizing the azido group on blebbistatin in the

M.ADP.VO$_4^{3-}$.Bleb complex demonstrates that the azido group does not cause steric hindrance of the inhibitor (**Figure 54**).
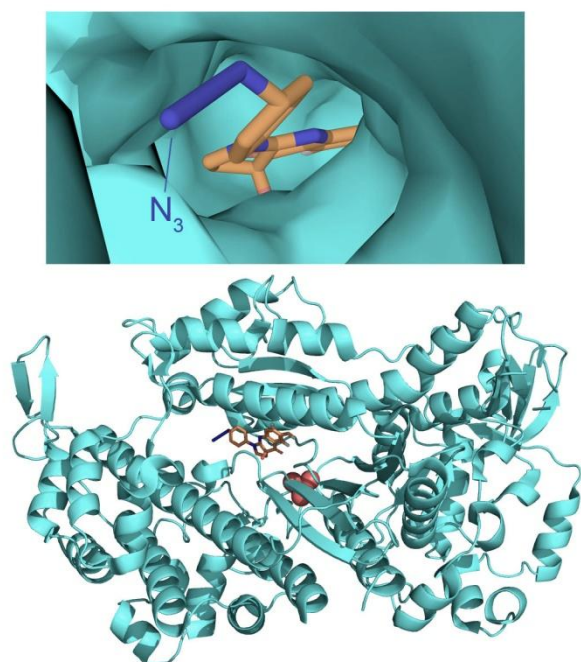
Figure 54. The structure of the myosin.ADP.VO$_4$.blebbistatin complex extended with an azido group at the C15 position of blebbistatin. Myosin residues form a cavity halfway from the nucleotide-binding pocket to the actin-binding cleft, where the binding site of blebbistatin is situated. Blebbistatin and ADP.VO$_4$ are shown by stick and space-fill representations, respectively. Inset: blebbistatin fits well into the binding pocket, together with the inserted azido substituent on the C15 position, even without energy minimization and molecular dynamic relaxation of the complex. (PDB code: 1YV3)

Improving the characteristics of blebbistatin

In spite of the widespread use of blebbistatin in developmental biology, cell motility or cancer research [162, 207-209], the inhibitor has serious limitations. Blue light irradiation (450-490 nm) causes photoconversion and citotoxicity of blebbistatin. It induces structural changes within the molecule, which are accompanied by the generation of reactive oxygen species [210]. Blebbistatin's own fluorescence hinders the detection of fluorescent signals, such as GFP. Additionally, slow precipitation of blebbistatin in aqueous media (due to its low water solubility) hampers fluorescent imaging and blocks the circulatory system of organisms in *in vivo* studies [211]. By the substitution of blebbistatin at its C15 position with an azido group, we reduced its fluorescence. Additionally, we have observed that para-azidoblebbistatin is not phototoxic on *Dictyostelium* or HeLa cells at blue light illumination where blebbistatin has severe effects on cell mortality. Moreover, we retained blebbistatin's inhibitory properties on myosin II (6.4 ± 0.9 μM and 5.2 ± 0.3 μM for Bleb and ABleb, respectively). In contrast, by the attempt to increase blue light photostability of blebbistatin, the C7 substitution of blebbistatin's tricyclic ring with a nitro group resulted in reduced affinity of myosin to the derivative significantly (27.5 ± 3μM) [212]. On the other hand, it resulted in a reduced fluorescent, photostable and non-photocitotoxic derivative of blebbistatin. These results suggest, that the substitution of the C15 position of blebbistatin by an electron-withdrawing group (cloro or nitro) may result in a non-fluorescent, photostable, non-photocitotoxic and

retained inhibitory featured myosin II inhibitor. Our yet unpublished results of a C15 nitro substitution of blebbistatin (para-nitroblebbistatin) provides all of these qualities. As it is not photoreactive as the azido derivative, para-nitroblebbistatin can serve as a comprehensive replacement of blebbistatin in every aspect by its improved characteristics in experiments where the reversible effect of the inhibitor is essential.

VII. Final Conclusion

Structural Background of Force Generation in Myosins and Allosteric Regulation of Motor Proteins

Despite functional differences between myosin isoforms, they share a common mechanistic framework of kinetic pathway selection mechanism. A manifestation of the kinetic pathway selection can be seen in the case of actin activation of myosin, which is enabled by the discovered interaction between activation loop and actin N-terminal region described in this study (**Figure 55**). Structural communication pathways are initiated by activation loop– actin interaction from the actin-binding region towards both the nucleotide-binding pocket and relay/converter region of myosin. The structural reorientations of these regions induce an extra primed state of myosin in the initial powerstroke actomyosin complex, which structural state has not been resolved until now. An intermediate state of the powerstroke, the M.ADP.ABleb complex awaits for its structure to be revealed by crystallographers. Further knowledge of the structures of the parallel powerstroke pathways, of the routes a myosin can explore through its enzymatic cycle will lead us towards the understanding of the mechanism of powerstroke and the allosteric activation of myosin (**Figure 55**).
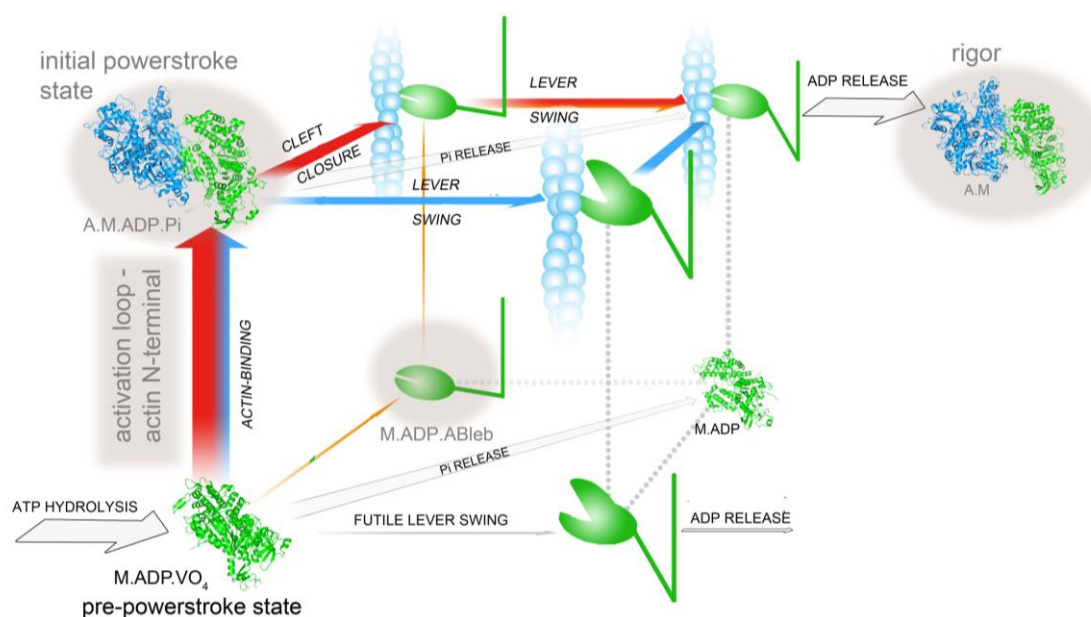
Figure 55. The different structural states in the mechanistic model of parallel powerstroke pathways. Known and unknown structures of different states of the mechanistic model are showed by cartoon or schematic representations of the myosin motor domain (green) and actin (blue), respectively. The structural states resolved in this study or contributions to reveal a structure (initial powerstroke state, rigor and M.ADP.ABleb) are highlighted by grey background, as well as activation loop–actin interaction, which enables the allosteric activation of myosin by actin. The widths of the arrows represent the relative fluxes of the pathways. The red, blue and orange pathways are three possible routes of the powerstroke. Modified on the basis of [156] (PDB codes: 1VOM, pre-powerstroke; 1MMA, M.ADP)

The mechanistic knowledge of myosin's actin activation will help us to understand the general mechanism of allosteric activation among P-loop NTPases, such as kinesins, dyneins, DNA and RNA polymerases, initiation and elongation factors in ribosomal translation and signaling enzyme complexes [213-215]. Upon receptor binding of the signal recognition particle SRP54, it goes through a conformational change that leads to the activation of GTP hydrolysis and the translocation of the cargo protein through the endoplasmic reticulum [215]. The high fidelity of protein synthesis is also ensured by kinetic pathway selection mechanism of translation factors. When the correct codon-anticodon complex is formed, the elongation factor Tu− aminoacyl-tRNA complex is allosterically activated, inducing aminoacyl-tRNA transfer and peptide bond formation. In case of DNA polymerases, after the formation of the correct Watson-Crick geometry, DNA activates a rate-limiting conformational change which results in the chemical displacement of the nucleotide. This mechanism is also an example of providing high fidelity during replication. All of these examples represent a similar mechanism of allosteric activation, providing the high efficiency of various systems through the population of productive complexes. This similarity may reflect similar structural backgrounds that would reveal further evolutionary conserved functions of P-loop NTPases.

VIII. Materials and Methods

Constructs and Cloning

W501+ *Dd* MD construct has one Trp at the 501 position in the myosin motor domain, which is sensitive to conformational changes occurring at the base of the lever arm [142]. Other native Trp amino acids in the motor domain (Trp36, Trp432 and Trp584) were changed to Phe (**Figure 56).**
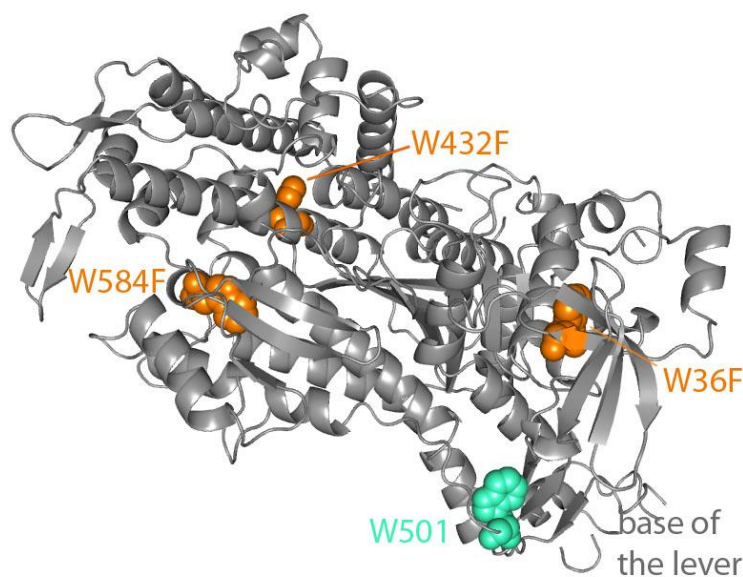
Figure 56. The W501+ *Dd* MD construct. The construct applied as wild type for the experiments contains a single tryptophan in the W501 position, at the base of the lever.

The W501+ *Dd* MD construct starts with a D_1GTEDP_6- motif and continues with the first 761 amino acids of the wild type *Dd* myosin II [180] and ends in an additional LGSTRDALH$_8$ sequence at the C-terminus, containing a His-tag. The W501+ *Dd* MD is referred to as 'wild type' (MD$_{wt}$), as its kinetic parameters are identical to the wild type *Dd* MD [142, 143, 177]. The *Dd* MD was cloned into pDXA-3H plasmid [216]. This plasmid is a shuttle vector that can be used in prokaryotic and eukaryotic systems as well. It contains the origo to replicate in *Escherichia coli* (*E. coli*) as well as an ampicillin resistance gene (β-lactamase) to be able to select with ampicillin the *E. coli* cells that contain the plasmid. It also has a replication origo for *Dictyostelium discoideum*, a constitutive actin promoter and terminator with STOP codon, with the myosin II motor domain sequence located in between. Its geneticin resistance gene enables the selection of *Dictyostelium* cells containing the plasmid.

Site-specific mutagenesis applying PCR was used to generate activation loop mutations in W501+ *Dd* MD. The following primers were used for each mutation, with red labeling the site of the mutations:

1. MD$_{\Delta519-523}$: 5'-GCCACTATCGATTTAATTGAT△GGTATTTTAGCTCTTTTGGATGA
ACAATCTGTTTTCCC-3'

2. MD$_{R520E}$: 5'-CGATTTAATTGATGGTGAACAACCACCAGG-3'

3. MD$_{R520Q}$: 5'-CGATTTAATTGATGGTCAACAACCACCAGG-3'

4. MD$_{R520K}$: 5'-CGATTTAATTGATGGTAAACAACCACCAGG-3'

Nucleotide changes favored *Dictyostelium*-specific codon usage. The PCR was carried out in two steps, with a megaprimer method (**Figure 57. and 58.**). In the first PCR, the mutant forward and a wild type reverse primer was used, resulting in an incomplete DNA sequence of the myosin II motor domain gene, but already containing the mutation (mutant megaprimer). In the second PCR the product of the first PCR is used as the reverse primer with a wild type forward primer. The product of the second PCR contains the whole sequence of the *Dd* MD.
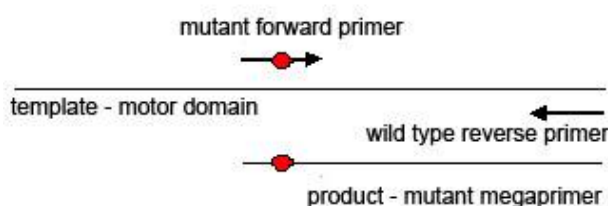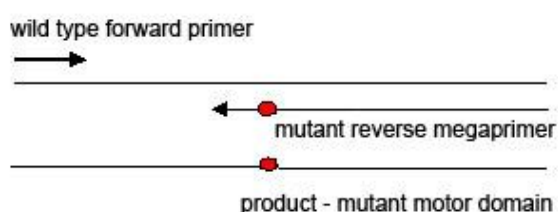
Figure 57. The megaprimer PCR method. After the two-step PCR, the mutant motor domain product was obtained. The site of the mutation is indicated with red circles.

The mutant myosin motor domain genes were cloned into pDXA-3H by restriction and ligation (Eco72I, BpiI and T4ligase, *Fermentas* protocol). DNA separation was carried out by agarose gelectrophoresis (1 m/V % agarose, 120 mA) in TAE buffer (40 mM Tris-acetate pH 8, 1 mM EDTA), DNA was detected by SYBR Safe (*Invitrogen*) and 0.5 µg/µl DNA ladder (Generuler 1 kb DNA ladder, *Fermentas*) and DNA loading dye (6-fold dilution, *Fermentas*) was applied as well. DNA isolation was performed with QIAquick Gel Extraction Kit (*Qiagen*). The amplification of the plasmids containing the mutant motor domain constructs was carried out in DH5α strain of *E. coli*. QIAprep MiniPrep Kit (*Qiagen*) was used for the isolation of the plasmids from bacterial cells.
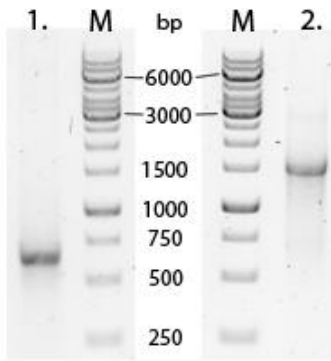
Figure 58. PCR products visualized after agarose gel-electrophoresis. The first PCR product (1.) was 604 basepairs (bp) long, while the second PCR resulted in a product of 1455 basepairs (2.), also verified by the DNA marker (M). Visualization of DNA was achieved by dying with SYBR Safe and UV illumination of the gel.

Mm myosin Va S1 cDNA of the N-terminal 820 amino acids of myosin gene was cloned into pFastBac1 baculovirus transfer vector containing Flag-tag (DYKDDDDK) that is fused with the C-terminal of the protein upon translation. This plasmid (constructed by collaborators) was used to generate K502E mutation with QuikChange II XL Site-directed Mutagenesis Kit (*Stratagene*), using the following primer, with red indicating the site of mutation:

myo5$_{K502E}$: 5'- CCTTGTATCAATCTTATAGAATCTGAGCTGGGAATTCTCG-3'

Plasmids containing mutant myosin Va S1 construct were amplified in XL10Gold ultracompetent cells.

C. elegans body-wall myosin gene, *unc-54* (WBGene00006789) with 4400 basepairs of promoter region, introns and exons was used to generate K525E mutation. Wild type and mutant unc-54 were cloned into pPD95.77 expression vector (through SalI and SphI restriction sites) containing a C-terminal GFP fusion protein and a 3' UTR region for proper expression (**Figure 59**.). After amplification of plasmids in DH5α bacterial cells, they were bombarded into *unc-54(e1092) C. elegans* strains (*Δunc-54*) (from Caenorhabditis Genetics Center) by microparticle bombardment.
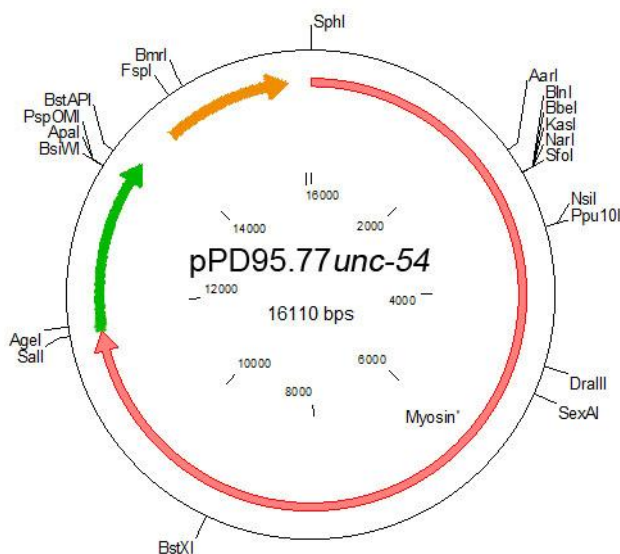
Figure 59. The plasmid map of pPD95.77 containing *unc-54*. *Unc-54* (red) is expressed with a C-terminal GFP (green) fusion. Ampicillin (orange) resistance gene can also be found on the plasmids. The restriction sites of endonucleases are indicated.

Protein Expression and Purification

Wild type and mutant *Dd* MD plasmid constructs were electroporated (Gene Pulser II, *Bio-Rad,* protocol for *Dictyostelium discoideum*) into *Dictyostelium* cells and expressed in cell cultures. Cells were grown by shaking (150 rpm, 21°C) in HL-5 medium (*Formedium*) complemented with penicillin-streptomycin (Sigma, in 100-fold dilution), glucose (12,4 g/l) and geneticin (0,03 mg/ml, *Gibco*) until reaching $4x10^6$/ml cell concentration . Cells for protein purification were collected by centrifugation (7 minutes, 2700 rpm, Jouan KR22i, 4°C) and washed with PBS buffer (10.1 mM $Na_2HPO_4.7H_2O$, 18 mM KH_2PO_4, 1.4 mM NaCl, 27 mM KCl, pH 7,3). After weighing the cells, 4ml/g lysis buffer was added to them (50 mM Tris-HCl, pH 8, 2 mM EDTA, 0.2 mM EGTA, 1-3 mM DTT, 5 mM benzamidin, 2000-fold diluted protease inhibitor mix: 15 mg pepstatin, 2 mg leupeptin, 66 mg TPCK, 25 mg TLCK, 66 mg PMSF in 1 ml DMSO). Total cell lysis was achieved by adding 2 ml/g lysis buffer containing 1 V/V% Triton-X100 (*Sigma*) and sonication (4x2 minutes, 70% performance, *Sonifier 250, Branson*). After 1 hour of incubation on ice, cell lysates were ultracentrifuged (60 minutes, 55000 rpm, Beckman L7-65, 4^{0}C) and the pellets were washed with extraction buffer (50 mM HEPES, pH 7.3, 30 mM potassium acetate, 10 mM magnesium acetate, 3 mM mercaptoethanol, 5 mM benzamidine, 40 mg/ml PMSF). After a second round of ultracentrifugation (45 minutes, 45000 rpm, 4^{0}C) the pellets were homogenized in 1.6 ml/g extraction buffer containing 20 mM ATP and 10 mM MgCl. After the last ultracentrifugation (60 minutes, 55000 rpm, 4^{0}C) myosin motor domains were in the supernatant, as ATP resulted in the dissociation of the actomyosin complexes. The His-tagged motor domain constructs were further purified by Ni-NTA affinity chromatography (*Novagen*). The column was equilibrated with low salt buffer (50 mM HEPES, pH 7.3, 30 mM potassium acetate, 3 mM benzamidine, 3 mM mercaptoethanol) then the supernatant of the last centrifugation was applied on the column and further washed for the elimination of non-specifically bound proteins. Washing with high salt buffer (50 mM HEPES, pH 7.3, 300 mM potassium acetate, 3 mM benzamidine, 3 mM mercaptoethanol) resulted in the elimination of proteins adhering with ionic bonds to the column, while low salt buffer containing 10 V/V% imidazole (50 mM imidazole, 3 mM NaN_3, pH 7.3) washes off proteins with His-rich regions. His-tagged motor domain was eluted by low salt buffer containing 450 mM imidazole (90 V/V%). Protein content of the eluted fractions was checked with Bradford reagent. Imidazole was dialyzed from the protein in dialysis buffer (40 mM NaCl, 1 mM $MgCl_2$, 20 mM HEPES, 3 mM benzamidine, 3 mM mercaptoethanol, pH 7.3) in dialysis tubes (High Retention Dial Tube, 3 kDa, *Sigma*). SDS-PAGE (4-20% Tris-Glycine Gel, *Invitrogen*) and staining of proteins with Coomassie Brilliant Blue was applied for
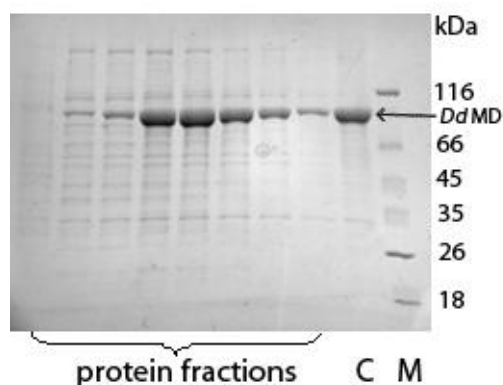
Figure 60. Visualization of *Dd* MD after SDS-PAGE. Fractions containing *Dd* MD (89 kDa) of the elution from the Ni-NTA affinity column were run on SDS-PAGE and stained by Coomassie Brilliant Blue. Control protein (C) and protein marker (M) were also applied. Purity of the eluted fractions can be also checked, in this case there were many other proteins co-eluting with *Dd* MD, but in a much smaller amount.

detection of the proteins using GeneSnap from SynGene softwares (**Figure 60.**). Concentration of the proteins was determined by Bradford reagent using known concentrations of BSA.

Wild type and mutant *Mm* myosin V S1 pFastBac constructs were used to create bacmids (carrying the myosin gene) by using BAC-TO-BAC Baculovirus Expression System from Life Technologies (*Gibco BRL*). Bacmids were transfected into Sf9 (*Spodoptera frugiperda*) insect cells by the help of Cellfectin (*Invitrogen*), which creates liposomes around bacmid DNA enabling their passage through the cell membrane of insect cells. 72 hours after the transfection of Sf9 cells, the supernatant of cells contains the first generation of viruses, P1. P1 was further used to infect cells and create the next generation of viruses, P2, then similarly P3, always selecting for the most efficient viruses by checking protein expression. Large-scale expression of proteins started after optimizing for virus concentration (1, 3 or 5 vol/vol%) and incubation time (48-72 hours), checking protein expression on SDS-PAGE/Western Blot. $2*10^6$/ml cell concentration cultures were infected with the determined volume of virus. Calmodulin was co-expressed with myosin V (P3 virus generation obtained from collaborating partners), as light chain is needed for its proper functioning. Sf9 cells were grown by shaking (120 rpm, 27**°**C) in cell medium (InsectExpress, *Lonza*) containing penicillin-streptomycin (*Sigma*) until the determined incubation time. Cells were collected by centrifugation (5 minutes, 3000 rpm, Jouan KR22i, 4˚C), washed with PBS and frozen in liquid nitrogen. Unfreezing of the cells was in Sf9 extraction buffer (10 mM MOPS pH 7.3, 200 mM NaCl, 10 mM $MgCl_2$, 1 mM EGTA, 3 mM NaN_3, 2 mM ATP, 0.1 mM DTT, protease inhibitor mix) and lysis was obtained by sonication (3x2 minutes, 70% performance). Elimination of the cell debris was by centrifugation (15 minutes, 20000 rpm, Jouan KR22i, 4˚C). FLAG affinity resin was given to the supernatant and incubated overnight with mild shaking. The resin was centrifuged (2 minutes, 1000 rpm, Janetzki K23) and washed with buffer containing ATP (10 mM HEPES pH 7.2, 0.1 mM EGTA, 3 mM NaN_3, 0.5 M NaCl, 0.1 mM DTT, 1 mM ATP, 5 mM $MgCl_2$) to get rid of actin binding to myosin, then placed into

a chromatography column. The column was further equilibrated with HMM buffer (10 mM HEPES pH 7.2, 0.1 mM EGTA, 3 mM NaN_3, 0.1 mM DTT). Recombinant myosin S1 was eluted by 0.3 mg/ml FLAG-peptide. Protein fractions were verified by Bradford reagent. FLAG-peptide was dialyzed from myosin in myosin V dialysis buffer (10 mM HEPES pH 7.2, 0.1 mM EGTA, 3 mM NaN_3, 50 mM KCl, 1 mM DTT). Purity of the protein was checked by SDS-PAGE and concentration was determined by Bradford reagent using known concentration of BSA.

Actin preparation was performed as published by Spudich&Watt [217] from α-actin powder isolated from rabbit skeletal muscle. Covalent labeling of Cys374 of actin by N-(1-pyrene)iodoacetamide (pyrene) (*Sigma*) was performed based on published protocol [218]. Actin filaments were stabilized by 1.5-fold molar excess of phalloidin (*Molecular Probes*).

Actomyosin covalent cross-linking by EDC.

30 μM *Dd* MD (either wild type or R520K) was mixed with 60 μM F-actin in assay buffer, and 5 mM EDC (*Fluka*) was added to initiate the zero-length crosslinking reaction at 20 °C. The reaction was terminated with 10 mM β-mercapto-ethanol, and the cross-linked products were analyzed by SDS-PAGE (with a 5–15% gradient minigel) using a Pharmacia Biotech Phast system.

Fluorescence Spectroscopy and Transient Kinetic Measurements
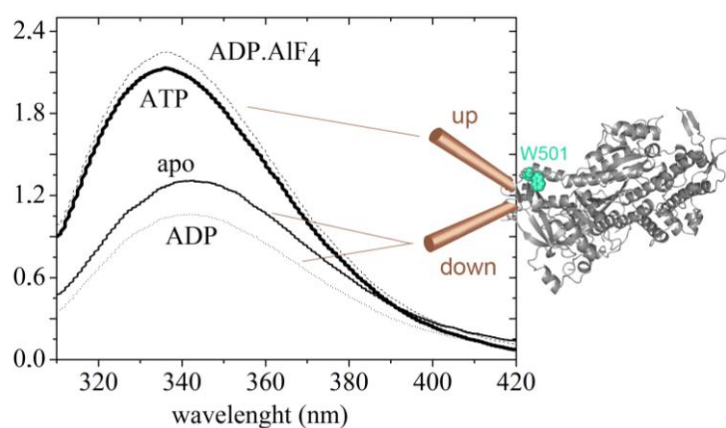
Figure 61. Steady-state emission spectra of W501+ *Dd* MD with and without bound nucleotides. Nucleotides inducing a myosin up-lever structure in steady-state conditions result in a fluorescence enhancement of W501, whereas ADP-binding to apo myosin down-lever structure induce a further decrease of fluorescence compared to apo state, detected at 340 nm.

Intrinsic fluorescence change of W501 of *Dd* MD constructs is detected upon nucleotide binding to myosin. Different nucleotides or their analogs induce conformational changes in myosin, resulting in different orientation of the lever, which can be distinguished by fluorescence increase or decrease of W501 (**Figure 61.**). The increase or decrease in fluorescence

sensed by W501, pirene of actin or mant fluorophor of nucleotides can be detected on a transient scale, measuring nucleotide or actin binding and dissociation with stopped-flow. An example for ATP binding toW501+ *Dd* MD is presented below, determining the observed rate of binding (k_{obs}) by detecting fluorescence change of W501 in time and fitting single exponential to the transient (**Figure 62.**). The initial quenching of fluorescence upon ATP binding to *Dd* MD W501+ (M†.ATP in Scheme 1B) cannot be detected at 20°, as myosin populates to the high-fluorescent, up lever M.ADP.Pi state (M*.ADP.Pi in Scheme 1B). Similarly, fluorescence change of mant or pyrene fluorophores can be detected in time.
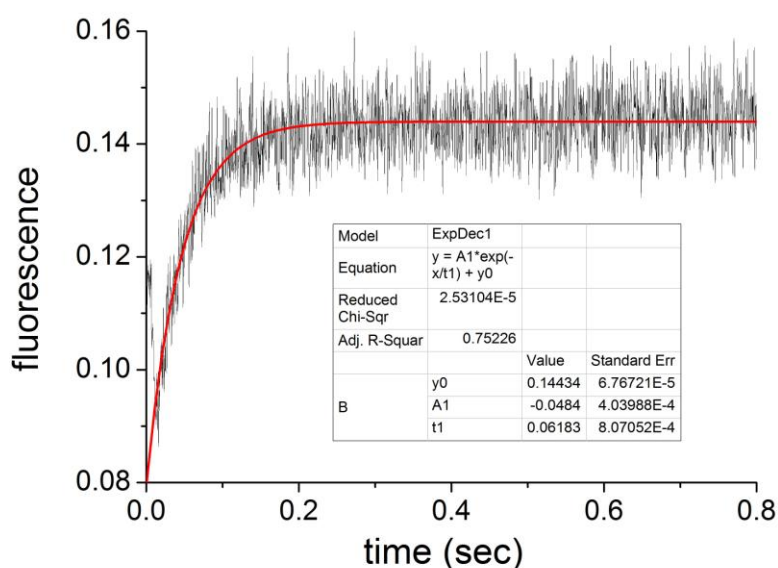
Figure 62. Fluorescence change on a transient time scale upon ATP binding to W501+ *Dd* MD at 20°. The absolute increase of fluorescence is detected in time at 340 nm, exciting W501 at 297 nm. A single exponential is fitted to the signal, yielding k_{obs}= 16 s^{-1} at 50 µM ATP concentration

Transient kinetic experiments were carried out by using BioLogic SFM 300 stopped-flow apparatus equipped with a Super-Quiet Mercury-Xenon Lamp (Hamamatsu Photonics). In stopped-flow experiments, 25 µl-s from each syringe were mixed in a µFc08 fluorescence cuvette with 8 ml/sec total flow-rate and 1.5 ms dead time. In ATP binding experiments, myosin's W501 was excited at 297 nm, the slit was 2 nm, and a 340 nm interference filter (*Corion* CFS-001999 9LI34) was used on the emission side. 2 µM myosin MD was rapidly mixed with 0-1 mM ATP. In ADP and actin binding experiments, mant-ADP and actin-pyrene were excited at 365 nm and a WG420 cutoff filter (*Comar Instruments*) was used for detection. 0-60 µM mant-ADP was mixed with 2 µM myosin MD while 0.2 µM pyrene actin was mixed with increasing concentration of MD (0-10 µM) in apo state or complexed with 1mM ADP. Pyrene fluorescence is proportional to the extent of newly formed actomyosin complexes. ATP induced actomyosin dissociation was followed after mixing 1 µM pyrene-actin MD complex

with increasing concentration of ATP (0-16 mM). All experiments were carried out at 20ºC in assay buffer (20 mM HEPES pH7.3, 40 mM NaCl, 4 mM $MgCl_2$, 4.5 mM mercaptoethanol). Fitting and data analysis were performed using Bio-Kine and OriginLab 7.5.

Steady-state Basal and Actin-activated ATPase Measurements

Basal and actin-activated ATPase activity of the *Dd* wild type, R520E, Δ519-523, R520Q MDs and Mm myosin Va wild type and K502E S1 constructs were measured using a Schimadzu UV-2101 PC spectrophotometer by a pyruvate kinase/lactate dehydrogenase coupled assay (NADH-coupled assay) [145] at 20ºC in a low ionic strength buffer (in case of *Dd* MD: 5 mM HEPES, 2mM $MgCl_2$, 1 mM DTT, pH 7.2; in case of *Mm* myosin V: 10 mM HEPES, 2 mM $MgCl_2$, 0.15 mM EGTA, 1 mM DTT, pH 7.2). Measurements were carried out at 2 μM (*Dd* MD) and 0.1 μM (*Mm* myosin Va S1) myosin concentrations while actin concentration was varied between 0 μM and 113 μM.

Dd MD – actin co-sedimentation Assay

Samples of 2 μM *Dd* MD in the presence of 2 mM ATP and increasing amounts of F-actin (0–130 μM) were ultracentrifuged at 350,000g for 20 min at 4 °C. The resulting supernatants at each concentration of actin were collected, and the pellets were dissolved in the same volume of buffer (1 mM HEPES, 2 mM MgCl2 and 1 mM DTT, pH 7.2) as the volume of the appropriate supernatants. After SDS-PAGE, a densitometric method (GeneTools from SynGene softwares) was used to detect the amount of myosin in the pellets and supernatants, and the fractional actin attachment of myosin at each actin concentration was determined (calculated as the volume of the pellet over the volume of the pellet plus the supernatant). Myosin without actin or ATP was used as a control (resulting in no myosin in the pellet), and 2 μM myosin with 40 μM actin and no ATP was used as a second control (resulting in all the myosin being in complex with actin in the pellet). Before the assay, nonfunctional myosin heads were eliminated by ultracentrifugation with actin in the presence of 5 mM ATP.

Data Analysis of Steady-state and Transient Kinetic Experiments

In actin activated ATPase activity measurements, activity values are plotted in the function of increasing actin concentration. The values of maximal actin-activated ATPase (V_{max}) and actin concentration at half of the maximal ATPase (K_{actin}) are obtained from the

fitted hyperbola. The mean values of basal ATPase activites (V_{basal}, at 0 μM actin) were determined from three independent experiments.

In the case of ATP binding to *Dd* MD, observed rate constants (k_{obs}) were plotted in the function of increasing ATP concentrations and fitted with a hyperbola (**Figure 63**), as myosin could be saturated with ATP. From the fitted hyperbola, values of the maximal k_{obs} (P1) and the ATP concentration at half saturation was determined (P2). Their quotient equals to the binding rate constant (k_{on}) of ATP to myosin MD (P1/P2). Also the P1 value determines the rate of hydrolysis ($k_{hydrolysis}$).
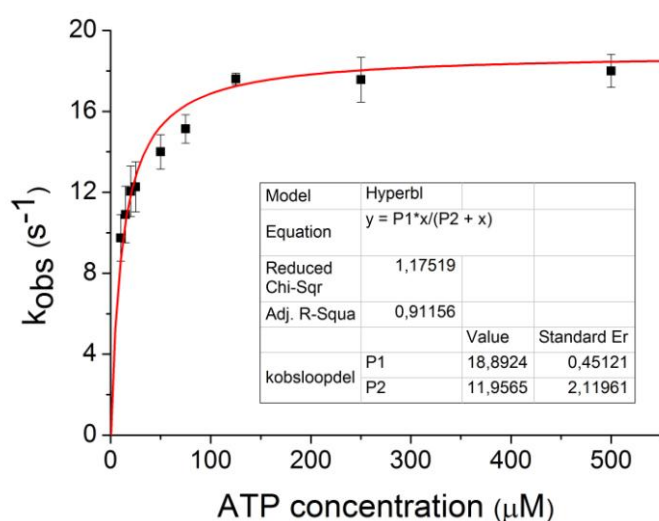
Figure 63. ATP binding of W501+ *Dd* MD. Observed rate constants (k_{obs}) are plotted in the function of increasing ATP concentration. $k_{hydrolysis}$ (P1)and k_{on} (P1/P2) are determined from the fitted hyperbole.

MD was not saturated by ADP or actin, therefore linear function was fitted to data. The gradient of the line gives the binding rate constant (k_{on}), while the intercept gives the dissociation rate constant (k_{off}). Dissociation equilibrium constant (K_d) is calculated from these values (k_{off}/k_{on}).

Actomyosin dissociation in the presence of ATP also saturates at the rate constant ($k_{actindissoc}$) obtained from the fitted hyperbola.

In cosedimentation experiments, the fractional actin attachment of myosin at each actin concentration was determined and plotted. The dissociation equilibrium constant (K_d) of actin binding to myosin in the presence of high ATP concentration is obtained from the fitted hyperbola to data, as the concentration at half saturation of the curve.

In Vitro Motility Assays

In vitro motility experiments were carried out according to published protocol [219, 220] at 20ºC, and detected by Olympus IX71 microscope. The internal volume of the flow-through microchamber was 10 μl. The following solutions were added to the microchamber : 10 μl 0.2 mg/ml Penta-His Antibody (*Quiagen*) incubated for 5 minutes for the positioning of MDs, 20 μl 10 mg/ml BSA incubated for 2 minutes for blocking, 20 μl wash buffer (25 mM imidazol pH 7.4, 25 mM KCl, 4 mM $MgCl_2$, 1 mM EGTA, 10 mM DTT and 0.5 mg/ml BSA), 10 μl 1-10 μM MD incubated for 5 minutes, 20 μl wash buffer, 20 μl of unlabelled F-actin for covering unfunctional MDs, after 2 minutes 20 μl wash buffer containing 2 mM ATP, after 20 μl wash buffer 20 μl of 2 μM TRITC-labelled actin (Molecular Probes, Eugene), 20 μl wash buffer and then 20 μl of anti-bleach solution (5 mg/ml glucose, 0.1 mg/ml glucose oxidase and 0.02 mg/ml catalase added to wash buffer). Motility of actin filaments was initiated by adding 20 μl anti-bleach solution containing 2 mM ATP. Images of moving filaments were visualized, recorded and digitized as described by [219] and average velocities of filaments were determined.

Microparticle Bombardment

Synchronised *unc-54(e1092) C. elegans* culture was grown on 8.5 cm plates containing nematode growth medium (NGM) seeded with OP50 until they reached young adult stage. Preparation of 1 μm gold particles (Bio-Rad), coating of linearized DNA and bombardment was carried out according to Berezikov et al [221] using Biolistic PDS-1000/He Particle Delivery System (*BIO-RAD*). M9 buffer used for washing *C. elegans* contains 3g KH_2PO_4 (*Sigma*), 6g Na_2H PO4, 5g NaCl (Sigma) dissolved in distilled water, autoclaved and 1 ml sterile $MgSO_4$ (*Sigma*) added afterwards. Screening for transformant animals started 1 week after bombardment. From integrated lines homozygous strains were selected.

Confocal Microscopy

Confocal pictures were taken by Zeiss Laser Scanning Confocal Microscope LSN 710 using Zen 2009 software. GFP was excited at 458 nm and 488 nm with 10 % laser intensity. Either EC Plan-Neofluar 10x/0.30 M27 or Plan-Apochromat 63x/1.40 OilDIC M27 objectives were used. Emission between 495 and 650 nm was detected.

Egg-production and Lifespan Assays of *C. elegans*

All assays were carried out at 25ºC with synchronized *C. elegans* cultures. For egg-production assay 20 animals of each strain were monitored from young adult stage until death. Animals were put to a new plate every day and offsprings were counted. For the lifespan assay L4 animals were transferred to NGM plates supplemented with 300 mg/ml FUDR. Surviving animals were counted each day. Animals were considered dead when they stopped pharyngeal pumping and responding to touching. Lifespan statistics were calculated from Keplen-Meier analysis.

Physiological and Motility Assays of *C. elegans*.

All assays were carried out at 25 °C with synchronized *C. elegans* cultures. For the FUDR-treated motility assays, the worms were maintained at 20 °C until the L4 larval stage and were then transferred to nematode growth media plates supplemented with 300 mg/ml FUDR for 1 day. Sterile adult worms were then transferred to the assay plates. Twenty worms from each strain were recorded every 24 h from the young adult stage until death. Worms were considered dead when they stopped pharyngeal pumping and stopped responding to touching. For the FUDR-untreated motility assay, the worms were maintained at 20 °C until the second day of their adult stage, and 40 worms from each strain were recorded. Nematodes were tapped with a glass rod to evoke motion, and δVision software was used for tracking the movement and the tail velocity of the worms.

Atomic Force Microscopy.

Individual *C. elegans* worms on an agarose plate were mechanically manipulated with an AsylumResearch MFP3D atomic force microscope. Olympus AC160 cantilevers were used, which were calibrated using the thermal method53. In the cantilever assay, the worms were exposed to an average initial force of 30 μN. Then, the change in force was monitored as a function of time for a period of 10 s. To quantify the vigor in the force response, the differences between the initial force and the force after 10 s were calculated and visualized. The difference in the y intercepts of the curves was the result of a shift between the curves present for display purposes. Experiments were carried out at 25 °C. Data were analyzed using Igor Pro 6.04.

***In Silico* Preparation of Protein Structures**

Dd MD up lever state (1VOM) was extended with the missing amino acids (Ala205 to Ser208, Asn711, Ala716 to Ser719, Asp724 to Leu730, and Ala748 to Glu759) based on the unpublished structure by Jon Kull (referred to as M_{up}). Missing residues of squid S1 apo state (2OVK referred to as $M_{apo,sq}$: Lys203 to Lys216, Pro626 to Ala642) and *Dd* MD down lever sate (1MMD: 615 to 634) were completed with Modeller 9.2 [222]. Coordinates of all the atoms of *Dd* MD apo state (1Q5G, referred to as $M_{apo,Dd}$) are well defined. Vanadate in the nucleotide binding pocket of 1VOM was replaced by Pi. We calculated the partial charges and coordinates by using the AMBER force field. The ADP parameters applied in the AMBER force field was provided by Meagher *et al* [223] . RESP (Restrained Electrostatic Potential) charges of $H_2PO_3^-$ (the most dominant ionized state at pH=7.2, verified by quantum mechanical calculations under CHARMM force field) were calculated by Gaussian 03 and ANTECHAMBER [224, 225]. The calculations were carried out for a set of structural conformations of the $H_2PO_3^-$ group by covering the accessible space in the system. The density functional algorithm with the B3LYP exchange and the 6-312+g (d,p) basis set were selected for calculation in Gaussian 03. The resulting charges were averaged over all of the conformations. All crystal waters were stripped except for two in the nucleotide binding pocket of 1VOM, which stabilize the position of ADP and Pi through interactions with the magnesium ion. The missing N-terminus of the actin trimer [89, 111] was sequentially extended and capped with acetylate preceding the molecular minimization (Acetyl-Asp_1-Glu-Asp-Glu_4-actin).

Protein-protein Docking

In case of myosin structures of Result I, randomization of orientations, rigid body energy minimization and semi-rigid simulated annealing in torsion angle space were carried out. Structures of Result II were relaxed by a 20 ns-long molecular dynamic simulation after preparation of their structures and before docking (resulting in $_{rel}M_{up}$, $_{rel}M_{apo,Dd}$ and $_{rel}M_{apo,sq}$). All structures were docked to the refined actin trimer by using HADDOCK V2.1 program (High Ambiguity Driven Docking) (resulting in $_{dock}A.M_{up}$, $_{dock}A.M_{rigor,Dd}$, $_{dock}A.M_{rigor,sq}$ and the docked actomyosin structures of Results I). Intermolecular restraint residues for docking were defined by experimentally determined actomyosin interface [226-228], regarded as flexible segments and divided into active and passive amino acids for protein-protein docking. Active residues take part in actomyosin binding and passive residues are the neighboring residues of active residues. Overall, six active and ten passive residues were selected from myosin, five active and five passive residues were selected from actin. Ambiguous interaction restraints

(AIR) identified from these residues was used to drive the docking process, with a maximum effective distance of 8.0 Å [229], which was available for the active-active and active-passive, but not for the passive-passive residues. The best 200 of 1000 refined complexes were obtained from rigid body energy minimization and then submitted to the semi-rigid simulated annealing process. These structures were exposed to a 12 Å shell of TIP3P water solvent for molecular dynamic simulations with a cutoff value of 5 Å. The best 100 complexes were selected according to the evaluation score of their average interaction energies and buried surface area. The HADDOCK score, as the main criteria for selection, was calculated on the basis of the equation $HADDOCK_{SCORE}=E_{VDW}+0.2E_{ELEC}+0.1E_{AIR}+E_{DESO}$, where E_{VWD} is the Van der Waals, E_{ELEC} is the electrostatic, E_{AIR} is the ambiguous interaction restraint and E_{DESO} is the desolvation energy. Finally, optimal candidates with the lowest HADDOCK scores were collected into subsets with more than ten structures by a backbone-based RMSD clustering with a cut-off value of 7.5 Å. All parameters and processes were carried out through the HADDOCK online service, http://haddock.science.uu.nl/services/HADDOCK/haddock.php.

Molecular Dynamic Simulations

The module of sander in the molecular dynamics package AMBER11 was used for molecular dynamics simulations [230]. After docking, the actomyosin structures were relaxed by a 15 or 100 ns-long molecular dynamics, creating the up lever, down lever and rigor actomyosin structures of Result I and $_{rel}A.M_{up}$, $_{rel}A.M_{rigor,Dd}$ and $_{rel}A.M_{rigor,sq}$ of Result II. After introducing mutations into the $_{rel}A.M_{up}$ complex, the structures were relaxed again for 100 ns leading to $_{rel}A.M_{up,R520Q}$, $_{rel}A.M_{up,R562Q}$ and $_{rel}A.M_{up,K622Q/K623Q}$ complexes. All structures were neutralized by adding discrete number of Na^+ in the most appropriate electro-negative areas around proteins. Complexes were then solvated in a truncated octahedron box of TIP3P water with a 12Å cut-off value along each dimension [231]. Long-range electrostatic interactions were treated by particle-mesh Ewald method in periodic boundary conditions [232]. By a 1000 steps of the steepest descent and conjugate gradient energy minimization, the compact system is slowly heated up to 300K and equilibrated at 2 ns constant volume and 3 ns constant pressure (structures of Result I) or constant temperature (NVT) for 20 ns and then at constant pressure (NPT) ns for 80 ns (structures of Result II). The Berendsen coupling algorithm was used for the temperature control [233]. The SHAKE algorithm was applied for constraints on covalent bonds and all hydrogen atoms [234].

Binding Free Energy Calculation

Binding free energies of actomyosin complexes of Result II from 2500 snapshots of the last 60 ns of the MD simulations were calculated by the molecular mechanic Poisson-Boltzmann surface area method (MM/PBSA) [235]. The pbsa module in AMBER was used to evaluate the electrostatic contribution to the solvation free energy ($\Delta G_{solv}=\Delta G_{sol\text{-}pol}+\Delta G_{sol\text{-}np}$). The grid spacing of the cubic lattice was set at 2 Å, and the dielectric constant values for the interior and exterior of the system were 1 and 80. The non-polar contribution to the solvation free energy ($\Delta G_{sol\text{-}np}$) was calculated from the solvent-accessible surface area ($\Delta G_{solv\text{-}np} =\gamma SASA+\beta$) [236]. The surface tension γ and the offset β were set to 0.00542 kcal·mol^{-1}·Å^{-2} and 0.92 kcal·mol^{-1}, respectively. The contribution of entropy (*-TΔS)* based on ligand receptor association was performed with normal-mode analysis [237]. 1000 snapshots were collected and submitted to the molecular minimization with a distance-dependent dielectric constant E=4r. The end of convergence was not achieved until the RMSD of the gradient vector less than 1×10^{-4} kcal·mol^{-1}·Å^{-1}. Residues close to the binding surface with a distance less than 20Å were acquired to estimate the contribution of entropy.

Synthesis and Purification of Para-azidoblebbistatin

5 mg (-)-blebbistatin was dissolved in 300 µl methanol and transferred to a 10-ml microwave reaction vessel (*CEM Corporation*). During continuous stirring 700 µl boron trifluoride dihydrate and 5.7 mg (1.5-fold excess) N-Iodosuccinimide was added and the reaction mixture was placed into a microwave reactor (*CEM BenchMate* 300W) at 50°C for 30 minutes with magnetic stirring. Purification of the resulted iodoblebbistatin was carried out on a Strata XL 500 mg SPA column (*Phenomenex*), equilibrated with 50 ml acetonitrile then 50 ml water and the crude reaction mixture was pipetted onto the column. It was sequentially washed with 20 ml water, 3 ml sodium bisulfite, 3 ml saturated sodium bicarbonate, 20 ml water, and then eluted with 20 ml acetonitrile containing 1 % trifluoroacetic acid and dried in vacuum. The brownish powder was dissolved in 0.5 ml acetonitrile containing 0.15 % triethylamine (TEA) and it was further purified by HPLC (*Agilent 1100* instrument) using a Luna 250x10 mm C18(2) column (*Phenomonex*). HPLC conditions were as follows: isocratic elution (water containing 0.15 V/V% TEA and acetonitrile containing 0.15 V/V% TEA in a ratio of 3:7), flow rate: 3.5 ml/min, detected at 254 nm. Pure iodoblebbistatin was dissolved in 1 ml of DMSO:H2O mixture (5:1 V/V%) and pipette into a 10 ml reaction vessel containing 15 mg sodium azide, 2 mg copper(I) iodide and 1 mg sodium ascorbate. 2 µl N,N′-

dimethylethylenediamine was added and the reaction mixture was stirred for 30 minutes at room temperature. The purification of para-azidoblebbistatin was performed in the same way as in case of iodoblebbistatin.

Analytical Data of Para-azidoblebbistatin

The exact position of the substituated azido group was determined by NMR. The analytical data is as follows: (-)-para-azido-blebbistatin: 1H chemical shifts , ppm: 2.26 (2, 2H, multiplet), 2.30 (11, 3H, singlet), 3.95 (3A, 1H, multiplet), 4.05 (3B, 1H, multiplet), 6.84 (12, 1H, singlet), 7.12 (8, 1H, doublet, $3JHH=8.1Hz$), 7.19 (3', 2H, doublet, $3JHH=8.9Hz$), 7.40 (7, 1H, dd, $3JHH=8.1Hz$, $4JHH=1.8Hz$), 7.54 (5, 1H, doublet, $4JHH=1.8Hz$), 8.15 (2', 2H, doublet, $3JHH=8.9Hz$). 13C chemical shifts, ppm: 20.0 (11), 28.0 (2), 47.2 (3), 73 (3a), 119.1 (3'), 120.8 (2'), 121.1 (10), 125.5 (8), 126.0 (5), 132.4 (6), 134.4 (1'), 136.0 (7), 138.1 (4'), 148.9 (9), 165.4 (2x), 194.7 (4). ES-MS. (Q-TOF Premier mass spectrometer, Waters Corporation): (M+1) 334.1306. Calculated for $C_{18}H_{16}N_5O_2$, 334.1304. Brownish yellow powder. Storage: -20°C. Protect from light. No degradation in 1 year.

Degradation Kinetics of Para-azidoblebbistatin

0.5 ml 5 µM para-azidoblebbistatin solution in assay buffer (40 mM NaCl, 4 mM $MgCl_2$, 20 mM HEPES pH 7.3) was irradiated at 247, 278 and 310 nm (with 10 nm slit width) for 0 (control), 1, 2 and 5 minutes using an Edinburgh Instruments F900 Fluorescence Spectrometer equipped with a 450 W Xenon Lamp. At each time point 10 µl solution was taken and analyzed by HPLC using conditions described above.

Cross-linking Myosin with Para-azidoblebbistatin

Before cross-linking, *Dd* MD was dyalized in assay buffer without mercaptoethanol, under argon atmosphere. Myosin for crystallization was concentrated by centrifugal filters (*Amicon Ultra*, 30 K) to 120 µM concentration, then incubated with 1 mM ADP and 15 mM $MgCl_2$ for 1 hour to get rid of possible ATP contamination. 2x60 µM of the inhibitor was added to the protein, or in the case of apo myosin, 10 µM para-azidoblebbistatin was added to 8 µM myosin. Samples were incubated on ice for 10 minutes, then irradiated at 310 nm for 4 minutes (slit width: 10 nm) (*Edinburgh Instruments F900* Fluorescence Spectrometer, 450 W Xenon lamp). Samples were taken from the cross-linked myosin.ADP.ABleb or myosin.ABleb

solutions for basal ATPase measurements. Addition of inhibitor, incubation and irradiation was repeated until reaching saturation of inhibition. His-tag affinity chromatography was carried out similarly as described above. The buffer used for equilibration of the column was assay buffer without mercaptoethanol (additional 1 mM ADP was present in case of crystallization). After applying the cross-linked myosin.ADP.ABleb or myosin.ABleb onto the coloumn, the complex was eluted in 500 mM imidazole. Myosin.ADP.ABleb complex for crystallization was dyalized in buffer containing 10 mM HEPES, 60 mM NaCl, 5 mM $MgCl_2$, 0.5mM ADP, 1mM NaN_3 (pH7.5) and 1mM TCEP, and myosin.ABleb was dialyzed in dialysis buffer.

Tryptic Digestion of M.ADP.ABleb

The myosin.ADP.ABleb complex was first reduced and alkylated. 6 M urea was given to the protein and pH was adjusted to 7.4 with the help of 25 mM Tris-HCl. 400-fold dithiothreitol was added to the SH-groups of the protein and stirred for two hours at room temperature. 1000-fold iodoacetamide was given to the SH-groups and stirred for 30 minutes in dark, surplus of iodoacetamide was eliminated by 2000-fold mercaptoethanol. The reduced and alkylated complex was dialyzed in 0.5 % ammonium carbonate. Dialyzed sample was subjected to 1 m/m % TPCK-treated trypsin (*Sigma*) and 1 mM $CaCl_2$. Digestion was carried out at 37°C for 18-20 hours. Digested samples were lyophilized.

Mass Spectrometry of ABleb-peptide Fragments

Lyophilized samples of M.ADP.ABleb were solvated in buffer of 50 V/V% water, 50 V/V% acetonitrile and 0.1 V/V% formic acid. Mass spectrometry was carried out using a Waters SQ instrument. Data were analyzed using the Findmod program.

Materials

ATP and ADP were purchased from Sigma-Aldrich and Roche. Traces of ATP were carefully removed from ADP stock solutions by extensive preincubation with *Dd* MD proteins. Mant(N-Methyl-anthraniloyl)-dADP was prepared from mant-dATP (Jen Bioscience) with excess of *Dd* MD and time. (-)-Blebbistatin, N-iodosuccinimide, boron trifluoride dihydrate, sodiumbisulfite, sodium bicarbonate, triethylamine, trifluoroacetic acid, sodium azide, copper(I) iodide, sodium ascorbate, N,N′-dimethylethylenediamine, acetonitrile, and methanol were purchased from Sigma-Aldrich.

IX. Acknowledgements

I am thankful for my supervisor, András Málnási-Csizmadia, who guided the way for me in science, and showed how to be most enthusiastic about research even at hard times. Together with Mihály Kovács, they provided their colleagues an inspiring atmosphere to work in, and always loaded us with new ideas that we were eager to follow.

I cannot be greatful enough for my friends and colleagues Nikolett Nagy, Kata Sarlós and Zoltán Simon, who helped to get through the obstacles of everyday life in the lab. I am especially thankful for Máté Gyimesi and Bálint Kintses, who taught me cloning and using the stopped flow when I arrived to the lab. I would also like to thank all my colleagues for their help in my research and patience for my struggles, Prof. György Hegyi, Zhenhui Yang, Ilona Ozoróczyné Szász, László Végner, István Lőrincz, Wanda Imrich, Ágnes Peragovics, Anna Rauscher, Gábor Szegvári, Szilva Ráti, Gergő Vörös, Balázs Takács, Gábor Harami, Zsuzsa Kocsis, Veronika Ferencziová, Kitti Szamosvölgyi and last but not least Balázs Jelinek, whose work is essential in the prospering of the lab.

I would like thank Prof. László Gráf and Prof. László Nyitray for operating such a successful Biochemistry Department, giving the opportunity for many students to study.

I would like to thank the work and help of our collaborators as well, Miklós Kellermayer, Tibor Vellai, Irén Bárdos-Nagy, Péter Erdélyi, Attila L. Kovács, Péter Hári, László Drahos, Andrea Bodor and Anne Houdusse and her group.

I am greatly thankful for my parents, Anna and Attila Várkuti, from where my scientific interest and persistence originates. I also think about my brother, Botond Várkuti with great gratitude, from whom I have learned an attitude that can be invested successfully in research.

I am most grateful for para-azidoblebbistatin, for providing a colleague, friend and companion in research and life, Miklós Képiró, who is a constantly inspiring mind offering challenges for every day.

X. Appendix, Tables

Table A1. Survival times of the four *C. elegans* strains

	Mean[a]			Median		
		95% Confidence Interval			95% Confidence Interval	
	Estimate	Lower Bound	Upper Bound	Estimate	Lower Bound	Upper Bound
wild type	12.647 ± 0.270	12.117	13.177	13.000 ± 0.417	12.182	13.818
Δunc-54	11.368 ± 0.344	10.695	12.042	11.000 ± 0.484	10.052	11.948
unc-54::gfp	10.632 ± 0.406	9.835	11.428	11.000 ± 0.338	10.338	11.662
unc-54$_{K525E}$::gfp	11.294 ± 0.567	10.182	12.406	12.000 ± 0.225	11.560	12.440
overall	11.458 ± 0.218	11.032	11.885	12.000 ± 0.188	11.631	12.369

Means and medians for survival time of the four C. elegans strains. Mean values ± s.d. are given.

[a] Estimation is limited to the largest survival time if it is censored.

Table A2. Pairwise comparisons of the survival of the four *C. elegans* strains

		wild type		Δunc-54		unc-54::gfp		unc-54$_{K525E}$::gfp	
		Chi-Square	Sig.	Chi-Square	Sig.	Chi-Square	Sig.	Chi-Square	Sig.
Log Rank (Mantel-Cox)	wild type			5.406	0.020	13.467	0.000	5.435	0.020
	Δunc-54	5.406	0.020			1.602	0.206	0.087	0.768
	unc-54::gfp	13.467	0.000	1.602	0.206			2.916	0.088
	unc-54$_{K525E}$::gfp	5.435	0.020	0.087	0.768	2.916	0.088		

Pairwise comparisons of the survival of the four *C. elegans* strains. There is no or little difference in survival time between the investigated strains.

Table A3. Converter/lever positions of different myosin and actomyosin states

	angle (°)	lever state
M$_{apo,Dd}$	221±4	down
$_{rel}$M$_{apo,Dd}$	221±4	down
$_{rel}$A.M$_{rigor,Dd}$	222±3	down
M$_{apo,sq}$	221±4	down
$_{rel}$M$_{apo,sq}$	221±3	down
$_{rel}$A.M$_{rigor,sq}$	245±4	further down
$_{EM}$A.M$_{rigor,ch}$	238	down

Angles were measured between the C$_\alpha$ atom of residues Gly684 and Arg689 of SH1 helix and Ala748 of the converter domain.

Table A4: Energy contributions to the binding free energies of the simulated actomyosin complexes

structure	ΔE_{VdW}[1] (kcal/mol)	ΔE_{ele}[2] (kcal/mol)	ΔE_{PBSA}[3] (kcal/mol)	ΔE_{SASA}[4] (kcal/mol)	ΔH[5] (kcal/mol)	$T\Delta S$[6] (kcal/mol)	ΔG_{bind}[7] (kcal/mol)
$_{rel}$A.M$_{up}$	-127.3 ±9.6	-103.4 ±8.8	230.0 ±16.6	-13.5 ±1.6	-14.1 ±1.3	-6.5 ±0.6	-7.6 ±0.8
$_{rel}$A.M$_{rigor,Dd}$	-152.2 ±11.7	-128.3 ±10.0	281.9 ±19.2	-20.9 ±1.3	-19.6 ±1.2	-7.1 ±0.8	-12.4 ±1.3
$_{rel}$A.M$_{rigor,sq}$	-167.3 ±12.4	-129.2 ±11.0	300.1 ±16.3	-22.4 ±1.6	-18.9 ±1.9	-7.3 ±1.1	-11.4 ±1.0

[1]Van der Waals contribution. [2]Electrostatic energy contribution. [3]Polar contribution to the solvation free energy (Poisson-Boltzmann surface area). [4]Non-polar contribution to the solvation free energy based on the solvent-accessible surface area. [5]Enthalpic contribution based on $\Delta H = \Delta E_{VdW} + \Delta E_{ele} + \Delta E_{PBSA} + \Delta E_{SASA}$. [6]Entropic contribution based on the normal-mode analysis. [7]Binding free energy is calculated on the basis of $\Delta G_{bind} = \Delta H - T\Delta S$.

Table A5. Interactions of actomyosin complexes

| actin-binding loops	type of interaction	*weak actin-binding* $_{rel}$A.M$_{up}$ myosin – actin	*strong actin-binding* $_{rel}$A.M$_{rigor,Dd}$ myosin – actin	$_{rel}$A.M$_{rigor,sq}$ myosin – actin	$_{EM}$A.M$_{rigor, ch}$ myosin – actin
Loop 2 (*upper 50 kDa domain*)	*salt bridges*	**Lys622 – Asp25**	**Lys622 – Asp24/Asp25 Lys635 – Asp1**	**Lys640 – Asp25**/Asp3/Glu4	Glu629 – Arg28 **Lys640 – Asp25** Lys642 – Glu334
	H-bonds			Ser641 – Asp24 Ala642 – Asp24 Ala643 – Asp25 Lys652/657 – Glu2/4 Lys660 – Glu1/2	Gly635 – Asp24 Lys637 – Gly23/Ser348 Gly638 – Gly23 Lys642 – Glu334 Gly643 – Ser145
Loop 4	*salt bridges*	Glu365 – Lys328	Glu365 – Arg147	Glu373 – Arg147	Arg371 – Asp311 Glu372 – Lys328/Arg335 Glu373 – Arg147
	H-bonds				Arg371 – Lys328/Gln314/Ile329
CM loop	*salt bridges*	<u>Arg402 – Glu334</u>	Arg402 – Glu93		Glu411 – Lys336
	H-bonds		Gly401 – Pro27 Gln407 – Glu334 Leu399 – Arg28	Gln415 – Glu334 Gly416 – Glu334 Lys407 – Asp25	Asn410 – Tyr337/Arg28
Activation loop (*lower 50 kDa domain*)	*salt bridges*	**Arg520 – Asp1**	Arg520 – Asp3/Glu4	**Lys528 – Asp1**/Glu4	
	H-bonds	Gln521 – Gln354			Pro529 – Thr351
H-loop	*H-bonds*	Asn537 – Arg147 Thr545 – Gln49 **Lys546 – Met44**	Asn537 – Gly146 Thr542 – Gln49 **Lys546 – Met44**	Lys544 – Gly48 Asn552 – Gln49/Lys50	Ser549 – Gln49 Asn552 – Lys50 Lys553 – Gly46/Gly48
Loop 3	*salt bridges*	**Arg562 – Glu99**	**Arg562 – Glu99**	Lys567 – Asn92	**Lys569 – Glu99**
	H-bonds	Ser564 – Arg95 Lys565 – Tyr91 **Glu567 – Arg95**		Lys567 – Glu99/100 Lys572 – Asp1/Glu2 Lys572 – Asp1/Glu2 Lys572 – Glu100 **Glu577 – Arg95**	Pro570 – Arg95 Ala571 – Tyr91 Lys572 – Arg95 Ala575 – Arg95 **Glu576 – Arg95**

Interactions present in both open and closed actin-binding cleft states of myosin are bolded.

All interactions have >75% occurrence during molecular dynamics.

XI. Appendix, Figures

Figure A1. Synthesis of para-azidoblebbistatin.

blebbistatin — para-iodoblebbistatin — para-azidoblebbistatin
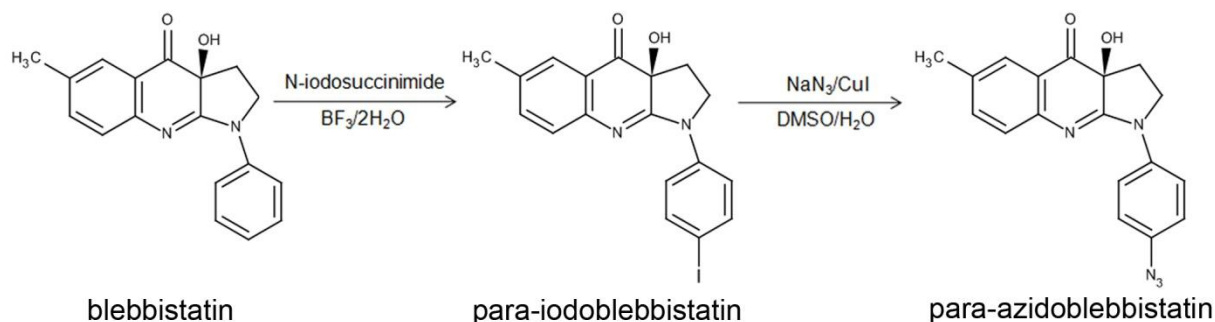
Para-azidoblebbistatin was synthesized in a two-step reaction. Blebbistatin was treated with N-iodosuccinimide in the presence of boron trifluoride dihydrate. After purification the iodinated product was converted into the azide by using sodium azide and copper (I) iodide catalyst.

Figure A2.
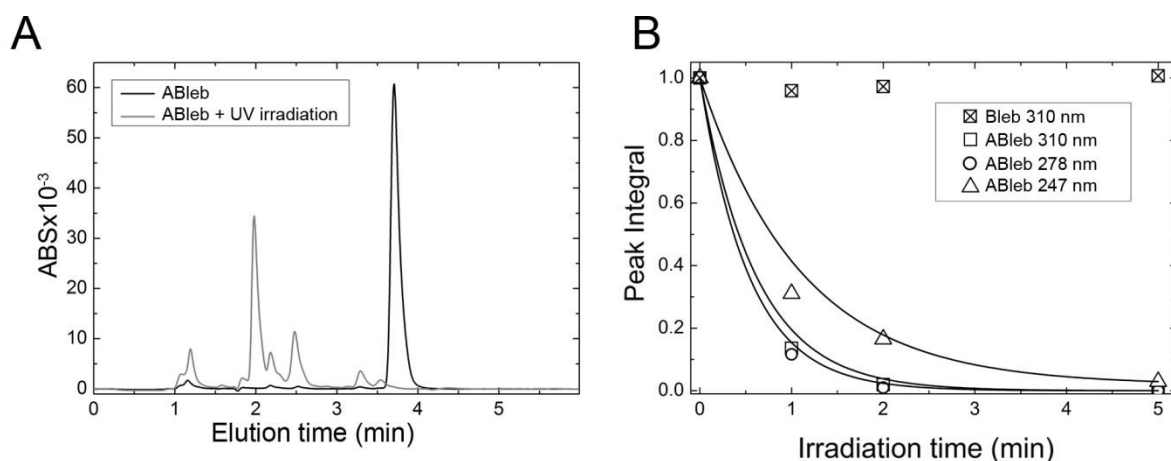
(A) Successive cycles of irradiation of para-azidoblebbistatin by UV light caused the disappearance of the para-azidoblebbistatin peak in HPLC elution profiles, with the parallel appearance of novel peaks at shorter elution times. **(B)** Gradual disappearance of the HPLC peak of para-azidoblebbistatin upon treatment by 310, 278 and 247 nm UV light in the absence of protein, reporting degradation of para-azidoblebbistatin. Under the same conditions blebbistatin degradation did not occur.

XII. Abbreviations

ABleb	para-azidoblebbistatin
AFM	atomic force microscopy
AMP	adenosine monophosphate
ADP	adenosine diphosphate
ATP	adenosine triphosphate
ATPase	adenosine triphosphatase
ATPN	amido− adenosine triphosphate
AlF_4^-	aluminium fluoride
Arg	arginine
AsCy3	biarsenic cyanine 3
Asp	aspartate
BeF_3^-	beryllium fluoride
Bleb	blebbistatin
cDNA	complementary deoxyribonucleic acid
Ca	calcium
C. elegans	*Caenorhabditis elegans*
Cys	cysteine
DMS	dimethyil suberimidate
DMSO	dimethyl sulfoxide
DNA	deoxyribonucleic acid
Dd	*Dictyostelium discoideum*
DTT	dithiothreitol
ELC	essential light chain
EDC	1-ethyl-3-(3-dimethylaminopropyl)carbodiimide
EDTA	ethylene diamine tetraacetic acid
EGTA	ethylene glycol tetraacetic acid
F-actin	filamentous actin

FlAsH	biarsenical fluorescein
FRET	Förster Resonance Energy Transfer
FUDR	floxuridine, 5-Fluoro-1-[4-hydroxy-5-hydroxymethyl) tetrahydrofuran-2-yl]-1H-pyrimidine-2,4-dione
G-actin	globular actin
GEF	guanine nucleotide exchange factor
GFP	green fluorescent protein
Glu	glutamate
Gly	glycine
GTPase	guanosine triphosphatase
HEPES	4-(2-hydroxyethyl)-1-piperazineethanesulfonic acid
HMM	heavy meromyosin
LC-MS	Liquid Chromatography–Mass Spectrometry
LMM	light meromyosin
Lys	lysine
mant-dADP	3'-(N-methylantraniloyl)-2'-deoxy–ADP
MD	motor domain
Mg	magnesium
Mm	*Mus musculus* (mouse)
MOPS	3-(N-morpholino)propanesulfonic acid
n	number of animals
N2	wild type Bristol isolate of *C. elegans*
NTP	nucleoside triphosphate
NTPase	nucleoside triphosphatase
p	probability value
PBS	phosphate
PCR	Polymerase Chain Reaction
PDB	Protein Data Bank

PDZ domain	**P**ost synaptic density protein (PSD95), **D**rosophila disc large tumor suppressor (Dlg1), **Z**onula occludens-1 protein (zo-1)
Phe	phenylalanine
Pi	inorganic phosphate group
PMSF	phenylmethanesulfonyl fluoride
Pro	proline
Ras	Rat sarcoma
ReAsH	biarsenic resorufin
RLC	regulatory light chain
Rn	*Rattus norvegicus* (rat)
S1	subfragment 1
S2	subfragment 2
s.d.	standard deviation
SDS-PAGE	sodium dodecyl sulfate-polyacrylamide gel electrophoresis
SH3 domain	Src homology 3 domain
SH2 domain	Src homology 2 domain
TAE	Tris-acetate EDTA
TLCK	tosyllysine chloromethylketone
TPCK	tosyl phenylalanyl chloromethyl ketone
TRITC	tetramethylrhodamine-5-isothiocyanate
Trp	tryptophan
UV	ultraviolet
VO_4^{3-}	vanadate

XIII. List of Tables

XIV. List of Figures

XV. Publications Concerning this Thesis

Boglárka H.Várkuti, , Zhenhui Yang, Bálint Kintses, Péter Erdélyi, Irén Bárdos-Nagy, Attila L. Kovács, Péter Hári, Miklós Kellermayer, Tibor Vellai and András Málnási-Csizmadia. "A novel actin binding site of myosin required for effective muscle contraction." Nature structural & molecular biology 19, no. 3 (2012): 299-306.

Miklós Képiró, **Boglárka H. Várkuti**, Andrea Bodor, György Hegyi, László Drahos, Mihály Kovács and András Málnási-Csizmadia. "Azidoblebbistatin, a photoreactive myosin inhibitor." Proceedings of the National Academy of Sciences 109, no. 24 (2012): 9402-9407.

Boglárka H. Várkuti, Zhenhui Yang and András Málnási-Csizmadia. " A structural model of actomyosin in the prepowerstroke state: actin induced 'extra priming' of myosin " – under submission

Conference Proceedings (the presenting author is underlined)

A structural model of actomyosin in the prepowerstroke state: actin-binding induced extra priming of myosin
<u>Boglárka Várkuti</u> *Zhen Hui Yang, András Málnási-Csizmadia*
2013 Philadelphia, US, Biophysical Society 57th Annual Meeting, poster presentation

An actomyosin model of the initial state of the powerstroke
<u>Boglárka H. Várkuti</u>,*Yang Zhe Hui, Málnási-Csizmadia András*
2012 Rhodes, European Muscle Conference, oral presentation

Structural Model of the Pre-Powerstroke State of the Actomyosin Complex
Zhen Hui Yang, **Boglárka H. Varkuti**, *Anna Rauscher, Miklos Kepiro, <u>Andras Malnasi-Csizmadia</u>*
2012 San Diego, US, Biophysical Society 56th Annual Meeting, oral presentation

A novel actin binding site enables effective muscle contraction
<u>Boglárka H. Várkuti</u>, *Bálint Kintses, Zhen Hui Yang, Péter Erdélyi, Irén Bárdos-Nagy, Péter Hári, Miklós Kellermayer, Tibor Vellai, András Málnási-Csizmadia*
2011 Berlin, European Muscle Conference, oral presentation

Synthesis and functional characterization of azido-blebbistatin, a photoreactive myosin inhibitor

Miklós Képiró, **Boglárka H. Várkuti**, *György Hegyi, Mihály Kovács, András Málnási-Csizmadia*

2011 Berlin, European Muscle Conference, oral presentation

Sythesis and functional characterization of azido-blebbbistatin, a photoreactive myosin inhibitor

Miklós Képiró, **Boglárka Várkuti** *and András Málnási-Csizmadia*

2011 Budapest, Hungary, 4th European Conference on Chemistry for Life Siences, poster presentation

A novel actin binding site of myosin is responsible for effective muscle contraction

Boglárka Várkuti, *Bálint Kintses, Zhen Hui Yang, Péter Erdélyi, Irén Bárdos-Nagy, Péter Hári, Miklós Kellermayer, Tibor Vellai, András Málnási-Csizmadia*

2011 Baltimore, US, Biophysical Society 55th Annual Meeting, poster presentation

The molecular mechanism of actin activation of myosin

Boglárka Várkuti, *Bálint Kintses, Zhen Hui Yang, András Málnási-Csizmadia*

2009 Lille, France, European Muscle Conference, poster presentation

The role of the proline-rich loop in the enzyme mechanism of myosin II

Boglárka Várkuti, *Kintses Bálint, Yang Zhenhui, Málnási Csizmadia András*

2008 Szeged, Annual Meeting of the Hungarian Society of Biochemistry, poster presentation, poster prize

The role of the proline-rich loop in the communication of actomyosin

Boglárka Várkuti, *Málnási-Csizmadia András*

2007 Temesvár, 10. International Students' Conference of Technological Sciences, oral presentation, special award

XVI. References

1. Noji, H., et al., *Direct observation of the rotation of F1-ATPase.* Nature, 1997. **386**(6622): p. 299-302.

2. Odronitz, F. and M. Kollmar, *Drawing the tree of eukaryotic life based on the analysis of 2,269 manually annotated myosins from 328 species.* Genome Biol, 2007. **8**(9): p. R196.

3. Szent-Gyorgyi, A.G., *The early history of the biochemistry of muscle contraction.* J Gen Physiol, 2004. **123**(6): p. 631-41.

4. Sellers, J.R., *Myosins: a diverse superfamily.* Biochim Biophys Acta, 2000. **1496**(1): p. 3-22.

5. Fujita-Becker, S., et al., *Changes in Mg2+ ion concentration and heavy chain phosphorylation regulate the motor activity of a class I myosin.* J Biol Chem, 2005. **280**(7): p. 6064-71.

6. Jontes, J.D. and R.A. Milligan, *Brush border myosin-I structure and ADP-dependent conformational changes revealed by cryoelectron microscopy and image analysis.* J Cell Biol, 1997. **139**(3): p. 683-93.

7. Reck-Peterson, S.L., et al., *Class V myosins.* Biochim Biophys Acta, 2000. **1496**(1): p. 36-51.

8. Tang, F., et al., *Regulated degradation of a class V myosin receptor directs movement of the yeast vacuole.* Nature, 2003. **422**(6927): p. 87-92.

9. Bahler, M., *Are class III and class IX myosins motorized signalling molecules?* Biochim Biophys Acta, 2000. **1496**(1): p. 52-9.

10. Rayment, I., C. Smith, and R.G. Yount, *The active site of myosin.* Annu Rev Physiol, 1996. **58**: p. 671-702.

11. Itakura, S., et al., *Force-generating domain of myosin motor.* Biochem Biophys Res Commun, 1993. **196**(3): p. 1504-10.

12. Ketchum, A.S., et al., *Complete sequence of the Drosophila nonmuscle myosin heavy-chain transcript: conserved sequences in the myosin tail and differential splicing in the 5' untranslated sequence.* Proc Natl Acad Sci U S A, 1990. **87**(16): p. 6316-20.

13. Montell, C. and G.M. Rubin, *The Drosophila ninaC locus encodes two photoreceptor cell specific proteins with domains homologous to protein kinases and the myosin heavy chain head.* Cell, 1988. **52**(5): p. 757-72.

14. Spudich, J.A., *How molecular motors work.* Nature, 1994. **372**(6506): p. 515-8.

15. Cope, M.J., et al., *Conservation within the myosin motor domain: implications for structure and function.* Structure, 1996. **4**(8): p. 969-87.

16. Goodson, H.V. and J.A. Spudich, *Molecular evolution of the myosin family: relationships derived from comparisons of amino acid sequences.* Proc Natl Acad Sci U S A, 1993. **90**(2): p. 659-63.

17. Stracher, A., *Evidence for the involvement of light chains in the biological functioning of myosin.* Biochem Biophys Res Commun, 1969. **35**(4): p. 519-25.

18. Dreizen, P. and L.C. Gershman, *Relationship of structure to function in myosin. II. Salt denaturation and recombination experiments.* Biochemistry, 1970. **9**(8): p. 1688-93.

19. Szent-Györgyi, A.G., *Calcium regulation of muscle contraction.* Biophys J, 1975. **15**(7): p. 707-23.

20. Gordon, A.M., E. Homsher, and M. Regnier, *Regulation of contraction in striated muscle.* Physiol Rev, 2000. **80**(2): p. 853-924.

21. Hartshorne, D.J. and A.J. Persechini, *Phosphorylation of myosin as a regulatory component in smooth muscle.* Ann N Y Acad Sci, 1980. **356**: p. 130-41.

22. Conti, M.A. and R.S. Adelstein, *Nonmuscle myosin II moves in new directions.* J Cell Sci, 2008. **121**(Pt 1): p. 11-8.

23. Houdusse, A. and C. Cohen, *Structure of the regulatory domain of scallop myosin at 2 A resolution: implications for regulation.* Structure, 1996. **4**(1): p. 21-32.

24.   Zhang, Y., et al., *Calcium-dependent regulation of the motor activity of recombinant full-length Physarum myosin.* J Biochem, 2012. **152**(2): p. 185-90.

25.   Hidalgo, C., et al., *Mechanism of phosphorylation of the regulatory light chain of myosin from tarantula striated muscle.* J Muscle Res Cell Motil, 2001. **22**(1): p. 51-9.

26.   Zhu, J., et al., *Analysis of tarantula skeletal muscle protein sequences and identification of transcriptional isoforms.* BMC Genomics, 2009. **10**: p. 117.

27.   Brzeska, H. and E.D. Korn, *Regulation of class I and class II myosins by heavy chain phosphorylation.* J Biol Chem, 1996. **271**(29): p. 16983-6.

28.   De La Cruz, E.M., E.M. Ostap, and H.L. Sweeney, *Kinetic mechanism and regulation of myosin VI.* J Biol Chem, 2001. **276**(34): p. 32373-81.

29.   Wang, F., et al., *Regulated conformation of myosin V.* J Biol Chem, 2004. **279**(4): p. 2333-6.

30.   Trybus, K.M., et al., *Effect of calcium on calmodulin bound to the IQ motifs of myosin V.* J Biol Chem, 2007. **282**(32): p. 23316-25.

31.   Kühne, W., *Untersuchungen über das Protoplasma und die Contractilitat. W. Engelmann.* 1864: Leipzig.

32.   Engelhardt, W.A. and M.N. Lyubimova, *Myosin and adenosinetriphosphate.* Nature, 1939.

33.   Banga, I. and A. Szent-Gyorgyi, *Preparation and properties of myosin A and B.* Stud. Inst. Med. Chem. Univ., 1942(5-15).

34.   Needham, J.A., et al., *Is muscle contraction essentially an enzyme-substrate combination?* Nature, 1942. **150**: p. 46-49.

35.   Szent-Györgyi, A., *The contraction of myosin threads.* Stud. Inst. Med.Chem. Univ., 1942. **I**: p. 17–26.

36.   Szent-Györgyi, A., *The crystallization of myosin and some of its properties and reactions.* Stud. Inst. Med. Chem. Univ. Szeged, 1943. **III**: p. 76–85.

37.   Straub, F.B., *Actin.* Stud. Inst. Med. Chem. Univ. Szeged., 1942. **II**: p. 3-15.

38.   Straub, F.B., *Actin II.* Stud. Inst. Med. Chem. Univ. Szeged., 1943. **III**: p. 23–37.

39.   Banga, I., *The phosphatase activity of myosin.* Stud. Inst. Med. Chem. Univ. Szeged., 1942. **I**: p. 27-36.

40.   Guba, F., *Observations on myosin and actomyosin.* Stud. Inst. Med. Chem. Univ. Szeged., 1943. **III**: p. 40-45.

41.   Erdős, T., *Rigor, contracture and ATP.* Stud. Inst. Med. Chem. Univ. Szeged., 1943. **III**: p. 51-56.

42.   Biró, N.A. and A.G. Szent-Gyorgyi, *The effect of actin and physicochemical changes on the myosin ATPase system, and on washed muscle.* Hung. Acta Physiol., 1949. **II**: p. 1-14.

43.   Szent-Gyorgyi, A., *Free-energy relations and contraction of actomyosin.* Biol Bull, 1949. **96**(2): p. 140-61.

44.   Gergely, J., *On the relationship between myosin and ATPase.* Fed. Proc., 1950. **9**: p. 176.

45.   Perry, S.V., *The adenosinetriphophatase activity of myofibrils isolated from skeletal muscle.* Biochem. J., 1951. **48**: p. 257-265.

46.   Szent-Györgyi, A.G., *Meromyosins, the subunits of myosin.* Arch Biochem Biophys, 1953. **42**(2): p. 305-20.

47.   Philpott, D.E. and A.G. Szent-Gyorgyi, *The structure of light-meromyosin: an electron microscopic study.* Biochim Biophys Acta, 1954. **15**(2): p. 165-73.

48.   Huxley, H.E., *X-ray analysis and the problem of muscle.* Proc R Soc Lond B Biol Sci, 1953. **141**(902): p. 59-62.

49.   Mueller, H. and S.V. Perry, *The degradation of heavy meromyosin by trypsin.* Biochem J, 1962. **85**: p. 431-9.

50.   Lowey, S., et al., *Substructure of the myosin molecule. I. Subfragments of myosin by enzymic degradation.* J Mol Biol, 1969. **42**(1): p. 1-29.

51.   Lowey, S., et al., *Proteolytic degradation of myosin and the meromyosins by a water-insoluble polyanionic derivative of trypsin: properties of a helical subunit isolated from heavy meromyosin.* J Mol Biol, 1967. **23**(3): p. 287-304.

52.   Sutoh, K., T. Karr, and W.F. Harrington, *Isolation and physico-chemical properties of a high molecular weight subfragment-2 of myosin.* J Mol Biol, 1978. **126**(1): p. 1-22.

53.   Huxley, H.E., *Electron Microscope Studies on the Structure of Natural and Synthetic Protein Filaments from Striated Muscle.* J Mol Biol, 1963. **7**: p. 281-308.

54.   Slayter, H.S. and S. Lowey, *Substructure of the myosin molecule as visualized by electron microscopy.* Proc Natl Acad Sci U S A, 1967. **58**(4): p. 1611-8.

55.   Woods, E.F., S. Himmelfarb, and W.F. Harrington, *Studies on the structure of myosin in solution.* J Biol Chem, 1963. **238**: p. 2374-85.

56.   Applegate, D., A. Azarcon, and E. Reisler, *Tryptic cleavage and substructure of bovine cardiac myosin subfragment 1.* Biochemistry, 1984. **23**(26): p. 6626-30.

57.   Bertrand, R., J. Derancourt, and R. Kassab, *Selective cleavage at lysine of the 50 kDa-20 kDa connector loop segment of skeletal myosin S-1 by endoproteinase Arg-C.* FEBS Lett, 1989. **246**(1-2): p. 171-6.

58.   Chaussepied, P., et al., *Selective cleavage of the connector segments within the myosin-S1 heavy chain by staphylococcal protease.* FEBS Lett, 1983. **161**(1): p. 84-8.

59.   Mornet, D., K. Ue, and M.F. Morales, *Proteolysis and the domain organization of myosin subfragment 1.* Proc Natl Acad Sci U S A, 1984. **81**(3): p. 736-9.

60.   Balint, M., et al., *The substructure of heavy meromyosin. The effect of Ca2+ and Mg2+ on the tryptic fragmentation of heavy meromyosin.* J Biol Chem, 1975. **250**(15): p. 6168-77.

61.   Okamoto, Y. and T. Sekine, *A new, smaller actin-activatable myosin subfragment 1 which lacks the 20-kDa, SH1 and SH2 peptide.* J Biol Chem, 1987. **262**(17): p. 7951-4.

62.   Waller, G.S., et al., *A minimal motor domain from chicken skeletal muscle myosin.* J Biol Chem, 1995. **270**(25): p. 15348-52.

63.   Chen, T., J. Liu, and E. Reisler, *Proteolysis and binding of myosin subfragment 1 to actin.* J Mol Biol, 1987. **194**(3): p. 565-8.

64.   Xie, X., et al., *Structure of the regulatory domain of scallop myosin at 2.8 A resolution.* Nature, 1994. **368**(6469): p. 306-12.

65.   Huxley, H.E., *Electron microscope studies of the organisation of the filaments in striated muscle.* Biochim Biophys Acta, 1953. **12**(3): p. 387-94.

66.   Huxley, H.E., *The double array of filaments in cross-striated muscle.* J Biophys Biochem Cytol, 1957. **3**(5): p. 631-48.

67.   Huxley, A.F. and R. Niedergerke, *Structural changes in muscle during contraction; interference microscopy of living muscle fibres.* Nature, 1954. **173**(4412): p. 971-3.

68.   Huxley, H. and J. Hanson, *Changes in the cross-striations of muscle during contraction and stretch and their structural interpretation.* Nature, 1954. **173**(4412): p. 973-6.

69.   Huxley, H.E., *The contraction of muscle.* Sci Am, 1958. **199**(5): p. 67-72 passim.

70.   Reedy, M.K., K.C. Holmes, and R.T. Tregear, *Induced changes in orientation of the cross-bridges of glycerinated insect flight muscle.* Nature, 1965. **207**(5003): p. 1276-80.

71.   Huxley, H.E., *The mechanism of muscular contraction.* Science, 1969. **164**(3886): p. 1356-65.

72.   Kanazawa, T. and Y. Tonomura, *The pre-steady state of the myosin-adenosine triphosphate system. I. Initial rapid liberation of inorganic phosphate.* J Biochem, 1965. **57**(5): p. 604-15.

73.   Lymn, R.W. and E.W. Taylor, *Mechanism of adenosine triphosphate hydrolysis by actomyosin.* Biochemistry, 1971. **10**(25): p. 4617-24.

74. Cooke, R., *The mechanism of muscle contraction.* CRC Crit Rev Biochem, 1986. **21**(1): p. 53-118.

75. Holmes, K.C., *The swinging lever-arm hypothesis of muscle contraction.* Curr Biol, 1997. **7**(2): p. R112-8.

76. Cheung, H.C. and M.F. Morales, *Studies of myosin conformation by fluorescent techniques.* Biochemistry, 1969. **8**(5): p. 2177-82.

77. Kishino, A. and T. Yanagida, *Force measurements by micromanipulation of a single actin filament by glass needles.* Nature, 1988. **334**(6177): p. 74-6.

78. Spudich, J.A., *Optical trapping: Motor molecules in motion.* Nature, 1990. **348**(6299): p. 284-5.

79. Kron, S.J. and J.A. Spudich, *Fluorescent actin filaments move on myosin fixed to a glass surface.* Proc Natl Acad Sci U S A, 1986. **83**(17): p. 6272-6.

80. Finer, J.T., R.M. Simmons, and J.A. Spudich, *Single myosin molecule mechanics: piconewton forces and nanometre steps.* Nature, 1994. **368**(6467): p. 113-9.

81. Manstein, D.J., K.M. Ruppel, and J.A. Spudich, *Expression and characterization of a functional myosin head fragment in Dictyostelium discoideum.* Science, 1989. **246**(4930): p. 656-8.

82. Manstein, D.J., et al., *Manipulation and expression of molecular motors in Dictyostelium discoideum.* J Cell Sci Suppl, 1991. **14**: p. 63-5.

83. Sweeney, H.L., et al., *Heterologous expression of a cardiomyopathic myosin that is defective in its actin interaction.* J Biol Chem, 1994. **269**(3): p. 1603-5.

84. Trybus, K.M., *Regulation of expressed truncated smooth muscle myosins. Role of the essential light chain and tail length.* J Biol Chem, 1994. **269**(33): p. 20819-22.

85. Onishi, H., et al., *Functional chicken gizzard heavy meromyosin expression in and purification from baculovirus-infected insect cells.* Proc Natl Acad Sci U S A, 1995. **92**(3): p. 704-8.

86. Kabsch, W., et al., *Atomic structure of the actin:DNase I complex.* Nature, 1990. **347**(6288): p. 37-44.

87. McLaughlin, P.J., et al., *Structure of gelsolin segment 1-actin complex and the mechanism of filament severing.* Nature, 1993. **364**(6439): p. 685-92.

88. Schutt, C.E., et al., *The structure of crystalline profilin-beta-actin.* Nature, 1993. **365**(6449): p. 810-6.

89. Oda, T., et al., *The nature of the globular- to fibrous-actin transition.* Nature, 2009. **457**(7228): p. 441-5.

90. Fujii, T., et al., *Direct visualization of secondary structures of F-actin by electron cryomicroscopy.* Nature, 2010. **467**(7316): p. 724-8.

91. Rayment, I., et al., *Three-dimensional structure of myosin subfragment-1: a molecular motor.* Science, 1993. **261**(5117): p. 50-8.

92. Rayment, I., et al., *Structure of the actin-myosin complex and its implications for muscle contraction.* Science, 1993. **261**(5117): p. 58-65.

93. Volkmann, N., et al., *Evidence for cleft closure in actomyosin upon ADP release.* Nat Struct Biol, 2000. **7**(12): p. 1147-55.

94. Yengo, C.M., et al., *Actin-induced closure of the actin-binding cleft of smooth muscle myosin.* J Biol Chem, 2002. **277**(27): p. 24114-9.

95. Conibear, P.B., et al., *Myosin cleft movement and its coupling to actomyosin dissociation.* Nat Struct Biol, 2003. **10**(10): p. 831-5.

96. Sweeney, H.L. and A. Houdusse, *The motor mechanism of myosin V: insights for muscle contraction.* Philos Trans R Soc Lond B Biol Sci, 2004. **359**(1452): p. 1829-41.

97. Fisher, A.J., et al., *X-ray structures of the myosin motor domain of Dictyostelium discoideum complexed with MgADP.BeFx and MgADP.AlF4.* Biochemistry, 1995. **34**(28): p. 8960-72.

98.   Coureux, P.D., H.L. Sweeney, and A. Houdusse, *Three myosin V structures delineate essential features of chemo-mechanical transduction.* EMBO J, 2004. **23**(23): p. 4527-37.

99.   Yang, Y., et al., *Rigor-like structures from muscle myosins reveal key mechanical elements in the transduction pathways of this allosteric motor.* Structure, 2007. **15**(5): p. 553-64.

100.   Kurzawa, S.E., D.J. Manstein, and M.A. Geeves, *Dictyostelium discoideum myosin II: characterization of functional myosin motor fragments.* Biochemistry, 1997. **36**(2): p. 317-23.

101.   Smith, C.A. and I. Rayment, *X-ray structure of the magnesium(II).ADP.vanadate complex of the Dictyostelium discoideum myosin motor domain to 1.9 A resolution.* Biochemistry, 1996. **35**(17): p. 5404-17.

102.   Dominguez, R., et al., *Crystal structure of a vertebrate smooth muscle myosin motor domain and its complex with the essential light chain: visualization of the pre-power stroke state.* Cell, 1998. **94**(5): p. 559-71.

103.   Houdusse, A., A.G. Szent-Gyorgyi, and C. Cohen, *Three conformational states of scallop myosin S1.* Proc Natl Acad Sci U S A, 2000. **97**(21): p. 11238-43.

104.   Fischer, S., et al., *Structural mechanism of the recovery stroke in the myosin molecular motor.* Proc Natl Acad Sci U S A, 2005. **102**(19): p. 6873-8.

105.   Mesentean, S., et al., *The principal motions involved in the coupling mechanism of the recovery stroke of the myosin motor.* J Mol Biol, 2007. **367**(2): p. 591-602.

106.   Koppole, S., J.C. Smith, and S. Fischer, *The structural coupling between ATPase activation and recovery stroke in the myosin II motor.* Structure, 2007. **15**(7): p. 825-37.

107.   Kintses, B., Z. Yang, and A. Malnasi-Csizmadia, *Experimental investigation of the seesaw mechanism of the relay region that moves the myosin lever arm.* J Biol Chem, 2008. **283**(49): p. 34121-8.

108.   Warshaw, D.M., et al., *The light chain binding domain of expressed smooth muscle heavy meromyosin acts as a mechanical lever.* J Biol Chem, 2000. **275**(47): p. 37167-72.

109.   Purcell, T.J., et al., *Role of the lever arm in the processive stepping of myosin V.* Proc Natl Acad Sci U S A, 2002. **99**(22): p. 14159-64.

110.   Kohler, D., et al., *Different degrees of lever arm rotation control myosin step size.* J Cell Biol, 2003. **161**(2): p. 237-41.

111.   Holmes, K.C., et al., *Electron cryo-microscopy shows how strong binding of myosin to actin releases nucleotide.* Nature, 2003. **425**(6956): p. 423-7.

112.   Coureux, P.D., et al., *A structural state of the myosin V motor without bound nucleotide.* Nature, 2003. **425**(6956): p. 419-23.

113.   Kollmar, M., et al., *Crystal structure of the motor domain of a class-I myosin.* EMBO J, 2002. **21**(11): p. 2517-25.

114.   Reubold, T.F., et al., *A structural model for actin-induced nucleotide release in myosin.* Nat Struct Biol, 2003. **10**(10): p. 826-30.

115.   Schroder, R.R., et al., *Three-dimensional atomic model of F-actin decorated with Dictyostelium myosin S1.* Nature, 1993. **364**(6433): p. 171-4.

116.   Lorenz, M. and K.C. Holmes, *The actin-myosin interface.* Proc Natl Acad Sci U S A, 2010. **107**(28): p. 12529-34.

117.   Behrmann, E., et al., *Structure of the rigor actin-tropomyosin-myosin complex.* Cell, 2012. **150**(2): p. 327-38.

118.   Holmes, K.C., et al., *The structure of the rigor complex and its implications for the power stroke.* Philos Trans R Soc Lond B Biol Sci, 2004. **359**(1452): p. 1819-28.

119.   Root, D.D., *A computational comparison of the atomic models of the actomyosin interface.* Cell Biochem Biophys, 2002. **37**(2): p. 97-110.

120. Kojima, S., et al., *Functional roles of ionic and hydrophobic surface loops in smooth muscle myosin: their interactions with actin.* Biochemistry, 2001. **40**(3): p. 657-64.

121. Onishi, H., S.V. Mikhailenko, and M.F. Morales, *Toward understanding actin activation of myosin ATPase: the role of myosin surface loops.* Proc Natl Acad Sci U S A, 2006. **103**(16): p. 6136-41.

122. Furch, M., et al., *Stabilization of the actomyosin complex by negative charges on myosin.* Biochemistry, 2000. **39**(38): p. 11602-8.

123. Sasaki, N., et al., *Deletion of the myopathy loop of Dictyostelium myosin II and its impact on motor functions.* J Biol Chem, 1999. **274**(53): p. 37840-4.

124. Gyimesi, M., et al., *Kinetic characterization of the function of myosin loop 4 in the actin-myosin interaction.* Biochemistry, 2008. **47**(1): p. 283-91.

125. Liu, Y., et al., *Protein-protein interactions in actin-myosin binding and structural effects of R405Q mutation: a molecular dynamics study.* Proteins, 2006. **64**(1): p. 156-66.

126. Milligan, R.A., *Protein-protein interactions in the rigor actomyosin complex.* Proc Natl Acad Sci U S A, 1996. **93**(1): p. 21-6.

127. Onishi, H. and M.F. Morales, *A closer look at energy transduction in muscle.* Proc Natl Acad Sci U S A, 2007. **104**(31): p. 12714-9.

128. Roopnarine, O. and L.A. Leinwand, *Functional analysis of myosin mutations that cause familial hypertrophic cardiomyopathy.* Biophys J, 1998. **75**(6): p. 3023-30.

129. Joel, P.B., K.M. Trybus, and H.L. Sweeney, *Two conserved lysines at the 50/20-kDa junction of myosin are necessary for triggering actin activation.* J Biol Chem, 2001. **276**(5): p. 2998-3003.

130. Miller, C.J., et al., *Mutational analysis of the role of the N terminus of actin in actomyosin interactions. Comparison with other mutant actins and implications for the cross-bridge cycle.* Biochemistry, 1996. **35**(51): p. 16557-65.

131. Van Dijk, J., et al., *Differences in the ionic interaction of actin with the motor domains of nonmuscle and muscle myosin II.* Eur J Biochem, 1999. **260**(3): p. 672-83.

132. Sutoh, K., *Mapping of actin-binding sites on the heavy chain of myosin subfragment 1.* Biochemistry, 1983. **22**(7): p. 1579-85.

133. Jontes, J.D., E.M. Wilson-Kubalek, and R.A. Milligan, *A 32 degree tail swing in brush border myosin I on ADP release.* Nature, 1995. **378**(6558): p. 751-3.

134. Whittaker, M., et al., *A 35-A movement of smooth muscle myosin on ADP release.* Nature, 1995. **378**(6558): p. 748-51.

135. Nagy, N.T., et al., *Functional adaptation of the switch-2 nucleotide sensor enables rapid processive translocation by myosin-5.* FASEB J, 2010. **24**(11): p. 4480-90.

136. Kintses, B., et al., *Reversible movement of switch 1 loop of myosin determines actin interaction.* EMBO J, 2007. **26**(1): p. 265-74.

137. Yount, R.G., D. Lawson, and I. Rayment, *Is myosin a "back door" enzyme?* Biophys J, 1995. **68**(4 Suppl): p. 44S-47S; discussion 47S-49S.

138. Lawson, J.D., et al., *Molecular dynamics analysis of structural factors influencing back door pi release in myosin.* Biophys J, 2004. **86**(6): p. 3794-803.

139. Bagshaw, C.R., et al., *The magnesium ion-dependent adenosine triphosphatase of myosin. Two-step processes of adenosine triphosphate association and adenosine diphosphate dissociation.* Biochem J, 1974. **141**(2): p. 351-64.

140. Bagshaw, C.R. and D.R. Trentham, *The characterization of myosin-product complexes and of product-release steps during the magnesium ion-dependent adenosine triphosphatase reaction.* Biochem J, 1974. **141**(2): p. 331-49.

141. Werber, M.M., A.G. Szent-Gyorgyi, and G.D. Fasman, *Fluorescence studies on heavy meromyosin-substrate interaction.* Biochemistry, 1972. **11**(15): p. 2872-83.

142. Malnasi-Csizmadia, A., R.J. Woolley, and C.R. Bagshaw, *Resolution of conformational states of Dictyostelium myosin II motor domain using tryptophan (W501) mutants:*

implications for the open-closed transition identified by crystallography. Biochemistry, 2000. **39**(51): p. 16135-46.

143. Malnasi-Csizmadia, A., et al., *Kinetic resolution of a conformational transition and the ATP hydrolysis step using relaxation methods with a Dictyostelium myosin II mutant containing a single tryptophan residue.* Biochemistry, 2001. **40**(42): p. 12727-37.

144. Malnasi-Csizmadia, A., et al., *The dynamics of the relay loop tryptophan residue in the Dictyostelium myosin motor domain and the origin of spectroscopic signals.* J Biol Chem, 2001. **276**(22): p. 19483-90.

145. Gyimesi, M., et al., *The mechanism of the reverse recovery step, phosphate release, and actin activation of Dictyostelium myosin II.* J Biol Chem, 2008. **283**(13): p. 8153-63.

146. Conibear, P.B., A. Malnasi-Csizmadia, and C.R. Bagshaw, *The effect of F-actin on the relay helix position of myosin II, as revealed by tryptophan fluorescence, and its implications for mechanochemical coupling.* Biochemistry, 2004. **43**(49): p. 15404-17.

147. Dantzig, J.A., et al., *Reversal of the cross-bridge force-generating transition by photogeneration of phosphate in rabbit psoas muscle fibres.* J Physiol, 1992. **451**: p. 247-78.

148. De La Cruz, E.M., et al., *The kinetic mechanism of myosin V.* Proc Natl Acad Sci U S A, 1999. **96**(24): p. 13726-31.

149. Takagi, Y., H. Shuman, and Y.E. Goldman, *Coupling between phosphate release and force generation in muscle actomyosin.* Philos Trans R Soc Lond B Biol Sci, 2004. **359**(1452): p. 1913-20.

150. Caremani, M., et al., *Effect of inorganic phosphate on the force and number of myosin cross-bridges during the isometric contraction of permeabilized muscle fibers from rabbit psoas.* Biophys J, 2008. **95**(12): p. 5798-808.

151. Davis, J.S. and M.E. Rodgers, *Indirect coupling of phosphate release to de novo tension generation during muscle contraction.* Proc Natl Acad Sci U S A, 1995. **92**(23): p. 10482-6.

152. Davis, J.S. and N.D. Epstein, *Mechanistic role of movement and strain sensitivity in muscle contraction.* Proc Natl Acad Sci U S A, 2009. **106**(15): p. 6140-5.

153. Lionne, C., et al., *Evidence that phosphate release is the rate-limiting step on the overall ATPase of psoas myofibrils prevented from shortening by chemical cross-linking.* Biochemistry, 2002. **41**(44): p. 13297-308.

154. Lionne, C., et al., *Time resolved measurements show that phosphate release is the rate limiting step on myofibrillar ATPases.* FEBS Lett, 1995. **364**(1): p. 59-62.

155. Muretta, J.M., K.J. Petersen, and D.D. Thomas, *Direct real-time detection of the actin-activated power stroke within the myosin catalytic domain.* Proc Natl Acad Sci U S A, 2013. **110**(18): p. 7211-6.

156. Malnasi-Csizmadia, A. and M. Kovacs, *Emerging complex pathways of the actomyosin powerstroke.* Trends Biochem Sci, 2010. **35**(12): p. 684-90.

157. Ferenczi, M.A., et al., *The "roll and lock" mechanism of force generation in muscle.* Structure, 2005. **13**(1): p. 131-41.

158. Straight, A.F., et al., *Dissecting temporal and spatial control of cytokinesis with a myosin II Inhibitor.* Science, 2003. **299**(5613): p. 1743-7.

159. Kovacs, M., et al., *Mechanism of blebbistatin inhibition of myosin II.* J Biol Chem, 2004. **279**(34): p. 35557-63.

160. Ramamurthy, B., et al., *Kinetic mechanism of blebbistatin inhibition of nonmuscle myosin IIb.* Biochemistry, 2004. **43**(46): p. 14832-9.

161. Limouze, J., et al., *Specificity of blebbistatin, an inhibitor of myosin II.* J Muscle Res Cell Motil, 2004. **25**(4-5): p. 337-41.

162. Allingham, J.S., R. Smith, and I. Rayment, *The structural basis of blebbistatin inhibition and specificity for myosin II.* Nat Struct Mol Biol, 2005. **12**(4): p. 378-9.

163. Takacs, B., et al., *Myosin complexed with ADP and blebbistatin reversibly adopts a conformation resembling the start point of the working stroke.* Proc Natl Acad Sci U S A, 2010. **107**(15): p. 6799-804.

164. Bhattacharyya, R.P., et al., *The Ste5 scaffold allosterically modulates signaling output of the yeast mating pathway.* Science, 2006. **311**(5762): p. 822-6.

165. Vale, R.D., *Switches, latches, and amplifiers: common themes of G proteins and molecular motors.* J Cell Biol, 1996. **135**(2): p. 291-302.

166. Kull, F.J., R.D. Vale, and R.J. Fletterick, *The case for a common ancestor: kinesin and myosin motor proteins and G proteins.* J Muscle Res Cell Motil, 1998. **19**(8): p. 877-86.

167. Thomas, C., et al., *Structural evidence for a common intermediate in small G protein-GEF reactions.* Mol Cell, 2007. **25**(1): p. 141-9.

168. Goody, R.S. and W. Hofmann-Goody, *Exchange factors, effectors, GAPs and motor proteins: common thermodynamic and kinetic principles for different functions.* Eur Biophys J, 2002. **31**(4): p. 268-74.

169. Cook, R.K., W.T. Blake, and P.A. Rubenstein, *Removal of the amino-terminal acidic residues of yeast actin. Studies in vitro and in vivo.* J Biol Chem, 1992. **267**(13): p. 9430-6.

170. Vandekerckhove, J. and K. Weber, *At least six different actins are expressed in a higher mammal: an analysis based on the amino acid sequence of the amino-terminal tryptic peptide.* J Mol Biol, 1978. **126**(4): p. 783-802.

171. Varkuti, B.H., et al., *A novel actin binding site of myosin required for effective muscle contraction.* Nat Struct Mol Biol, 2012. **19**(3): p. 299-306.

172. Andreev, O.A. and Y.K. Reshetnyak, *Mechanism of formation of actomyosin interface.* J Mol Biol, 2007. **365**(3): p. 551-4.

173. Meiler, J. and D. Baker, *Coupled prediction of protein secondary and tertiary structure.* Proc Natl Acad Sci U S A, 2003. **100**(21): p. 12105-10.

174. Purcell, T.J., et al., *Nucleotide pocket thermodynamics measured by EPR reveal how energy partitioning relates myosin speed to efficiency.* J Mol Biol, 2011. **407**(1): p. 79-91.

175. Cooke, R., H. White, and E. Pate, *A model of the release of myosin heads from actin in rapidly contracting muscle fibers.* Biophys J, 1994. **66**(3 Pt 1): p. 778-88.

176. Nyitrai, M., et al., *What limits the velocity of fast-skeletal muscle contraction in mammals?* J Mol Biol, 2006. **355**(3): p. 432-42.

177. Takacs, B., et al., *Myosin cleft closure determines the energetics of the actomyosin interaction.* FASEB J, 2011. **25**(1): p. 111-21.

178. Forgacs, E., et al., *Switch 1 mutation S217A converts myosin V into a low duty ratio motor.* J Biol Chem, 2009. **284**(4): p. 2138-49.

179. Lin, T., et al., *A hearing loss-associated myo1c mutation (R156W) decreases the myosin duty ratio and force sensitivity.* Biochemistry, 2011. **50**(11): p. 1831-8.

180. Uyeda, T.Q., P.D. Abramson, and J.A. Spudich, *The neck region of the myosin motor domain acts as a lever arm to generate movement.* Proc Natl Acad Sci U S A, 1996. **93**(9): p. 4459-64.

181. Waterston, R.H., *The minor myosin heavy chain, mhcA, of Caenorhabditis elegans is necessary for the initiation of thick filament assembly.* EMBO J, 1989. **8**(11): p. 3429-36.

182. Moerman, D.G., et al., *Mutations in the unc-54 myosin heavy chain gene of Caenorhabditis elegans that alter contractility but not muscle structure.* Cell, 1982. **29**(3): p. 773-81.

183. Fire, A. and R.H. Waterston, *Proper expression of myosin genes in transgenic nematodes.* EMBO J, 1989. **8**(11): p. 3419-28.

184. Anderson, P. and S. Brenner, *A selection for myosin heavy chain mutants in the nematode Caenorhabditis elegans.* Proc Natl Acad Sci U S A, 1984. **81**(14): p. 4470-4.

185. Geeves, M.A. and P.B. Conibear, *The role of three-state docking of myosin S1 with actin in force generation.* Biophys J, 1995. **68**(4 Suppl): p. 194S-199S; discussion 199S-201S.

186. Kepiro, M., et al., *Azidoblebbistatin, a photoreactive myosin inhibitor.* Proc Natl Acad Sci U S A, 2012. **109**(24): p. 9402-7.

187. Vodovozova, E.L., *Photoaffinity labeling and its application in structural biology.* Biochemistry (Mosc), 2007. **72**(1): p. 1-20.

188. Marcinek, A., et al., *Evidence for stepwise nitrogen extrusion and ring expansion upon photolysis of phenyl azide.* Journal of the American Chemical Society, 1993. **115**(19): p. 8609-8612.

189. Murphy, C.T. and J.A. Spudich, *Dictyostelium myosin 25-50K loop substitutions specifically affect ADP release rates.* Biochemistry, 1998. **37**(19): p. 6738-44.

190. Jacobs, D.J., et al., *Kinetics and thermodynamics of the rate-limiting conformational change in the actomyosin V mechanochemical cycle.* J Mol Biol, 2011. **407**(5): p. 716-30.

191. Sweeney, H.L. and A. Houdusse, *Myosin VI rewrites the rules for myosin motors.* Cell, 2010. **141**(4): p. 573-82.

192. Cook, R.K., et al., *Enhanced stimulation of myosin subfragment 1 ATPase activity by addition of negatively charged residues to the yeast actin NH2 terminus.* J Biol Chem, 1993. **268**(4): p. 2410-5.

193. Furch, M., M.A. Geeves, and D.J. Manstein, *Modulation of actin affinity and actomyosin adenosine triphosphatase by charge changes in the myosin motor domain.* Biochemistry, 1998. **37**(18): p. 6317-26.

194. Menetrey, J., et al., *The structural basis for the large powerstroke of myosin VI.* Cell, 2007. **131**(2): p. 300-8.

195. Sweeney, H.L. and A. Houdusse, *Structural and functional insights into the Myosin motor mechanism.* Annu Rev Biophys, 2010. **39**: p. 539-57.

196. Adams, S.R. and R.Y. Tsien, *Preparation of the membrane-permeant biarsenicals FlAsH-EDT2 and ReAsH-EDT2 for fluorescent labeling of tetracysteine-tagged proteins.* Nat Protoc, 2008. **3**(9): p. 1527-34.

197. Cao, H., et al., *A red cy3-based biarsenical fluorescent probe targeted to a complementary binding peptide.* J Am Chem Soc, 2007. **129**(28): p. 8672-3.

198. Adams, S.R., et al., *New biarsenical ligands and tetracysteine motifs for protein labeling in vitro and in vivo: synthesis and biological applications.* J Am Chem Soc, 2002. **124**(21): p. 6063-76.

199. Fessenden, J.D. and M. Mahalingam, *Site-specific labeling of the type 1 ryanodine receptor using biarsenical fluorophores targeted to engineered tetracysteine motifs.* PLoS One, 2013. **8**(5): p. e64686.

200. Hoffmann, C., et al., *Fluorescent labeling of tetracysteine-tagged proteins in intact cells.* Nat Protoc, 2010. **5**(10): p. 1666-77.

201. Zurn, A., et al., *Site-specific, orthogonal labeling of proteins in intact cells with two small biarsenical fluorophores.* Bioconjug Chem, 2010. **21**(5): p. 853-9.

202. Chang, S. and E.M. Ross, *Activation biosensor for G protein-coupled receptors: a FRET-based m1 muscarinic activation sensor that regulates G(q).* PLoS One, 2012. **7**(9): p. e45651.

203. Scheck, R.A. and A. Schepartz, *Surveying protein structure and function using bis-arsenical small molecules.* Acc Chem Res, 2011. **44**(9): p. 654-65.

204. Nakanishi, J., et al., *FRET-based monitoring of conformational change of the beta2 adrenergic receptor in living cells.* Biochem Biophys Res Commun, 2006. **343**(4): p. 1191-6.

205. Yengo, C.M. and C.L. Berger, *Fluorescence anisotropy and resonance energy transfer: powerful tools for measuring real time protein dynamics in a physiological environment.* Curr Opin Pharmacol, 2010. **10**(6): p. 731-7.

206. Shu, S., X. Liu, and E.D. Korn, *Blebbistatin and blebbistatin-inactivated myosin II inhibit myosin II-independent processes in Dictyostelium.* Proceedings of the National Academy of Sciences of the United States of America, 2005. **102**(5): p. 1472-1477.

207. Eddinger, T.J., et al., *Potent inhibition of arterial smooth muscle tonic contractions by the selective myosin II inhibitor, blebbistatin.* J Pharmacol Exp Ther, 2007. **320**(2): p. 865-70.

208. Loudon, R.P., et al., *RhoA-kinase and myosin II are required for the maintenance of growth cone polarity and guidance by nerve growth factor.* J Neurobiol, 2006. **66**(8): p. 847-67.

209. Swaminathan, V., et al., *Mechanical stiffness grades metastatic potential in patient tumor cells and in cancer cell lines.* Cancer Res, 2011. **71**(15): p. 5075-80.

210. Mikulich, A., S. Kavaliauskiene, and P. Juzenas, *Blebbistatin, a myosin inhibitor, is phototoxic to human cancer cells under exposure to blue light.* Biochim Biophys Acta, 2012. **1820**(7): p. 870-7.

211. Swift, L.M., et al., *Properties of blebbistatin for cardiac optical mapping and other imaging applications.* Pflugers Arch, 2012. **464**(5): p. 503-12.

212. Lucas-Lopez, C., et al., *Absolute stereochemical assignment and fluorescence tuning of the small molecule tool, (-)-blebbistatin.* European Journal of Organic Chemistry, 2005(9): p. 1736-1740.

213. Johnson, K.A., *Conformational coupling in DNA polymerase fidelity.* Annu Rev Biochem, 1993. **62**: p. 685-713.

214. Gromadski, K.B. and M.V. Rodnina, *Kinetic determinants of high-fidelity tRNA discrimination on the ribosome.* Mol Cell, 2004. **13**(2): p. 191-200.

215. Egea, P.F., et al., *Substrate twinning activates the signal recognition particle and its receptor.* Nature, 2004. **427**(6971): p. 215-21.

216. Manstein, D.J., et al., *Cloning vectors for the production of proteins in Dictyostelium discoideum.* Gene, 1995. **162**(1): p. 129-34.

217. Spudich, J.A. and S. Watt, *The regulation of rabbit skeletal muscle contraction. I. Biochemical studies of the interaction of the tropomyosin-troponin complex with actin and the proteolytic fragments of myosin.* J Biol Chem, 1971. **246**(15): p. 4866-71.

218. Cooper, J.A., S.B. Walker, and T.D. Pollard, *Pyrene actin: documentation of the validity of a sensitive assay for actin polymerization.* J Muscle Res Cell Motil, 1983. **4**(2): p. 253-62.

219. Kellermayer, M.S. and H.L. Granzier, *Calcium-dependent inhibition of in vitro thin-filament motility by native titin.* FEBS Lett, 1996. **380**(3): p. 281-6.

220. Anson, M., et al., *Myosin motors with artificial lever arms.* EMBO J, 1996. **15**(22): p. 6069-74.

221. Berezikov, E., C.I. Bargmann, and R.H. Plasterk, *Homologous gene targeting in Caenorhabditis elegans by biolistic transformation.* Nucleic Acids Res, 2004. **32**(4): p. e40.

222. Eswar, N., et al., *Comparative protein structure modeling using Modeller.* Curr Protoc Bioinformatics, 2006. **Chapter 5**: p. Unit 5 6.

223. Meagher, K.L., L.T. Redman, and H.A. Carlson, *Development of polyphosphate parameters for use with the AMBER force field.* J Comput Chem, 2003. **24**(9): p. 1016-25.

224. Frisch, M.J., et al., *Gaussian 03, Revision C.02*. 2003.

225. Wang, J., et al., *Development and testing of a general amber force field.* J Comput Chem, 2004. **25**(9): p. 1157-74.

226. Chaussepied, P. and M.F. Morales, *Modifying preselected sites on proteins: the stretch of residues 633-642 of the myosin heavy chain is part of the actin-binding site.* Proc Natl Acad Sci U S A, 1988. **85**(20): p. 7471-5.

227. Bertrand, R., J. Derancourt, and R. Kassab, *Probing the hydrophobic interactions in the skeletal actomyosin subfragment 1 and its nucleotide complexes by zero-length cross-linking with a nickel-peptide chelate.* Biochemistry, 1997. **36**(32): p. 9703-14.

228. Bertrand, R., J. Derancourt, and R. Kassab, *The covalent maleimidobenzoyl-actin-myosin head complex. Cross-linking of the 50 kDa heavy chain region to actin subdomain-2.* FEBS Lett, 1994. **345**(2-3): p. 113-9.

229. Dominguez, C., R. Boelens, and A.M. Bonvin, *HADDOCK: a protein-protein docking approach based on biochemical or biophysical information.* J Am Chem Soc, 2003. **125**(7): p. 1731-7.

230. Gotz, A.W., et al., *Routine Microsecond Molecular Dynamics Simulations with AMBER on GPUs. 1. Generalized Born.* J Chem Theory Comput, 2012. **8**(5): p. 1542-1555.

231. Jorgensen, W., et al., *Comparison of simple potential functions for simulating liquid water.* The Journal of Chemical Physics, 1983. **79**(2): p. 926-935.

232. York, D., T. Darden, and L. Pedersen, *The effect of long-range electrostatic interactions in simulations of macromolecular crystals: A comparison of the Ewald and truncated list methods.* The Journal of Chemical Physics, 1993. **99**(10): p. 8345-8348.

233. Berendsen, H.J.C., Postma, J.P.M., van Gunsteren, W.F., Dinola, A. and Haak, J.R. , *Molecular dynamics with coupling to an external bath.* J. Chem. Phys, 1984. **81**: p. 3684-3690.

234. Ryckaert, J.-P., G. Ciccotti, and H. Berendsen, *Numerical integration of the cartesian equations of motion of a system with constraints: molecular dynamics of n-alkanes.* Journal of Computational Physics, 1977. **23**(3): p. 327-341.

235. Luo, R., L. David, and M.K. Gilson, *Accelerated Poisson-Boltzmann calculations for static and dynamic systems.* J Comput Chem, 2002. **23**(13): p. 1244-53.

236. Connolly, M., *Analytical molecular surface calculation.* Journal of Applied Crystallography, 1983. **16**(5): p. 548-558.

237. Kottalam, J. and D.A. Case, *Langevin modes of macromolecules: applications to crambin and DNA hexamers.* Biopolymers, 1990. **29**(10-11): p. 1409-21.